MODELING OF UNCONTROLLED FLUID FLOW IN WELLBORE AND ITS PREVENTION

A Dissertation

by

RUOCHEN LIU

Submitted to the Office of Graduate and Professional Studies of
Texas A&M University
in partial fulfillment of the requirements for the degree of

DOCTOR OF PHILOSOPHY

Chair of Committee,	M. Sam Mannan
Co-Chair of Committee,	A. Rashid Hasan
Committee Members,	M. Nazmul Krim
	Mahmoud El-Halwagi
Head of Department,	M. Nazmul Karim

May 2016

Major Subject: Chemical Engineering

ABSTRACT

Uncontrolled fluid flow in the wellbore is one of the most critical safety concerns for the oil and gas industry. The major focus of this dissertation is on blowout events given the most severe consequences associated with such incidents. The past tragedies reflect a strong need for not only understanding the mechanisms of blowout to accurately estimate the consequence, but also the approaches to managing and controlling the risks, uncertainties, and hazards associated with blowout events.

A fully integrated analytical model that couples the reservoir and wellbore has been proposed to investigate the fluid behaviors during the blowout events. This model could be used to simulate any potential blowout events for gas, oil, or oil/gas wells at onshore or offshore facilities. The reservoir, wellbore, and their interactions are coupled together to demonstrate a full picture of the potential well blowout incidents. The results reveal that understanding the importance of heat transfer and multi-phase flow behaviors is essential to accurately estimate the consequence of well blowouts. Well-established computational algorithms are developed to effectively estimate the blowout rate and total discharge amount during blowout incidents. The statistical analysis identifies the independent variables responsible for the maximum discharge; both reservoir permeability and the connected reservoir volume are the key variables.

The results of the blowout modeling could serve as the input for both consequence-based and risk-based approaches to assess the risk associated with the blowout events. The application of such approaches is demonstrated by the case study.

The consequence-based approach is easier to be implemented and provide guidance to the operators based on the realistic worst-case scenario. It would be useful for drilling site location selection and preparation of emergency response plan. On the other hand, the risk-based approach enables the operators to have a comprehensive understanding of the particular well that they are working on, so that the risk associated with the blowout events can be effectively managed and controlled. The risk reduction plan based on the blowout risk assessment is also discussed in this dissertation.

DEDICATION

To my wife, family and friends for all the endless support and grateful encouragement in facing all the challenges in completing this dissertation.

ACKNOWLEDGEMENTS

I would like to acknowledge and show my greatest appreciation to my advisor, Dr. M. Sam Mannan, for all his support and guidance throughout the course of this research. His professionalism and leadership has guided me to be ready for my next career, not only as an expert in the process safety field, but as a professional team player as well. I also would like to thank my co-advisor, Dr. A. Rashid Hasan, for his endless help on both technical and personal aspects during my Ph.D. program. My sincere thanks also goes to my committee members, Dr. Mahmoud El-Halwagi, and Dr. M. Nazmul Karim, for their continuous support and constructive suggestions.

I am very grateful to Dr. Ray Mentzer for providing me with valuable guidance as a team leader. Special thanks to all the people working on offshore safety, Dr. Tony Rocha, Dr. Josh Richardson, Ms. Tatiana Flechas, and Mr. MD Nafiz E Tamim, for providing me with great support during the initial stage of my research. I want to thank Ms. Valerie Green, Ms. Alanna Scheinerman, Ms. Amarette Renieri, Ms. Towanna Arnold, and Ms. Ashley Stokes, for all their continuous support. I would like to express my sincere gratitude to all the friends and colleagues at the Mary Kay O'Connor Process Safety Center.

Finally, thanks to my mother and father for their encouragement and to my wife for her patience and love.

TABLE OF CONTENTS

Page

LIST OF FIGURES

Page

LIST OF TABLES

Page

CHAPTER I

INTRODUCTION AND LITERATURE REVIEW

Uncontrolled fluid flow phenomena and the causes behind such flow must be understood in depth in order to improve safety performance in offshore operations. Anecdotal and statistical summaries of uncontrolled fluid flow phenomenon are discussed in the following sections. Also, a description of safety barriers to prevent uncontrolled fluid flow is discussed.

1.1 Uncontrolled Fluid Flow

1.1.1 Incident History

Uncontrolled fluid flow in the wellbore is one of the most critical safety concerns for the oil and gas industry. It can result from petroleum seepage, hydrate formation, gas-kicks, and blowouts. Petroleum seepage takes place when the seal above the reservoir is breached. The hydrocarbon escapes along the fractures due to the buoyancy forces to the surface of the earth. Hydrates are solid mixtures of gas and water forming under low temperature and high pressure. It may happen in offshore wells as the ocean water temperature is low. The hydrates can block the subsea equipment, resulting in costly delays or even some dangerous scenarios, such as sudden release of gas at the surface. In a variety of operational phases, if the wellbore pressure provided by drilling mud is less than the formation pressure, the formation fluid will flow into wells from the reservoir. This is known as kicks, and is described in many references (Bourgoyne, 1991). The rate of fluid influx is a function of reservoir parameters and the pressure

difference between the formation and wellbore. There are several indicators of kicks, including (Grace, 2003):

- Sudden change in drilling rate
- Increase in flow rate
- Change in pump pressure
- Reduction in drillpipe weight
- Gas, oil or water-cut mud

After detecting a kick, proper well control procedures must be performed immediately to eliminate the fluid influx and prevent further formation fluid from flowing into the well. The wellbore must be isolated from the surface by activating blowout preventers (BOP). Then the remaining fluid influx is circulated out to the surface. Once the influx has been displaced, heavier drilling mud is pumped into the well in order to regain control of the well. However, as can be seen from the past incident history of the oil and gas industry, such procedures do not always succeed. If the kick is out of control, it will lead to a blowout.

The definition of blowout event according to International Association of Oil & Gas Producers (OGP) is an incident where formation fluid flows out of the well or between the formation layers after all the predefined technical well barriers or the activation of the same have failed (OGP, 2010). Although the drilling and production well planning may be good, the measurement and detection systems used are sophisticated and accurate, and personnel receive comprehensive training, blowout

events can still occur and lead to severe consequences, such as the deepwater Macondo incident in the US Gulf of Mexico. These consequences include:

- Fatalities and injuries of personnel
- Fire, explosion, or toxic hazard
- Environmental impact
- Loss of production
- Loss of equipment
- Blowout control cost
- Loss of company credibility
- Penalties and fines due to oil spill
- Lawsuits and settlements

In this dissertation, the research focuses on the blowout event given the most severe consequences associated with such incidents. Blowouts have occurred since the later 19th and early 20th centuries, and was called gusher – an icon of oil exploration. With more and more workmen being killed or losing hearing permanently because of the gusher, and the extremely severe damage to the wildlife, people started to be aware that gushers were hazardous events, triggering the invention and application of BOPs. However, even with the advent of BOPs, a number of notable incidents have occurred since then all over the world. In this dissertation, several incidents are described to demonstrate the severity of the blowout incidents and the necessity to focus on the blowout risk.

Gulf War Oil Spill

The Gulf War oil spill in 1991 is known as one of the largest oil spills in history. When the Iraqi military retreated from Kuwait, over six hundred oil wells were set on fire in January 1991 to achieve the strategic goal—prevent potential landings of US Marines. The oil fire turned day into night due to the smoke. The fire lasted for about ten months. Until November 6, 1991, all blown-out oil wells due to the Gulf War were officially shut down (Grace, 2003). There were 11 fatalities associated with the Kuwait fires by that time. The oil spill left over 200 oil lakes throughout the desert, and some of them were more than six feet deep. The cleanup work is continuing until today.

Different parties conducted research to estimate the volume of oil spilled during the Gulf War. Initially, media estimated the spilled amount could reach about 11 million US barrels (Landrey, 1991). After all the wells were shut in, the US Committee on Merchant Marine and Fisheries reported to the US Congress that the volume of the oil spill ranged between four and six million barrels (US Committee on Merchant Marine and Fisheries, 1992). The methods adopted in the above two estimations are not clear. In 1993, Khordagui and Al-Ajmi (1993) reported that the maximum amount of spilled oil should be around two to four million barrels based on the historical and incident data.

Kaixin Blowout Incident

The incident happened on December 23, 2003 in Chongqing, China when the Luojia 16H well was being drilled by Chuandong Drilling Company. The production in that reservoir contained 82% methane, 9% hydrogen sulfide and 7% carbon dioxide (Xu,

2005). The blowout affected several villages that were only 300 to 500 m away from the well, and resulted in 243 fatalities, 1,242 hospitalizations, and over 65,000 evacuations (Li, 2009). The immediate causes for this tragedy include insufficient circulation time of drilling fluid during the pulling up operation, poor operating procedure compliance, missing back-pressure valve, malfunction of BOP, lack of hydrogen sulfide detectors, and poor emergency response planing. For example, igniting the production at the wellhead immediately when the sour gas well is out of control is considered as a typical industrial practice. However, in this incident, it took more than 13 hours to grant the permission for igniting. This incident also indicates the importance of conducting a consequence analysis and risk assessment to determine the minimum safety distance to the surrounding communities.

Deepwater Horizon Oil Spill

Deepwater Horizon Oil Spill is considered as the most severe marine oil spill incident in the history. The incident led to 11 fatalities, 17 injuries and serious environmental damage (CSB, 2014). The loss of well control event quickly turned into a surface blowout of hydrocarbon gas and liquid. The hydrocarbon gas was ignited on the platform, resulting in a fire and explosion. The Deepwater Horizon drilling rig was severely damaged and finally sank. During the incident, the BOP failed to prevent a kick event from escalating to the blowout event. The attempt to completely seal the well by the blind shear ram was not successful due to the off-center drill pipe. In addition, the platform personnel also made several questionable decisions, such as the failure in

interpreting negative pressure test, and diverting the overflow to the mud-gas separators instead of directly overboard. There have been a number of reports discussing the technical causes and root causes of the incident. However, until today, an accurate estimate of the total discharge amount of the hydrocarbons has not been reported yet given the various uncertainties during this incident. Before drilling the Macondo well, BP estimated that the worst-case scenario of the oil discharge during a blowout event would reach 162,000 bbls (BP, 2009). After the incident, the US Coast Guard and BP initially estimated the blowout rate at about 1,000 bbl/day (Goldenberg, 2010). This number kept increasing and the Federal District Court judge finally ruled that the total amount spilled was 3.19 million barrels. The basis of such ruling is that there was about 4 million barrels of oil discharged into the ocean and 810,000 barrels recovered (BP, 2015). This tragedy reflects the strong need of not only understanding the mechanisms of blowout to accurately estimate the blowout consequence, but also the approaches to managing and controlling the risks, uncertainties, and hazards associated with deepwater drilling activities.

1.1.2 Historical Statistics

Blowout events could happen at either onshore or offshore operations. The major concerns for onshore well blowouts include the toxic gas dispersion, fire, and explosion that could potentially affect the onsite personnel and offsite communities. All the concerns of onshore well blowouts stay valid for offshore blowout events. One additional hazard scenario is the environmental impact due to offshore oil spill. The

most widely known blowout database is SINTEF Offshore Blowout Database. This database was initiated in 1984 with 18 participants from both operators and service providers. It provides category and location, well description, operations, blowout causes, blowout characteristics, and other useful information of total 607 offshore blowout and well release events from 1950 to present. The SINTEF Offshore Blowout Database is believed to cover most blowout incidents in the North Sea and the US Gulf of Mexico (GOM). It should be noted that the Bureau of Safety and Environmental Enforcement (BSEE) also collects the GOM Outer Continental Shelf (OCS) loss of well control incidents, which have been an important information source for the SINTEF database. Besides SINTEF database, there are also other three databases documenting the onshore and offshore blowouts, including:

- World Offshore Incident Databank (WOAD)
- Energy Resources Conservation Board (ERCB) database
- Neal Adams Firefighters (NAF) database

WOAD is currently under operation and maintenance of DNV GL. It has collected over 6,000 incidents data for various offshore facilities since 1970. It also contains the location and operation mode of around 3,700 offshore units. ERCB database is an open access database established by the Alberta Energy Regulator. Over 61,000 onshore well and pipeline release events in Canada have been recorded since 1975. The NAF blowout database is not a public database. Many of the onshore blowouts in the NAF database come from the ERCB database with additional blowout data from Texas and Louisiana (Holland, 1997).

The value of the historical database is to provide information to enable us to understand the nature of the blowout events. Such statistical data often is associated with different operational phases. Consequently, the taxonomy of the main operations phases is presented as following:

- *Exploration drilling* is an activity to explore potential hydrocarbon productions in the reservoir or determine the size of the reservoir with relatively limited knowledge to the geological information.
- *Development drilling* is an activity to drill a production or injection well for the further development with relatively abundant knowledge about the geological information.
- *Completion* is an activity conducted after the drilling is completed to prepare the well for the purpose of production or injection. Various types of equipment are run into the well that might disable the safety barriers for a certain period.
- *Workover* is a well maintenance operation to solve the technical or production well issues. Similar to completion, equipment is run into the well that might disable the safety barriers for a certain period.
- *Production* is an activity to extract hydrocarbon production from the reservoir to the surface.
- *Wireline* is an activity to run the equipment into the well by a wireline through the tubing for the maintenance purposes. This operation will

disable the surface controlled subsurface safety valve (SCSSV), which is an important barrier to prevent blowout from happening.

Table 1 (SINTEF 2013) shows the number of blowouts during different operational phases from January 1980 to December 2013 in the GOM, the North Sea (Norwegian and UK waters), and other parts of the world based on the SINTEF Offshore Blowout Database. It reveals that almost two thirds of blowouts occurred during drilling operations. Additional 17% of the incidents occurred during workover, which ranks the most complicated and difficult types of well operations. The blowout incidents during the production accounted for another 12%. Therefore, blowout events during drilling require critical attentions.

Table 1. Offshore blowout/well release statistics between 1980 and 2011 (SINTEF, 2013)

Operations	US GOM	UK & Norway	Rest of World	Total
Drilling	108	43	96	247
Completion	13	7	6	26
Workover	41	9	18	68
Production	21	3	24	48
Wireline	5	4	0	9
Unknown	2	0	0	2
Total	190	66	144	400

It is also important to understand the nature of the discharge material during the well blowout events. As can be seen in Figure 1, gas is the most common blowout fluid.

A pure liquid blowout is rare because the oil usually contains a significant amount of gas in most of the reservoirs. Skalle *et al.* (1999) also conducted a statistical analysis on a database that contains about 1,120 blowout events at the GOM from 1960 to 1996. The trend of such analysis shows an agreement with the SINTEF database (Figure 2). Gas becomes the most common discharge materials during the blowout events. It can be concluded from the statistical analysis that the discharge materials of gas or liquid/gas should be focused when modeling the blowout events.

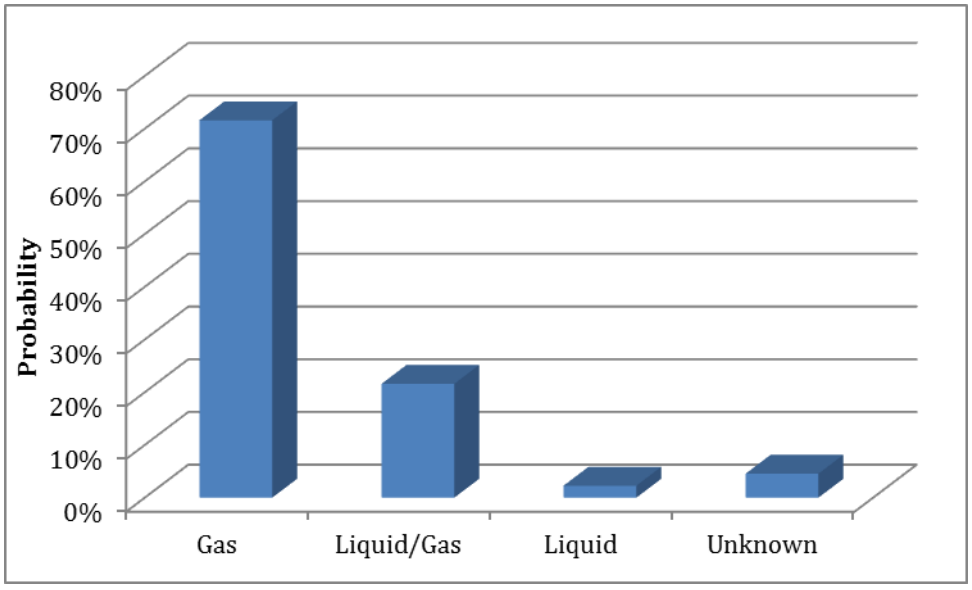

Figure 1. Blowout flow medium for US GOM and North Sea between 1980 and 2011 (SINTEF, 2013)

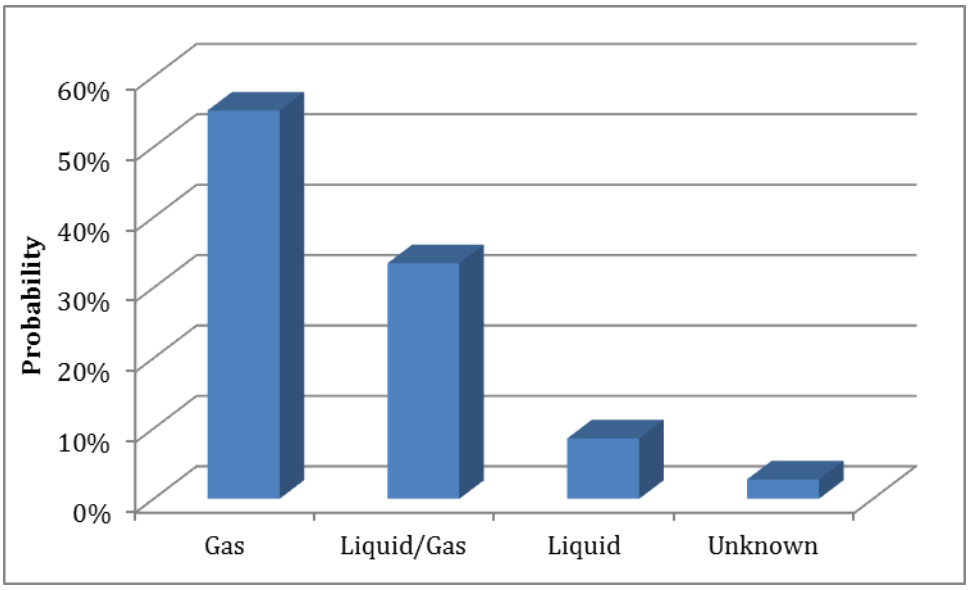

Figure 2. Blowout flow medium for US GOM from 1960 to 1996 (Skalle, 1999)

Blowout duration is also an important characteristic when analyzing blowout events. It can be obtained from the statistical analysis. The blowout durations depend on a number of factors, such as the location of wells (onshore or offshore), the depth of wells, the existence of fires and explosions, the availability of crews and equipment, blowout severity, intervention plans, and blowout control techniques. Skalle *et al.* (1999) indicated that blowout duration could range from 0 to 450 days. Figure 3 shows the duration distribution for investigated blowouts. Forty-six percent of the blowouts were brought under control in less than one day. More than 22% of the blowouts could not be controlled within 3 days. They also showed that the average duration of blowouts for the well depth greater than 10,000 ft is 519.6 hours. Figure 4 shows the duration of blowouts based on SINTEF database (SINTEF, 2013). It is concluded that 25% of the blowouts

can be controlled in 12 hours, 69% of the blowouts lasted for at most five days, and 31% continued flowing for more than five days.

The historical data suggests that the duration of blowouts ranges from hours to months and depends on many internal and external factors. The production loss, which determines the amount of oil spill, increases as the blowout continues. Therefore, long duration blowout incidents constituted the main focus of investigation in this dissertation.

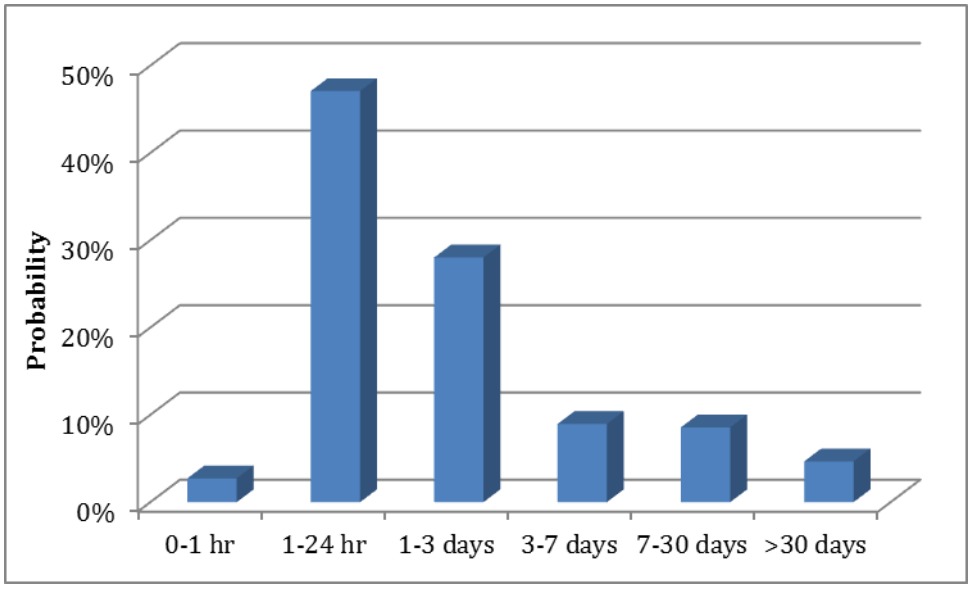

Figure 3. Blowout duration for US GOM blowouts from 1960 to 1996 (Skalle, 1999)

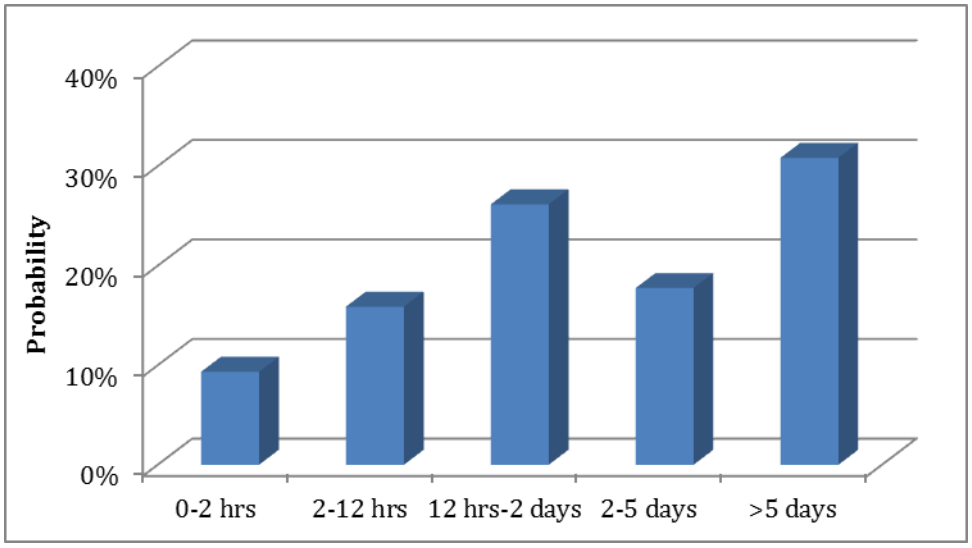

Figure 4. Blowout duration for US GOM and North Sea between 1980 and 2011 (SINTEF, 2013)

1.1.3 Safety Barriers

Safety barriers in the well are used to prevent hydrocarbon flows from the reservoir to flowing to the surface. NORSOK D010 (NORSOK, 2004) establishes the standards to the well barriers including:

- Two independent well barriers shall be available during all well activities and operations to prevent uncontrolled outflow from the well to the external environment.
- The two barriers shall be designed and selected to withstand the maximum anticipated differential pressure and environment exposure over time, and verified by leak test and function test.
- No single failure of the well barriers shall lead to the uncontrolled outflow from the well to the external environment.

- The physical location and integrity status shall be known and monitored all the time.

The two independent barriers include the primary and secondary barriers. The primary barrier usually refers to the hydrostatic pressure provided by the drilling mud, and the secondary barrier could include a variety of equipment, such as the BOP, wellhead, casing, tubing, and drilling string safety valve. Such barriers can also be grouped according to the functionality, how they are operated and how barrier failures are observed (Holland, 1997). Table 2 (Holland, 1997) shows some typical well barriers and the corresponding types. Figure 5 is an example demonstrating how the primary and secondary barriers are arranged during the drilling operation.

Table 2. Some typical well barriers (Holland, 1997)

Barrier Type	Description	Example
Operational barrier	A barrier that functions while the operation is carried out. A barrier failure will be observed when it occurs.	Drilling mud
Active barrier	An external action is required to activate the barrier. Barrier failures are normally observed during regular testing.	BOP, Christmas tree, SCSSV
Passive barrier	A barrier in place that functions continuously without any external action.	Casing, tubing, well packer
Conditional barrier	A barrier that is either not always in place or not always capable of functioning as a barrier	Stabbing valve

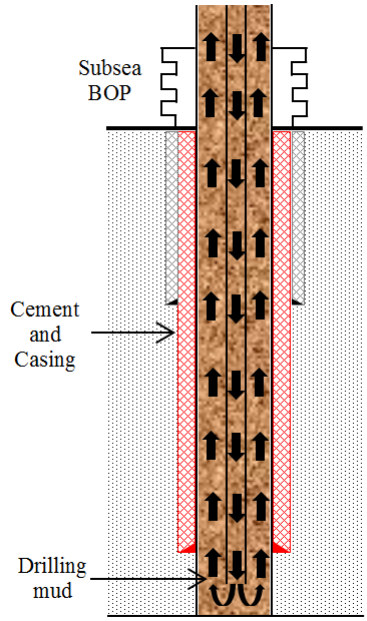

Figure 5. Example of barriers arrangement during drilling operation

Similar to NORSOK D-010, American Petroleum Institute (API) Recommended Practice (RP) 96 (API, 2013) requires a system of multiple physical barriers to be installed to prevent flow from formations from taking undesired paths (either to the surface or within the well). In addition, operational barriers are also considered in this RP, including human recognition and response, and institutional controls (e.g., casing design standards and policy manuals), to provide assurance that any failure of a physical barrier is detected early and managed without loss of well control. Moreover, it emphasizes that review of the barrier plan as part of a management of change (MOC) process shall be conducted if well conditions change. If a physical barrier is found to be

deficient during the operations and cannot be repaired, replacing such barrier or providing additional barriers, as a part of MOC should be considered.

A UK Health and Safety Executive (HSE) standard (HSE SPC/TECH/GEN/42) requires that the well completion operations should incorporate at least two barriers to flow between the reservoir and surface. UK requirements are less specific to the well barriers than the Norway and US regulations and standards (Holland, 1997).

1.2 Current Research and Practices to Address Blowout Events

1.2.1 Current Research

To properly assess and manage the blowout risk, past research mainly focused on the consequence modeling of blowout events at different conditions. Unfortunately, only a few papers have addressed the physical phenomenon of the blowout events. Clark and Perkins (1981) are perhaps the first researchers who presented a pioneering work to calculate the critical flow velocity, pressure, and temperature at the exit of an oil well blow-out. Hasan *et al.* (2000) also investigated the wellbore dynamics for an oil well blowout. In 1996, a method for blowout rate prediction for sour gas wells was presented by Kikani *et al.* (1996). Oudeman and his colleagues (Oudeman, 1998, Oudeman 2006, and Oudeman, 2010) accomplished a series of work focusing on simulating blowouts based on observations, such as wellhead pressure and temperature, plume shape and size, noise field around the wellhead, the pressure response of nearby wells, and production data of the wells with high flow rates, to develop proper well control strategies. Blowout events are dependent on not only the wellbore configurations, but also the reservoir

conditions. In addition, the interaction between the wellbore and the reservoir must be taken into consideration. However, none of the prior works mentioned earlier covered all these important components. Liu and others (2015) coupled the wellbore dynamics with a reservoir model to estimate blowout rate and the total discharge amount in an onshore gas well blowout for the first time. Such method, with extensive modification, can be adopted for the determination of offshore well blowout consequences.

1.2.2 Consequence-based Assessment

Due to the aftermath of the explosion and sinking of the Deepwater Horizon, and the personnel injuries and fatalities, the Bureau of Ocean Energy Management, Regulation, and Enforcement (BOEMRE) (formerly known as Minerals Management Service (MMS)) started requiring additional information for the operators' planned activities (BOEMRE, 2014). Therefore, the consequence-based assessment for blowout events is required in the US GOM region at present, which is known as worst-case discharge (WCD) calculation. According to 30 CFR 250.213(g), the definition to the blowout scenario for an Exploration Plan (EP) is:

"*A scenario for the potential blowout of the proposed well in your EP that you expect will have the highest volume of liquid hydrocarbons. Include the estimated flow rate, total volume, and maximum duration of the potential blowout. Also, discuss the potential for the well to bridge over, the likelihood for surface intervention to stop the blowout, the availability of a rig to drill a relief well, and rig package constraints. Estimate the time it would take to drill a relief well.*"

30 CFR 250.243(h) has the same requirement for a Development and Production Plan (DPP) and a Development and Coordination Document (DOCD). Such plans must be submitted to BOEM with a blowout scenario and worst-case discharge scenario.

The worst-case discharge scenario determination is governed by two important factors – daily blowout rate and blowout duration. The requirements of the evaluation of the daily blowout rate are slightly different for exploratory or development drilling operations and production activities. For exploratory or development drilling operations, the daily discharge rate is the greatest potential daily discharge from an uncontrolled blowout through an open borehole (BOEMRE, 2010), considering any known reservoir characteristics and any analog reservoir characteristics from the area if they are unknown. For production activities, the determination of the daily discharge rate must take reservoir characteristics, casing/production tubing sizes, and historical production and reservoir pressure data into account according to 30 CFR 254.47(a)(3).

The uncontrolled flow rate is obtained by using nodal-analysis, which is a standard petroleum engineering analysis tool (SPE, 2015). In such analysis, the inflow and tubing performance curves are plotted and the intersection of the two curves is considered as the discharge rate. The inflow performance curve is the mathematical model describing the pressure drop when the fluid flows from the reservoir to the wellbore through the porous medium. The model predicts the well bottomhole pressure at various flow rates considering a number of reservoir parameters and a given reservoir pressure. The tubing performance curve calculates the pressure drop when the fluid flows through the wellbore at constant wellhead pressure by taking the wellbore

characteristics into account. The purpose of nodal-analysis is to find the intersection of these two curves which determines the flow rate and pressure solution. Figure 6 shows an example of how the worst-case discharge rate is obtained from inflow and tubing performance curves.

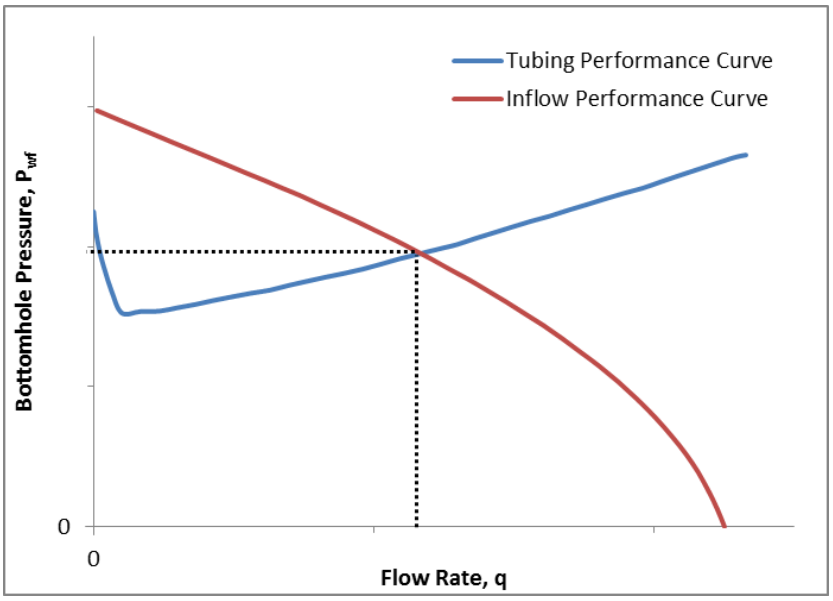

Figure 6. Example of inflow and tubing performance curves crossplot

Operators must use the maximum duration of the potential blowout to evaluate the WCD. The maximum duration is the summation of the time it would take to contract for a rig, move it onsite, and drill a relief well, including the possibility of drilling a relief well from a neighboring platform or an onshore location (BOEMRE, 2014). Combining the daily discharge rate and the maximum duration of a potential blowout

scenario yields the WCD value. Figure 7 shows a typical work flow diagram for the determination of WCD scenario.

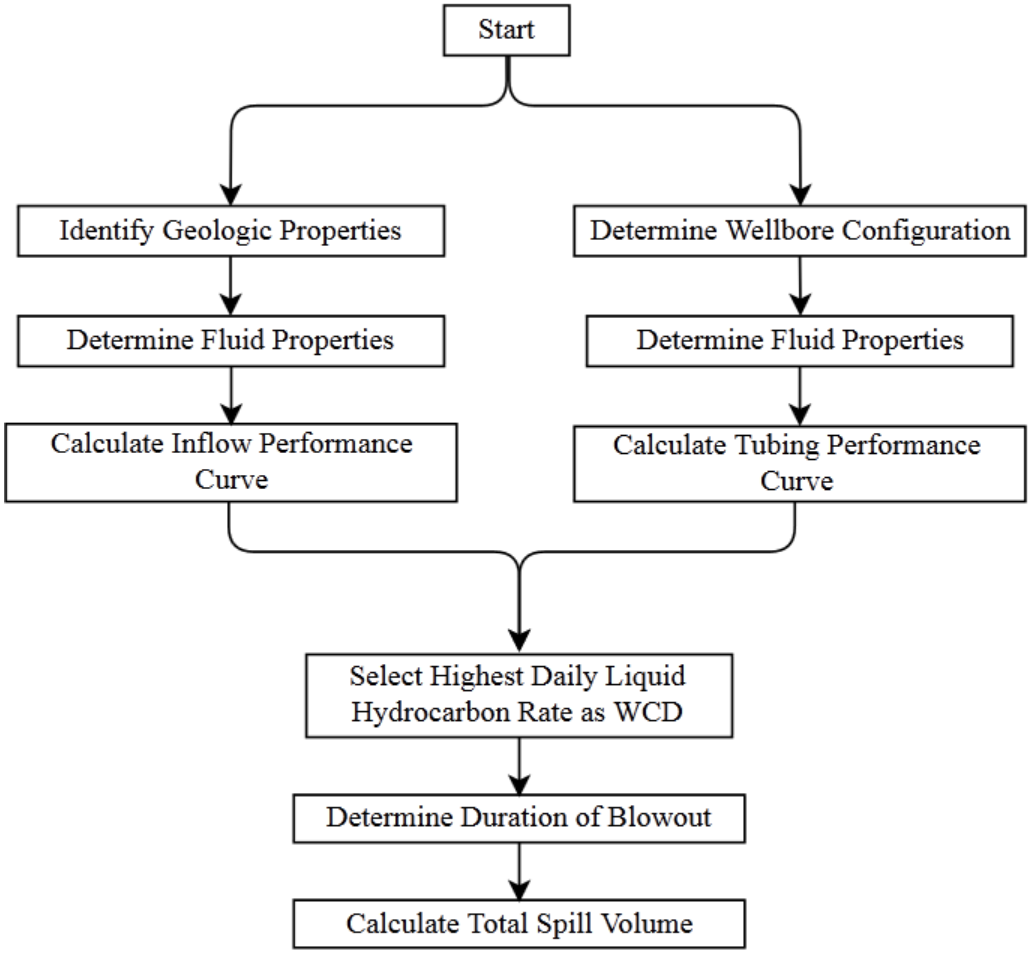

Figure 7. Typical workflow for WCD assessment

1.2.3 Risk-based Assessment

In the North Sea, the regulations require operators to determine the blowout risks duration during drilling, workover, intervention, and production operations. The major inputs for risk analysis are the frequency of blowout and release scenarios including release rate, duration, dispersion, and other factors (NORSOK, 2001). The blowout risk analysis covers the following components (NORSOK, 2001):

- Probability of blowout and its consequence
- Probability of occupational incidents and their consequence
- Probability of different amount of oil spilled, as input to the environmental risk analysis

Several reports investigating the environmental risk assessment of drilling activities are available in public domain (DNV, 2010 and ACONA, 2011). Such reports have served as the industrial benchmark for the risk-based assessment to the blowout events in the North Sea region. The first step of blowout risk assessment is to construct the statistical modeling of the blowout scenarios. The blowout scenarios are defined based on the flow path, blowout duration, penetration depth, and BOP status.

The three flow paths include fluid flowing through open hole, drill pipe and annulus with different probabilities illustrated by Figure 8. A blowout could be killed by a number of reasons, including:

- Bridging (self-killing due to collapse of formation near wellbore)
- Crew intervention
- Mechanical barriers (*e.g.*, capping)

- Drilling of relief wells
- Other causes

Literature reveals that about 84% of the past blowout events are stopped by bridging (Scandpower, 2011). It serves as the major reason for the well being killed. The bridging may result from the accumulation of sand or rock inside the wellbore, collapse owing to the high flow rate and significant pressure difference between the reservoir and bottomhole, and the hydrate formation. Crew intervention includes the activities performed by onboard personnel to the existing equipment on the offshore installation, such as repair, and replacement components and equipment. Mechanical barrier such as capping has drawn significant attentions after the Macondo Blowout. The adoption of mechanical barrier to stop the blowout requires the successful activation of disconnect function at the subsea BOP system. The capping device then could be lowered onto the blowing well and closed upon the successful landing and connection to stop the blowout. Typically, the delivery of the capping device to the offshore installation could take 10 days, and 5 to 15 days could be required to connect the device with the well depending on the weather, sea water depth and the well configuration (ACONA, 2012). When a blowout incident is confirmed, the plan of drilling relief well(s) needs to be discussed immediately. If all the above mentioned methods fail to stop the incident, relief well(s) will become necessary to regain the well control. The basic principle to drill a relief well is similar to drill an exploration well, except that the electromagnetic tools are required to ensure the precise interception with the blowing well. The blowing well could also be killed for other reasons, such as the reservoir pressure depletion, water injection, and

water breakthrough. All the approaches to kill the blowing well have possibilities to fail to regain the well control. Based on the SINTEF database, Figure 9 presents the probability that a blowing well is still flowing after the single intervention approach being applied, such as natural bridging, crew intervention, capping, and drilling relief well (ACONA, 2012 and Scandpower, 2011). The probabilities of blowout flow paths and blowout duration could be found from SINTEF Offshore Blowout Database, which is discussed in later section.

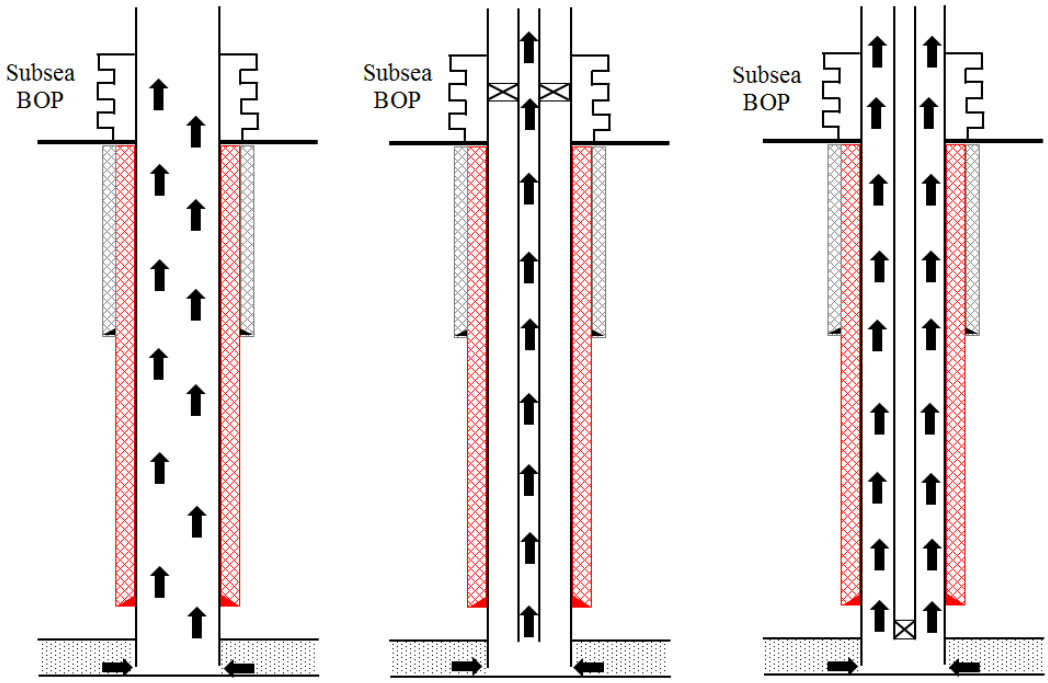

Figure 8. Possible flow paths for blowout scenarios (from left to right: open hole, drill pipe and annulus)

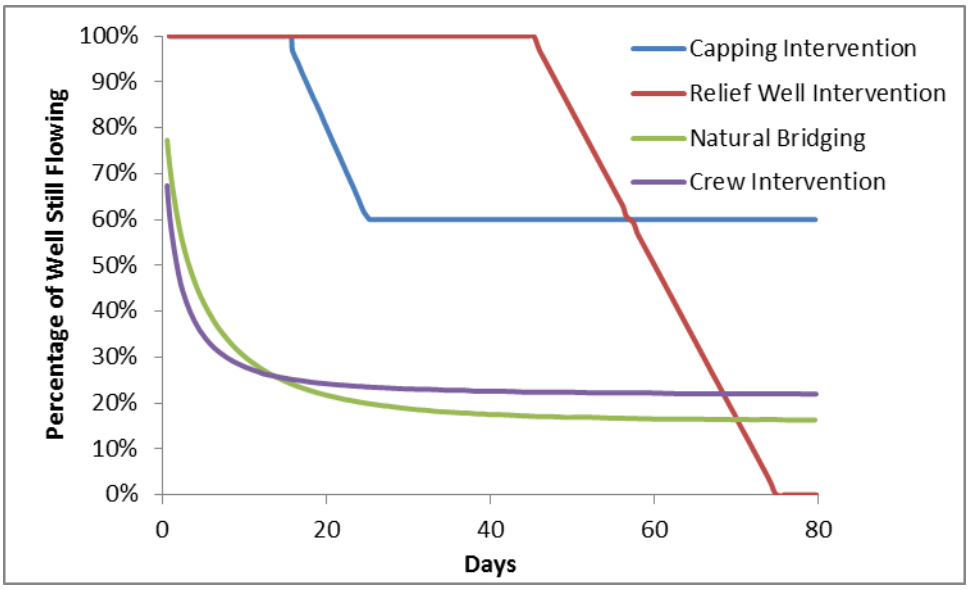

Figure 9. Reliability plots for each of possible remedial actions

When the drill bit reaches the reservoir, the hydrocarbons have the potential to form a blowout incident. The penetration depth to the reservoir is an important factor to determine the blowout rate. The typical industrial practice is to assume two penetration depths when assessing the blowout risk – partial penetration and fully penetration (DNV, 2011 and ACONA 2012). The probability of partial penetration is assumed to be 0.6 and 0.4 for fully penetration scenario when drilling exploration and development wells. BOP, as a secondary well barrier, has to fail or partially fail when the blowout occurs. OLF guidelines for estimation of blowout potential (OLF, 2004) suggest that BOP partial failure scenario would stand up 70% of the total blowout scenario, while the other 30% presents the total BOP failure scenarios. When all these uncertainties are combined together, a statistical model of blowout scenario could be established.

Another important component of the blowout risk assessment is the consequence analysis for blowout events. The blowout rate determination is similar to the WCD calculation. The inflow and tubing performance curves are plotted together and the intersection of two curves indicates the blowout rate. It should be noted that the value of blowout rate is different for each blowout scenario, taking the well configuration, blowout duration, BOP status, penetration depth, and flow paths into account. Given the blowout duration is a part of the blowout risk assessment, the change in flow rate must be properly addressed. Hence, OLF guideline (OLF, 2004) suggests two approaches. The first is to assume that the blowout rate is constant over a certain period of time. The inflow performance curve is then re-plotted based on the pressure depletion given the production loss. The new intersection between the inflow and tubing performance curve defines a new blowout rate. Such procedure is performed repeatedly until the end of the blowout event. As can be seen from Figure 10, very limited number of the blowout rates is identified with the uncertainties discussed above due to the lack of integrated tools to model both reservoir and wellbore. An alternative approach can be based on a simplified model, assuming the constant blowout rate over the entire duration of the blowout event with the uncertainties distribution (Figure 11). Although the second approach yields overestimation to the blowout risk, it is generally accepted by the industry at present due to the technology limitation to determine the dynamic blowout rates.

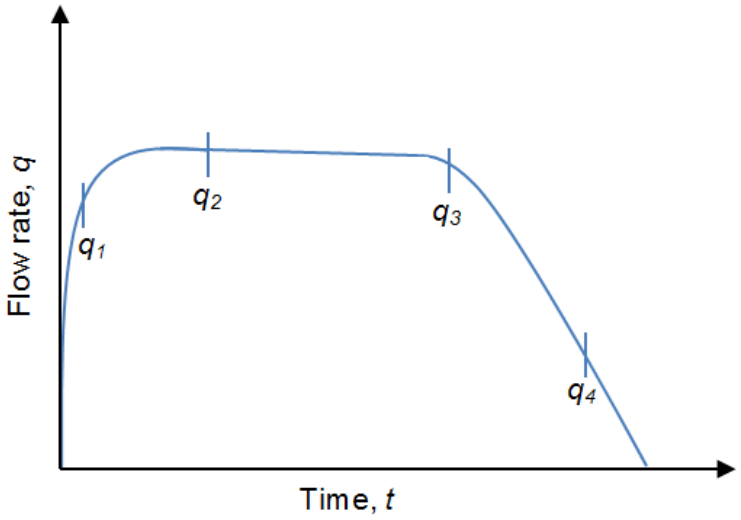

Figure 10. Example of flow rate change during blowout event

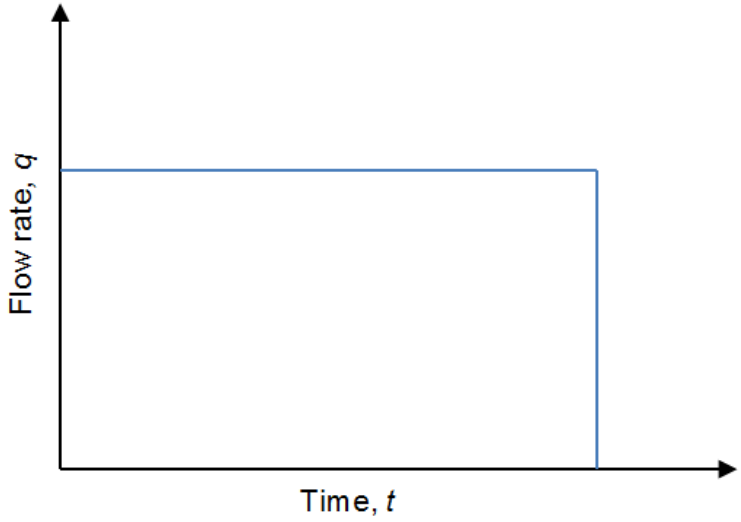

Figure 11. Example of constant flow rate during blowout event

When the blowout rate and probability are combined for each of the blowout scenarios, the total blowout risk picture could be depicted as shown in Figure 12.

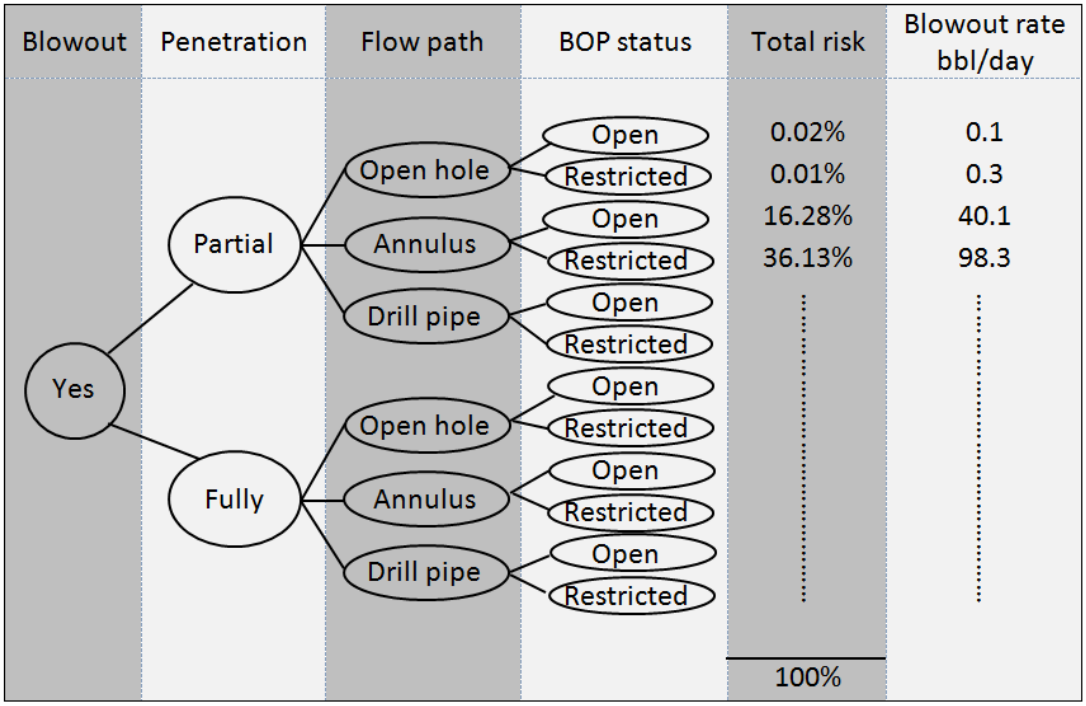

Figure 12. Example on blowout risk assessment results

1.3 Statement of Problems and Significance

1.3.1 Research Motivation

As can be seen from the historical data, blowout events have caused many deadly incidents with a number of fatalities, asset loss, and severe environment impact for more than one century. However, the total amount of discharge is still an argument for most of

the incidents due to the technology limitation. At present, both the consequence-based assessment approach and the risk-based assessment approach have drawbacks.

Requirements of reporting single value of WCD do not provide any additional values to manage the risk of the uncontrolled wellbore flow event and the impact to the marine environment. More importantly, it would be completely inadequate to represent the risk and mislead the risk picture to the general public.

The risk-based approach depicts the blowout risk by using the constant blowout rate for most of the studies. However, Liu (2015) showed that the reservoir pressure depletion was a dominating factor for the exponential decrease in blowout rate, and illustrated the overestimation of blowout event consequence/risk if a constant value of blowout rate is assumed during the event. In addition, only uncertainties, such as flow path, which are available in the historical database, are considered in current studies. During the well planning phase, the reservoir characteristics may not be fully known. It is important to be aware that the reservoir parameters could be different even for wells in the same field. As a result, introducing the well-specific uncertainties associated with the reservoir will enable us to estimate the blowout risk more precisely.

Moreover, most of the studies now are focusing on the offshore oil/gas well blowout events. However, the onshore gas well blowout could also impose great threat to the onsite personnel and offsite communities, as illustrated by the Kaixin incident. Therefore, a comprehensive methodology to fully assess the risks associated with various kinds of blowout events is needed, and such approach could serve as a benchmark for the industrial application.

1.3.2 Research Objectives

In view of the above discussion, the primary objective of the proposed research is the advancement of understanding the onshore/offshore gas or oil/gas blowout mechanism. To capture all the physical phenomena during a blowout event, blowouts need to be simulated from the beginning of the event to the time they are brought under control. An analytical model of blowouts needs to be established taking into account the mass balance in the reservoir, and energy balance, momentum balance, and mass balance in the wellbore. The interaction between the reservoir and the wellbore will be also described in this model. It is expected that the model could estimate the blowout rates as a function of time and corresponding volume of spill based on the parameters of the reservoir, the wellbore configuration, and other operational conditions. The uncertainties during the blowout events are investigated, including the characteristics of the event and the well-specific parameters.

The ultimate objective of the research is to quantitatively assess the blowout risk for the wells not only in the planning phase but also in the operational phase. A well-established blowout consequence model couples the nature of transient-fluid flow in the reservoir and the fluid and heat flows in the wellbore. Combining the consequence model and the uncertainties from both historical database and well-specific parameters provide great opportunities to understand and manage the blowout risk. In addition, this dissertation demonstrates how this method could be practically applied in typical industrial settings. The risk reduction plan is also discussed in the later sections using statistical and sensitivity analysis.

1.3.3 Research Methodology

To understand the risk associated with uncontrolled flow events, this research is divided into three parts – consequence modeling, uncertainties determination and assessing the risk associated with the blowout events. Figure 13 outlines the overall research plan.

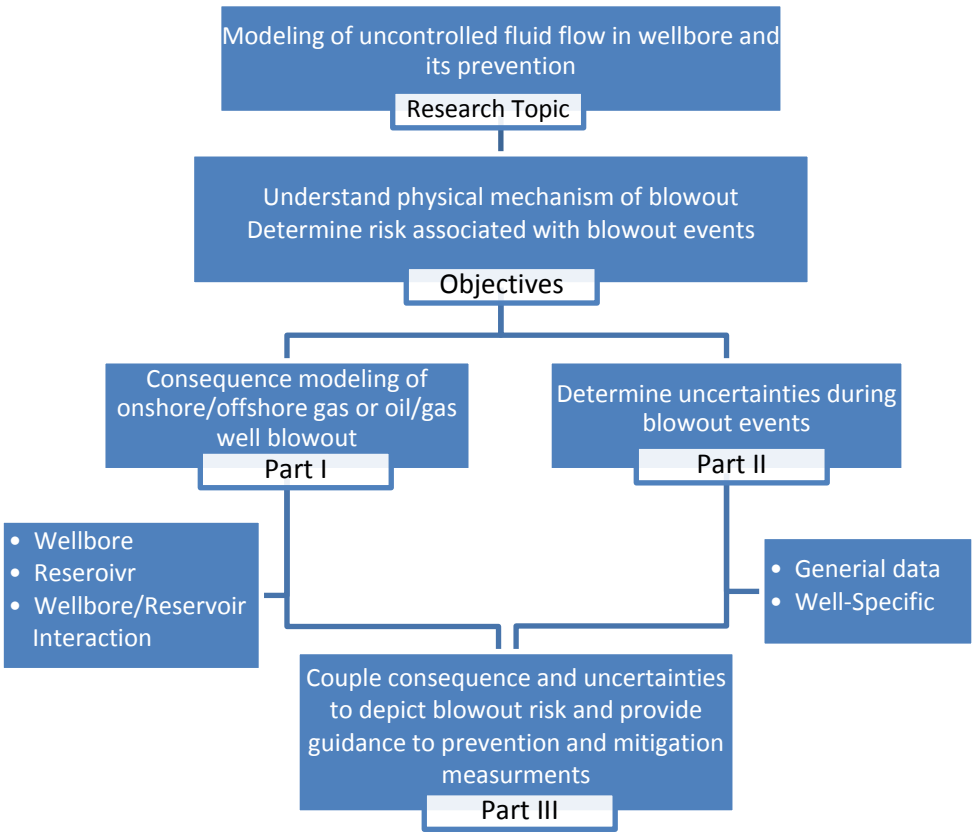

Figure 13. Proposed research outline

The consequence modeling is first established to couple the reservoir and wellbore. The reservoir pressure depletion, and fluid dynamics and heat transfer in the wellbore are taken into account. The results of the model are validated by the field data and existing models.

The uncertainties associated with the blowout events are scrutinized. Combining the generic statistical data from database, probability distribution according to the guidelines, and well-specific uncertainties based on the geological test information yields a full spectrum of the potential blowout scenarios.

Lastly, the consequence and uncertainties are coupled together for each of the scenarios to depict the blowout risk picture. Sensitivity and statistical analysis demonstrates the importance of the well barriers and provides guidance for the blowout prevention measurements and risk reduction plans.

CHAPTER II

CONSEQUENCE MODELING OF GAS WELL BLOWOUT[1]

To estimate the total discharge amount of hydrocarbons during a blowout event, the blowout rate, which depends on the well configuration and the reservoir conditions, must be dynamically obtained throughout the entire event. The interaction between the reservoir and the wellbore also needs to be taken into account. The reservoir pressure determines if the blowout rate can be sustained, while the discharged hydrocarbon flow depletes the pressure of the reservoir. As a result, in this chapter, the reservoir model, the wellbore model and the interactions between the reservoir and wellbore are studied separately. Then they are coupled together to understand the blowout mechanism. In the reservoir model, we assume that the reservoir is isothermal during the blowout event. The heat transfer model is therefore not considered in the reservoir. For onshore gas well blowout, one of the major challenges is the sonic velocity at the wellhead. With the high reservoir pressure and ambient pressure at wellhead, hydrocarbon gas tends to be choked at the wellhead. The determination of sonic velocity requires the estimation of the pressure and temperature profile of the fluid along the wellbore.

[1] Part of this chapter is reprinted with permission from "Flow rate and total discharge estimation in gas-well blowouts" by Liu, R., Hasan, A. R. and Mannan, M. S. (2015). *Journal of Natural Gas Science and Engineering*, 26, 438-445. Copyright 2015 Elsevier.

2.1 Reservoir Model

In this section, the behavior of the reservoir is studied. Given the duration of the blowout events, the extremely high flow rate at the wellhead depletes the reservoir. The depletion of a reservoir results in the decrease of reservoir pressure, and therefore leads to a decreased wellhead velocity. Thus, a material balance in the reservoir needs to be considered to calculate one of the most important variables that governs the blowout mechanism—average reservoir pressure.

G_i and G represent the initial and current gas-in-place within a drainage area of a reservoir. The cumulative production, G_p (production loss for the case of blowout), from a gas reservoir is calculated as:

$$G_p = G_i - G = G_i - G_i \frac{B_{gi}}{B_g} \tag{1}$$

where B_{gi} and B_g are initial and current gas formation volume factors, respectively. The gas formation volume factor relates the volume of 1 lb-mole of natural gas at reservoir conditions to its volume at standard conditions.

$$B_g = \frac{V}{V_{sc}} = \frac{ZnRT / p}{Z_{sc} nRT_{sc} / p_{sc}} \tag{2}$$

By substituting $Z_{sc} = 1$, $T_{sc} = 520^{\circ}$R, and $p_{sc} = 14.7$ psi, the above equation becomes:

$$B_g = 0.0283 \frac{ZT}{p} \tag{3}$$

If the reservoir is assumed to be isothermal, substituting Equation (3) into Equation (1) yields:

$$G_p = G_i(1-\frac{\bar{p}/Z}{p_i/Z_i}) \tag{4}$$

Given some basic reservoir parameters, the original gas in place, G_i, can be obtained by:

$$G_i = \frac{Ah\phi s_g}{B_{gi}} \tag{5}$$

where A is drainage area, h is payzone thickness, ϕ is porosity of the formation, and s_g is gas saturation. The importance of Equation (4) is that once the cumulative production/loss is known at any time t, the average reservoir pressure $\bar{p}$, which strongly affects the blowout rate, can be calculated. However, the average reservoir pressure and compressibility factor cannot be obtained directly, thus an iterative modeling approach is needed to determine the correct average reservoir pressure. It is discussed in later sections.

2.2 Wellbore Model

2.2.1 Wellbore Dynamic Model for Single Phase Gas

A gas well is inherently dangerous for any operation in the oil and gas industry. If an onshore gas well is out of control, a significant amount of gas will come out from the formation and into the atmosphere. The gas will diffuse to the surroundings, forming a mixture of air and hydrocarbon gases. Depending on the concentration, a single spark

could ignite this mixture and cause a huge explosion, resulting in personnel fatalities and injuries, and asset loss. In addition, the toxic content in the mixture cloud may put the onsite personnel and offsite populations into jeopardy illustrated by the Kaixian blowout incident.

Single phase gas flow in the wellbore is one of the most fundamental problems in production engineering of the oil and gas industry. The importance of single phase flow in vertical or inclined wells has led to the development of a variety of models. The basis of these models is the mechanical momentum balance. Mechanical momentum balance represents the pressure drop along the flow path:

$$(\frac{dp}{dz})_T = (\frac{dp}{dz})_F + (\frac{dp}{dz})_H + (\frac{dp}{dz})_A \quad (6)$$

Equation (6) shows the total pressure gradient, $(\frac{dp}{dz})_T$, is the summation of the frictional gradient, $(\frac{dp}{dz})_F$, the hydrostatic gradient, $(\frac{dp}{dz})_H$, and the acceleration gradient, $(\frac{dp}{dz})_A$. These three components of the total pressure drop are discussed in the following paragraphs.

For the fluid flow model in a wellbore, it is assumed that the fluid flows through a symmetric well, and the pressure in the cross section plane normal to flow remains constant. With such assumptions, the fluid flow model reduces to one dimensional analysis, as shown in Figure 14.

Among the three components of the total pressure drop, the hydrostatic gradient is convenient to be estimated, as it only needs the input of gas density and well deviation angle.

$$(\frac{dp}{dz})_H = -g\rho_g \sin\theta \tag{7}$$

Because the density of gas obeys the Equation of State, the static term will vary along the well.

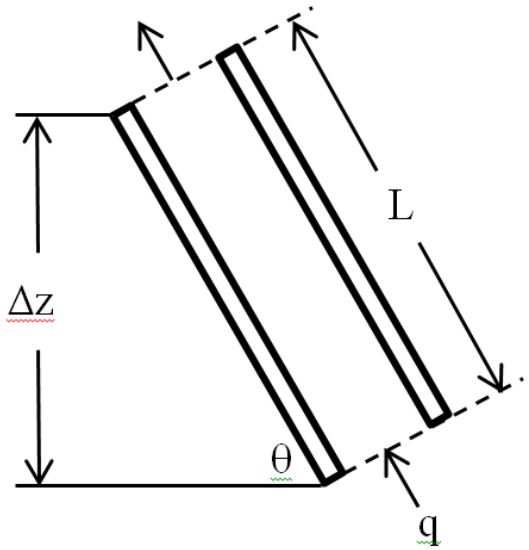

Figure 14. Flow geometry for pipe flow

The acceleration gradient is given by:

$$(\frac{dp}{dz})_A = -\rho_g v_{sg} \frac{dv_{sg}}{dz} \tag{8}$$

One simplified assumption is that the tubing has constant cross section area. However, in the multiple casing of offshore setting, such assumption needs to be adjusted accordingly. The gas velocity, v_{sg}, is a function of pressure and temperature. By chain rule, Equation (8) can be written as:

$$-(\frac{dp}{dz})_A = \rho_g v_{sg}[(\frac{\partial v_{sg}}{\partial p})_T \frac{dp}{dz} + (\frac{\partial v_{sg}}{\partial T})_p \frac{dT}{dz}] \tag{9}$$

From the Equation of State, we have:

$$v_{sg} = \frac{q_g}{A} = \frac{ZnR}{A}\frac{T}{p} \tag{10}$$

where q_g is volumetric flow rate and A is the area of cross section of tubing.

Differentiating of v_{sg} with respect to pressure and temperature yields:

$$\frac{\partial v_{sg}}{\partial p} = -\frac{ZnRT}{Ap^2} = -\frac{v_{sg}}{p} \tag{11}$$

$$\frac{\partial v_{sg}}{\partial T} = \frac{ZnR}{Ap} = \frac{v_{sg}}{T} \tag{12}$$

Thus, Equation (9) becomes:

$$-(\frac{dp}{dz})_A = -\frac{\rho_g v_{sg}^2}{p}(\frac{dp}{dz})_T + \frac{\rho_g v_{sg}^2}{T}(\frac{dT}{dz}) \tag{13}$$

The frictional pressure gradient is represented by:

$$(\frac{dp}{dz})_F = -\frac{f v_{sg}{}^2 \rho_g}{2d} \tag{14}$$

where f is the Moody friction factor, depending on the turbulence of the fluid and the pipe roughness, and d is tubing diameter. The friction factor is usually expressed as a function of the Reynolds number and roughness factor (ϵ / d). The roughness factor can be found in various references (Moody, 1944). Some charts are useful for all types of pipe roughness and Reynolds number. However, the implicit relationship between Moody friction factor and roughness factor is not easy to be implemented into the computational programs. Therefore, in this research, the following explicit expressions for the Moody friction factor calculation without the need of the iterative solution procedure is used (Chen, 1979):

$$f = \frac{4}{[4\log(\frac{\epsilon / d}{3.7065} - \frac{5.0452}{Re}\log\Lambda)]^2} \tag{15}$$

where the dimensionless parameter Λ is given by:

$$\Lambda = \frac{\epsilon / d}{2.8257} + (\frac{7.149}{Re})^{0.8981} \tag{16}$$

Combining Equations (7), (13) and (14), the total pressure gradient when gas flows through the wellbore can be expressed as:

$$\begin{aligned} -(\frac{dp}{dz})_T &= \rho_g g\sin\theta + \frac{f v_{sg}^2 \rho_g}{2d} + \rho_g v_{sg}\frac{dv_{sg}}{dz} \\ &= \rho_g g\sin\theta + \frac{f v_{sg}^2 \rho_g}{2d} - \frac{\rho_g v_{sg}^2}{p}(\frac{dp}{dz})_T + \frac{\rho_g v_{sg}^2}{T}(\frac{dT}{dz}) \end{aligned} \tag{17}$$

Therefore,

$$-(\frac{dp}{dz})_T = \frac{\rho_g g \sin\theta + \frac{f v_{sg}^2 \rho_g}{2d} + \frac{\rho_g v_{sg}^2}{T}(\frac{dT}{dz})}{1 - \frac{\rho_g v_{sg}^2}{p}} \tag{18}$$

The temperature gradient, $\frac{dT}{dz}$, can be calculated from the analytic expression for steady flow in a wellbore, which is discussed in a later section. Alternatively, the temperature gradient term can be estimated with respect to the pressure gradient. It is especially suitable for blowout scenarios. For a gas well blowout, the velocity of gas is subsonic near the wellhead. Thus, the heat exchange between the gas and its surroundings (formation) is greatly reduced. It is reasonable to assume that the gas is experiencing adiabatic expansion near the wellhead. First, Equation (9) is changed into the following form by utilizing Equations (11) and (12):

$$-(\frac{dp}{dz})_A = \rho_g v_{sg}[(\frac{\partial v_{sg}}{\partial p})_T \frac{dp}{dz} + (\frac{\partial v_{sg}}{\partial T})_p \frac{dT}{dp}\frac{dp}{dz}] = \rho_g v_{sg}^2 (\frac{1}{T}\frac{dT}{dp} - \frac{1}{p})\frac{dp}{dz} \tag{19}$$

Then, the total pressure gradient can be expressed as:

$$-(\frac{dp}{dz})_T = \frac{\rho_g g \sin\theta + \frac{f v_{sg}^2 \rho_g}{2d}}{1 - \rho_g v_{sg}^2 (\frac{1}{p} - \frac{1}{T}\frac{dT}{dp})} \tag{20}$$

To calculate the term $\frac{dT}{dp}$, we can assume that the gas near the wellhead is ideal given that the pressure near wellhead is approximately equal to the atmosphere due to

the high fluid velocity. Therefore, the following relationships are valid for an adiabatic process:

$$\frac{T}{T_0} = (\frac{p}{p_0})^{R/C_p} \tag{21}$$

$$\frac{dT}{dp} = \frac{RT_0}{C_p} \frac{p^{(\frac{R}{C_p}-1)}}{p_0^{R/C_p}} \tag{22}$$

where T_0 and p_0 are the temperature and pressure under standard conditions and C_p is heat capacity. Replacing $\frac{dT}{dp}$ by Equation (22), Equation (20) becomes a first order Ordinary Differential Equation, which can be solved analytically.

2.2.2 Heat Transfer

Significant heat exchange between the wellbore fluid and its surroundings is inevitably involved during the fluid flowing through the well. For an offshore well where sea water is present, the situation is more complicated due to the cold marine temperature. During a blowout event, formation fluid with high temperature comes from the reservoir. As it moves upward, it loses heat to the surroundings. The temperature difference between the wellbore fluid and the formation increases as the fluid flows up from the bottomhole to the wellhead. This heat transfer process affects the fluid properties, and therefore influences the fluid dynamics in the wellbore. For multi-phase flow, the flow regime is also impacted. Thus, the momentum balance equations need to

be solved with energy balance equations simultaneously. In the following paragraphs, the formation temperature distribution in the radial direction is first addressed. Then the heat exchange between the wellbore fluid and its surroundings is taken into account by performing the energy balance for the wellbore fluid. Lastly, these equations are solved to get analytic solutions for hydrocarbon gas.

When the hot wellbore fluid moves upward to the wellhead from the bottomhole, it provides a heat source to the formation. Therefore, it is reasonable to consider the wellbore as a heat sink. Several assumptions need to be made to model the heat flow and the resulting temperature distribution in the formation suggested by the literature (Hasan, 1994). The first assumption is that the formation is a homogeneous solid. In addition, assuming that the formation is symmetric around the well reduces the model from three dimensions to two dimensions. Moreover, due to the small temperature gradient in the vertical direction, the heat diffusion in the vertical direction is assumed to be negligible. Then an energy balance is derived in cylindrical coordinates as follows:

$$\frac{\partial^2 T_e}{\partial r^2} + \frac{1}{r}\frac{\partial T_e}{\partial r} = \frac{c_e \rho_e}{k_e}\frac{\partial T_e}{\partial t} \tag{23}$$

where T_e is formation temperature at time, t, and distance, r, measured from the center of the wellbore, c_e, ρ_e, and, k_e, represent heat capacity, density and thermal conductivity of the formation. One initial condition and two boundary conditions are needed to solve this partial differential equation. At initial time ($t = 0$), we assume that temperature is uniform throughout the formation horizontally, which leads to the following initial condition:

$$T_e(r, t=0) = T_{ei} \tag{24}$$

At a point very far away from the wellbore in the reservoir, the temperature gradient is zero. In addition, the heat exchange at the interface of the wellbore and formation must obey Fourier's law of heat conduction. Therefore, two boundary conditions could be written as:

$$Q = 2\pi k_e \frac{r\partial T_e}{\partial r}\Big|_{r=r_{wb}} \tag{25}$$

$$\frac{\partial T_e(r=\infty, t)}{\partial r} = 0 \tag{26}$$

where Q is the heat flow rate from the formation to the well and r_{wb} is the radius of the wellbore.

Equation (23) coupled with the initial condition (Equation (24)) and boundary conditions (Equations (25) and (26)) can be solved analytically by using Laplace transformations (Hasan, 1994 and Everdingen, 1949). The analytical solution of formation temperature is a function of radial distance and time:

$$T_{wb} = T_{ei} + \frac{Q}{\pi^2 k_e} I \tag{27}$$

where,

$$I = \int_0^\infty \frac{1 - e^{-u^2 t_D}}{u^2} \frac{Y_1(u)J_0(u) - J_1(u)Y_0(u)}{J_1^2(u) + Y_1^2(u)} du \tag{28}$$

In Equation (28), t_D is defined as dimensionless time ($t_D = \frac{k_e t}{\rho_e c_e r_{wb}^2}$). The dimensionless temperature, T_D, is defined as following:

$$T_D = -\frac{2\pi k_e}{Q}(T_{wb} - T_{ei}) \tag{29}$$

Evaluation of Equation (27) is computationally expensive because of the integration of modified Bessel functions of zero and first order. Hasan and Kabir (Hasan, 1994) found the following algebraic expressions for the dimensionless temperature could represent the solutions without losing accuracy.

$$T_D = \ln[e^{-0.2t_D} + (1.5 - 0.3719e^{-t_D})\sqrt{t_D}] \tag{30}$$

The temperature difference between the wellbore fluid and the surrounding formation is the driving force of energy exchange. Figure 15 shows the schematic of a typical well setting, based on which the energy balance of wellbore fluid is developed. In a control volume of length, dz, at a distance, z, from the wellhead, the energy balance is given by:

$$wH|_{z+dz} - (z+dz)wg\sin\theta + wv^2|_{z+dz} + Qdz = wH|_z - wg\sin\theta + wv^2|_z \tag{31}$$

where w is mass flow rate of fluid and H is fluid enthalpy. Changing Equation (31) into differential form yields:

$$\frac{dH}{dz} - g\sin\theta + v\frac{dv}{dz} = -\frac{Q}{w} \tag{32}$$

Enthalpy is a function of pressure and temperature, and is given by:

$$dH = (\frac{\partial H}{\partial T})_p dT + (\frac{\partial H}{\partial p})_T dp = c_p dT - C_J c_p dp \tag{33}$$

where C_J is the Joule-Thomson coefficient and c_p is the heat capacity of the fluid under constant pressure. By substituting Equation (33) into Equation (32), the wellbore fluid temperature as a function of depth can be expressed by:

$$\frac{dT_f}{dz} = C_J \frac{dp}{dz} + \frac{1}{c_p}[-\frac{Q}{w} - g\sin\alpha - v\frac{dv}{dz}] \tag{34}$$

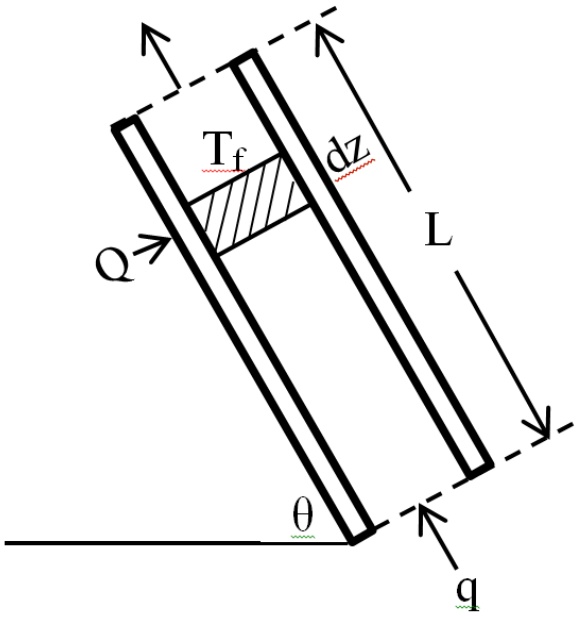

Figure 15. Energy balance for wellbore fluid

Combining Equations (29), (30), and (34), the expression of fluid temperature, T_f, can be obtained. However, the temperature at wellbore/formation interface, T_{wb}, cannot be easily measured. Therefore, an overall heat transfer coefficient for the wellbore is introduced to replace T_{wb}.

In typical wellbore configurations, there are tubing, tubing-casing annulus, casing and cement, as shown in Figure 16. They are considered as resistances that the radial heat transfer must overcome. During steady-state, the rate of heat flow through a wellbore Q can be expressed as:

$$Q = -2\pi r_{to} U_{to} (T_f - T_{wb}) \tag{35}$$

where U_{to} is the overall heat transfer coefficient. The rate of heat flow is determined by the overall heat transfer coefficient, the tubing outside surface area, and the temperature difference between the wellbore fluid and wellbore/formation interface. The heat flows through each of the elements from wellbore fluid to surrounding formations. Therefore, we can derive the expression for the overall heat transfer coefficient (Hasan, 1994):

$$\frac{1}{U_{to}} = \frac{r_{to}}{r_{ti} h_{to}} + \frac{r_{to} \ln(r_{to} / r_{ti})}{k_t} + \frac{1}{h_c} + \frac{r_{to} \ln(r_{co} / r_{ci})}{k_c} + \frac{r_{to} \ln(r_{wb} / r_{co})}{k_{cem}} \tag{36}$$

where r_{ti}, r_{to}, r_{ci} and r_{co} are tubing inner radius, tubing outer radius, casing inner radius, and casing outer radius, and h_{to} and h_c represent convective heat transfer coefficients for tubing and annular fluid.

In Equation (36), the resistances to heat transfer provided by annulus and tubing fluid need to be calculated as they cannot be directly measured in the field. The Sieder-

Tate correlation is used for forced convective heat transfer coefficient calculation for turbulent flow in pipes and wells (McCabe, 2004):

$$Nu = \frac{h_{to} d}{k} = 0.023(\frac{dv\rho}{\mu})^{0.8}(\frac{c_p \mu}{k})^{0.33}(\frac{\mu}{\mu_w})^{0.14} \tag{37}$$

where μ_w is the viscosity of the fluid at the wall temperature. In fact, neglecting the last term will not introduce significant error unless the viscosity of the fluid is high.

When a fluid is in contact with two parallel plates with different temperatures, both the heat conduction and natural convection will take place. The temperature difference between casing and tubing changes the density of fluid in the casing-tubing annulus. Consequently, it results in fluid circulation in the annulus, and enhances heat transfer. In this work, the correlation of the heat transfer coefficient for natural convection for the fluids between two vertical plates proposed by Dropkin and Sommerscales is adopted (Dropkin, 1965). The correlation for natural convection coefficient in a cylindrical coordinator is:

$$h_c = \frac{0.049(GrPr)^{0.333} Pr^{0.074} k_a}{r_{to} \ln(r_{ci} / r_{to})} \tag{38}$$

where Gr is the Grashof number and Pr is the Prandtl number. However, the evaluation of Grashof number requires the temperature difference between tubing and casing. Therefore, an iterative solution procedure is needed to obtain the natural convection coefficient. Then the overall heat transfer coefficient can be calculated.

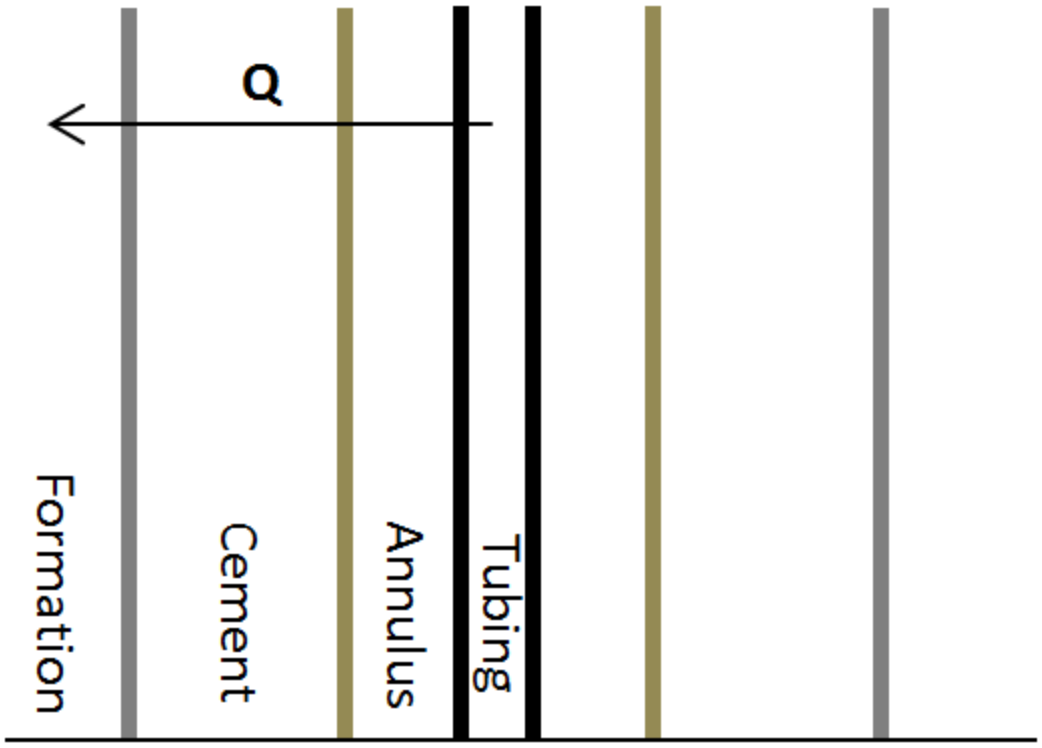

Figure 16. Heat flow through a series of resistances

Equation (29) is coupled with Equation (35) to replace T_{wb}. The heat flow crossing the wellbore/formation interface can be expressed as:

$$Q = -L_R w c_p (T_f - T_{ei}) \tag{39}$$

where the relaxation parameter, L_R, is defined as (Hasan, 2012):

$$L_R = \frac{2\pi}{c_p w}\left[\frac{r_{to}U_{to}k_e}{k_e + (r_{to}U_{to}T_D)}\right] \tag{40}$$

Substituting Equation (40) into Equation (34) yields:

$$\frac{dT_f}{dz} = C_J \frac{dp}{dz} - (T_f - T_{ei})L_R - g\sin\alpha - v\frac{dv}{dz} \tag{41}$$

In Equation (41), T_{ei} is the initial formation temperature, varying with depth nearly linearly. Therefore, for an inclined well of true vertical depth L, it can be expressed as:

$$T_{ei} = T_{eibh} - (L - z)g_G \sin\alpha \tag{42}$$

where T_{eibh} is initial bottomhole temperature that remains constant within the time and g_G is the geothermal gradient. Then Equation (41) can be written as:

$$\frac{dT_f}{dz} = -(T_f - T_{ei})L_R + g\sin\alpha - \phi \tag{43}$$

where

$$\phi = v\frac{dv}{dz} - C_J \frac{dp}{dz} \tag{44}$$

Equation (43) is a first order linear differential equation, which can be solved analytically based on different scenarios.

For typical gas production, the term ϕ is usually small and therefore negligible. However, considering the rapid expansion of gas near the wellhead and the resulting large pressure gradient, this term could be significant when evaluating the gas well blowout.

2.2.3 Sonic Velocity

The upper limit of the wellhead velocity is the sonic velocity of the hydrocarbon gas from the well during the blowout events. In the following paragraph, the explanation to the existence of this limit is given (Smith, 2005). From the continuity equation one can have:

$$d\frac{vA}{V}=\frac{dV}{V}-\frac{dv}{v}-\frac{dA}{A}=0 \tag{45}$$

When fluid flows through a constant cross section area (*e.g.*, pipeline, wellbore), the last term is zero. Equation (45) reveals the relationship between the control volume V and the fluid velocity v. The control volume of fluid is a function of entropy S and pressure P according to the thermodynamics laws. Therefore, it could be written as:

$$dV=(\frac{\partial V}{\partial S})_p dS+(\frac{\partial V}{\partial P})_S dp \tag{46}$$

The two terms on the right hand side can be expressed as:

$$(\frac{\partial V}{\partial p})_S=\frac{V^2}{c^2} \tag{47}$$

and

$$(\frac{\partial V}{\partial S})_p=\frac{\beta VT}{C_p} \tag{48}$$

where c is the speed of sound in a fluid and β is the volume expansion coefficient. Substituting Equation (47) and (48) into Equation (46) yields:

$$\frac{dV}{V} = \frac{\beta T}{C_P} dS - \frac{V}{c^2} dp \tag{49}$$

From the knowledge of thermodynamics, we also have:

$$TdS + Vdp = dH = -vdv \tag{50}$$

Therefore, combining Equations (45), (49), and (50) by assuming constant cross section area, we have:

$$(1 - M^2)Vdp + (1 + \frac{\beta v^2}{C_P})TdS = 0 \tag{51}$$

where the M is the Mach number, determined by the ratio of the velocity and sound speed in the fluid. A transformation of Equation (51) is:

$$\frac{dp}{dx} = -\frac{T}{V} \frac{1 + \frac{\beta v^2}{C_P}}{1 - M^2} \frac{dS}{dx} \tag{52}$$

Fluid always flows towards the negative pressure gradient direction. Based on the second law of thermodynamics, the entropy always increases. Therefore, the value of M cannot be larger than 1, indicating that the upper limit of the fluid speed must be the sonic velocity. The sonic velocity of gas is derived from thermodynamic knowledge of ideal gas behavior by Kieffer (1977), as

$$c = \left(\gamma \frac{R}{M} T \right)^{0.5} \tag{53}$$

where γ is the ratio of heat capacities (C_p / C_v), R is the universal gas constant, and M is the molecular weight.

2.3 Reservoir and Wellbore Interaction

This section describes the reservoir variable that governs the blowout rate under different conditions. Given that a blowout event could happen during any operational phase, such as drilling, completion and production, the theory of reservoir and wellbore interaction is applicable to all these phases. When the formation fluid flows from the reservoir, a pressure disturbance is initiated at the location of the well. Such disturbance travels toward the boundaries of the reservoir within the time. However, for the point that is far away from the disturbance generation location, such disturbance cannot be detected immediately. The furthest distance where the effect can be monitored is called the radius of investigation r_{inv}. It is given by:

$$r_{inv} = \sqrt{\frac{kt}{\phi \mu c_t}} \tag{54}$$

where k is reservoir permeability, t is time, ϕ is reservoir porosity, μ is reservoir fluid viscosity, and c_t is total compressibility accounting for the compressibility of reservoir fluid and rock. When t is small, it results in a minimum radius of investigation compared to the radius of the reservoir. This period is called transient period or infinite acting period.

2.3.1 Transient Period

For most of the fluid that flows from the reservoir into the well, it should obey Darcy's Law (Darcy, 1856). The expression of Darcy's law in radial coordinates is:

$$q = \frac{kA_r}{\mu}\frac{dp}{dr} \tag{55}$$

where A_r is a radial area at a distance r. The following classic diffusivity equation can describe the pressure profile in the reservoir:

$$\frac{\partial^2 p}{\partial r^2} + \frac{1}{r}\frac{\partial p}{\partial r} = \frac{\phi\mu c_t}{k}\frac{\partial p}{\partial t} \tag{56}$$

During the transient period, it is assumed that the well is a line source compared to the reservoir with large radius. The assumption leads to a general solution of Equation (56):

$$p_{wf} = p_i - \frac{qB\mu}{4\pi kh} Ei\left(\frac{\phi\mu c_t r^2}{4kt}\right) \tag{57}$$

In Equation (57), q represents the sandface flow rate, h is formation thickness, and $Ei(x)$ is the exponential integral function. The following equations are derived from Equation (57) for the interaction between the gas reservoir and the gas well during the transient period:

$$q = \frac{1.987\times10^{-5} T_{sc} kh[m(p_i) - m(p_{wf})]}{p_{sc} T\alpha} \tag{58}$$

where

$$\alpha = -0.5[\ln(\frac{r_w^2}{4At_{DA}}) + 0.5772 + \delta\sum_{i=2}^{\infty} Ei(-\frac{a_{iD}^2}{4t_{DA}})] + s + Dq \tag{59}$$

$$t_{DA} = \frac{2.637\times10^{-4} kt}{\phi\mu c_t A} \tag{60}$$

In Equation (58), $m(p)$ is the pseudo pressure. The purpose of introducing the pseudo pressure is to eliminate the nonlinearity due to the equation of state for gases. The method of images (Matthews, 1954) is used in Equation (59) to connect the infinite acting period and pseudo steady-state period, which is discussed in later paragraphs. The summation of the exponential integral function accounts for the partial boundary effect. The coefficient δ is a correction term to smooth the transition between the infinite acting flow and pseudo steady-state flow. Kabir (2006) suggested the value of δ ranges between 1.1 and 1.3. As time progresses, the radius of investigation becomes larger and comparable to the radius of the reservoir, so that the well cannot be assumed to be a line source any more. Then the reservoir is in a pseudo steady-state period.

2.3.2 Pseudo Steady-State Period

Earlougher (1977) has shown that the time at which pseudo steady-state begins is given by:

$$t_{pss} = \frac{\phi\mu c_t A}{0.000264k} t_{DA} \tag{61}$$

In a pseudo steady-state period, pressure disturbance could be detected at all the boundaries of the reservoir. From the radial diffusivity equation, the pressure, p_e, at the point of $r = r_e$ in a reservoir with radius, r_e, can be expressed as:

$$p_e = p_{wf} + \frac{141.2qB\mu}{kh}(\ln\frac{r_e}{r_w} - 0.5) \tag{62}$$

However, the value of p_e is immeasurable in the field. A more useful expression for pseudo steady-state flow is to use the average reservoir pressure that can be obtained based on Equation (4):

$$\bar{p} - p_{wf} = \frac{141.2qB\mu}{kh}(\ln\frac{0.472r_e}{r_w} + s + Dq) \tag{63}$$

where s is skin factor and D is the non-Darcy coefficient, which describes the condition of the wells (*e.g.*, damage or stimulation). For a gas reservoir, the formation volume factor is defined by Equation (3) with average value. Therefore:

$$\bar{B}_g = \frac{0.0283\bar{Z}T}{(p_e + p_{wf})/2} \tag{64}$$

and from Equation (62)

$$\bar{p}^2 - p_{wf}^2 = \frac{1424q\bar{\mu}\bar{Z}T}{kh}(\ln\frac{r_e}{r_w} + s) \tag{65}$$

To avoid the nonlinearity in Equation (65), Al-Hussainy *et al.* (Al-Hussainy, 1966) suggests introducing pseudo pressure defined as follows:

$$m(\bar{p}) = 2\int_{p_0}^{\bar{p}} \frac{p}{\mu(p)Z(p)}dp \tag{66}$$

Equation (65) therefore becomes:

$$m(\bar{p}) - m(p_{wf}) = \frac{1424qT}{kh}(\ln\frac{r_e}{r_w} + s + Dq) \tag{67}$$

2.3.3 Unified Model

When modeling the blowout events, the transition from transient period to pseudo steady-state period is common given that the high blowout rate depletes the reservoir pressure quickly. However, combination of Equations (58) and (67) usually leads to the discontinuity between the transition and highly depends on the value of δ. Therefore, a general solution (Matthews, 1967) that could cover both periods is adopted in this research:

$$m(p_i) - m(p_{wf}) = 1422\frac{qT}{kh}\{\frac{2t_{Dw}}{r_{eD}^2} + \ln r_{eD} - \frac{3}{4} + 2\sum_{n=1}^{\infty}\frac{\exp(-a_n^2 t_{Dw})J_1^2(a_n r_{eD})}{a_n^2[J_1^2(a_n r_{eD}) - J_1^2(a_n)]}\} \tag{68}$$

where

$$r_{eD} = \frac{r_e}{r_w} \tag{69}$$

$$r_{eD} = \frac{r_e}{r_w} \tag{70}$$

and the a_n values are the root of:

$$J_1(a_n r_{eD})Y_1(a_n) - J_1(a_n)Y_1(a_n r_{eD}) = 0 \tag{71}$$

where J_1 is the Bessel function of first kind and Y_1 is Bessel function of second kind. The Equation (71) has infinite number of solutions. Figure 17 shows the solutions for Equation (71) from the interval between 0 to 0.1. With sufficient number of the roots, the pseudo pressure difference could be relatively easy to obtain, which is computationally inexpensive.

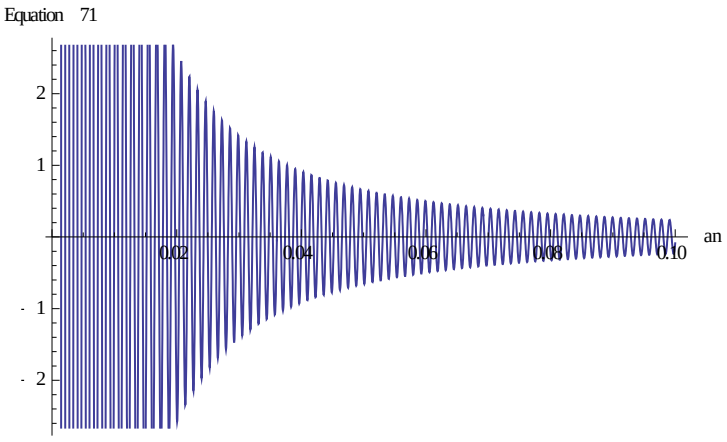

Figure 17. Solutions of Equation (71) from 0 to 0.1

In addition, the summation term in Equation (68), as shown in Figure 18, is significant compared to other terms at early times. However, this term becomes less important as time progresses, thereby indicating that the transition between early and late time is occurring. At late times, the summation term becomes negligible. Stated differently, the pseudo pressure difference bears a linear relationship with flow rate during the pseudo steady-state flow period when the effects of all the boundaries have

been felt at the wellbore. The advantage of Equation (68) is that it avoids the discontinuity between the two flow periods of interest, transient and pseudo steady-state.

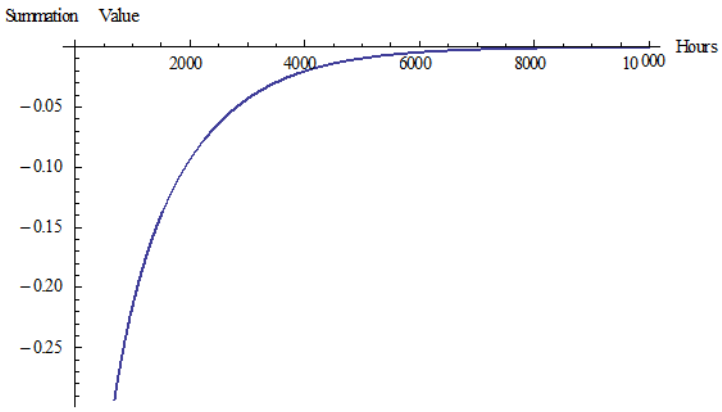

Figure 18. Summation term in Equation (68)

2.4 Computational Algorithm

The onshore gas well blowout duration is divided into small segments first, then at each time step:

1. Sonic velocity is assumed to exist, and the wellhead temperature is assumed to be ambient temperature. Then the flow rate in Mscf/D can be calculated.
2. Use the flow rate to calculate the compressibility factor in the reservoir at current time step by Equation (4):
   a) Initial pressure and compressibility factor are known, the cumulative production can be obtained by examining the flow rate history.
   b) The term of $\bar{p}/Z$ can be obtained readily.

c) Because the average reservoir pressure $\bar{p}$ is unknown and compressibility factor Z depends on the pressure, an iterative procedure is needed to calculate the compressibility factor.

d) Convergence is reached and the compressibility factor at current time step is obtained.

3. Use the flow rate in Step 2 to calculate the pseudo pressure difference.

4. The bottomhole pressure is then calculated by Equation (66)

5. Once the bottomhole pressure is known, a bottom-to-top calculation in wellbore could be performed so that the wellhead temperature and wellhead velocity can be calculated according to Equations (20) and (43).

a) Use the flow rate in Step 1 to calculate the wellhead conditions, including pressure, temperature, and velocity. If the wellhead pressure is large than ambient pressure, go to Step 5 b); otherwise, go to Step 5 d)

b) The blowout is in the wellhead pressure governed mode. Calculate the sonic velocity based on the computed wellhead temperature and compare with the computed wellhead velocity. If two values are not equal, go to Step 5 c); otherwise, go to Step 6.

c) Use the new sonic velocity and computed wellhead temperature in Step 5 b) to repeat Step 1 to 5 b) until the convergence is reached.

d) The blowout is in the reservoir pressure governed mode. Re-guess a new flow rate and repeat Step 1 to 5 a) until the wellhead pressure equals to the ambient pressure. Then go to Step 6.

6. Go to next time step.

2.5 Results and Discussion

First, Equation (68) is compared with commercial software for the scenarios of the constant rate drawdown test in a gas reservoir. As shown in Figure 19, a good agreement with the results of a commercial package for the reservoir response is indicated. The early-time transient period is over around 10,000 hr, followed by late-time, pseudo steady-state condition with a smooth transition.

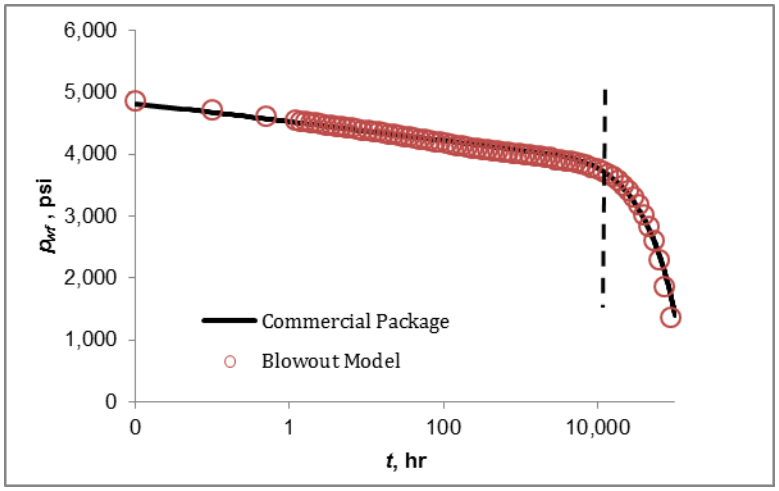

Figure 19. Constant rate drawdown test of gas reservoir

We used the results of Oudeman (2010) to validate the blowout model first. These data were obtained from the results of well testing of a small tight offshore gas reservoir at the North Sea. This gas well was drilled underbalanced and a series of well tests were performed. This example presented a great opportunity to verify the blowout

model because of the high flow rates associated with testing. Different wellhead pressures during testing may be construed as blowouts at various water depths. Given the wellhead pressure and the reservoir pressure, it is possible to calculate the blowout rate and bottomhole pressure. Figure 20 shows the comparison of the calculated and measured rates. In general, the calculated rates match the measured rates fairly well. Poor flow stabilization in the reservoir probably contributed to the scatter in Figure 20.

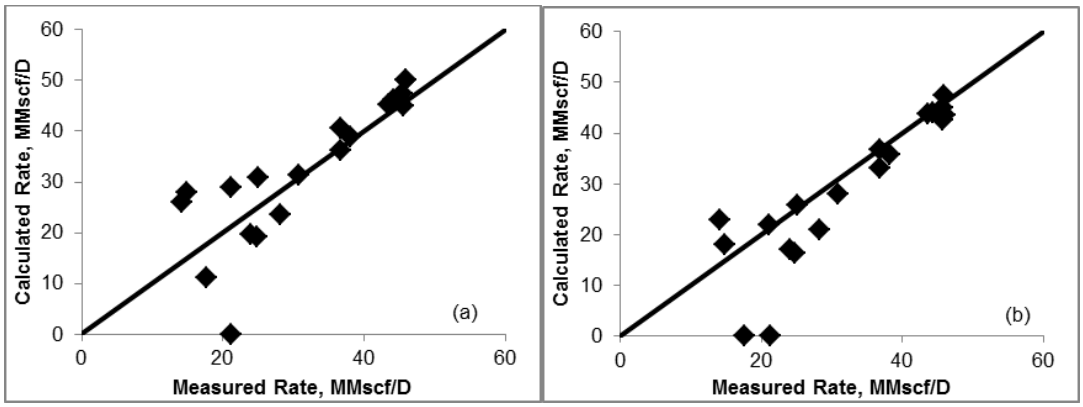

Figure 20. Comparison of measured and calculated blowout rates by our blowout model (b) comparison of measured and calculated blowout rates from Oudeman (2010)

Our model, discussed in the previous section, is applied to an onshore sour-gas well in Germany, as described by Kikani *et al.* (1996). The field data for this example is reported in Table 3. In this case, it should be noted that the flow is choked (sonic velocity is present) throughout the whole duration of the blowout.

Table 3. Data presented in the field example of Kikani *et al.* (1996)

Parameters	Value
Well Depth, ft	12,300
Reservoir Depth, ft	12,456
Net Thickness, ft	100
Porosity	0.149
Water Saturation	0.15
Reservoir Pressure, psia	5,985
Reservoir Temperature, ℉	276.8
Gas Gravity	0.83
H_2S concentration	0.2869
Tubing inner radius, ft	0.25
Drainage radius, ft	3,280
Skin	-2.5
Non-Darcy Coefficient, day/Mscf	2.57E-05
Permeability, md	4.3

Because Kikani *et al.* did not use a thermal model, we first matched their simulated blowout rates with our model allowing no temperature variation with time. The agreement of our model generated blowout rates with Kikani's numerical model appears very good as shown in Figure 21. However, when heat transfer effects are accounted in our model, a divergence of about 5% in estimated rate with Kikani's simulation is observed. Figure 21also shows our computed wellhead fluid temperature on the secondary y-axis. A wellhead fluid temperature increase of about 30 ℉ over 100 days of production is noted in Figure 21. This temperature difference appears to be the primary reason for higher blowout rate calculated by our model in later times.

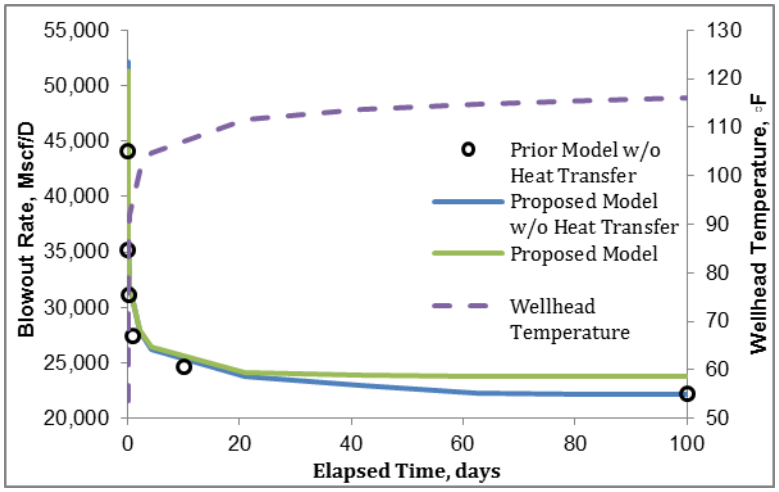

Figure 21. Comparison of model presented in this work and Kikani's results

Figure 22 shows the temperature profile in the wellbore when choked flow rate is achieved at the wellhead. Two interesting phenomena are observed from this figure. First, the fluid temperature starts to decrease as it moves up from the bottomhole and quickly declines near the wellhead. Second, the wellhead temperature increases over time, although the blowout rate may decline during the blowout event because of reservoir depletion. These observations can be explained by examining Equations (43) and (44). There are two important components that are taken into account in heat transfer equations, which are kinetic energy loss (KE) and Joule-Thomson Effect (JT); Equation (44) combines these two components.

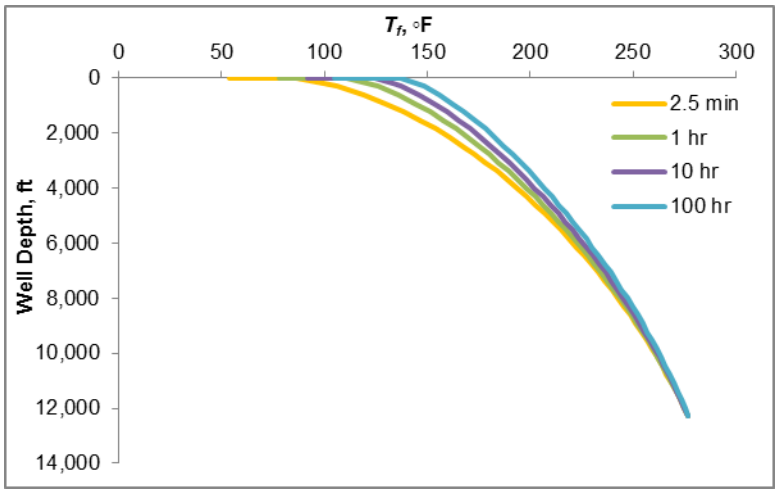

Figure 22. Fluid temperature in wellbore during a blowout event

Figure 23 shows these two components affecting the behavior of heat transfer in blowout events for a given situation with and without considerations of KE and/or JT near the wellhead. The contributions of KE and JT are significant when the fluid approaches to wellhead. The figure illustrates the fluid temperature profile in the wellbore starting from 20 feet below the wellhead for four cases—with JT and KE, with JT and without KE, with KE and without JT, and without JE or KE. When the rate approaches the choked flow rate at wellhead (potential blowout scenario), the gas experiences an extreme expansion near the wellhead, resulting in the significantly increase of pressure gradient in the wellbore. It leads to the increase of kinetic energy contribution in Equation (44), thereby explaining the quick decrease of fluid temperature near the wellhead.

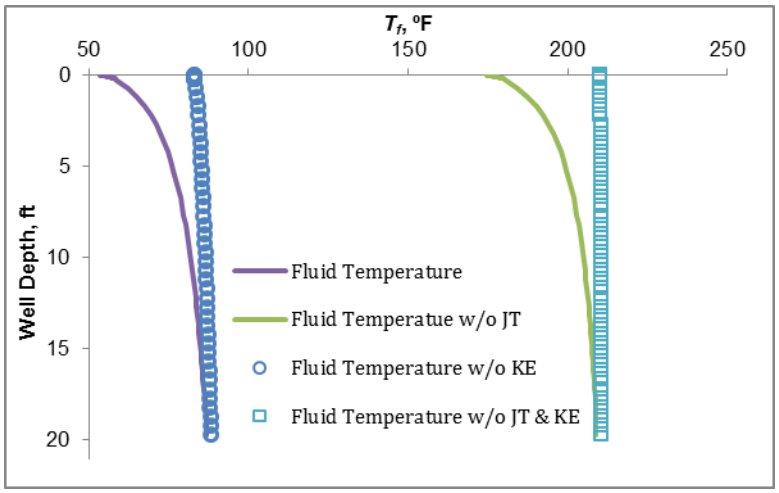

Figure 23. Fluid temperature profile in wellbore after 2.5 minutes near wellhead considering different components in heat transfer

If KE is not considered in heat transfer model, as shown in Figure 23, the fluid temperature near the wellhead in the wellbore will not change significantly. On the other hand, Joule-Thomson Effect describes the fluid temperature change owing to the pressure changes when the fluid flows. Figure 23 shows that the fluid temperature is overall higher when the JT effect is not considered. In conclusion, based on our observations, the KE contributes to the fluid temperature change near the wellhead, while the JT affects the fluid temperature in the entire wellbore.

Figure 24 illustrates how the KE and JT can affect the fluid temperature evolution in the blowout scenario. When KE term is neglected, the temperature is higher compared to the one considering KE, but has similar trend. The blowout rate declines with the increase in temperature. If the JT effect is not taken into account, the blowout rate and temperature decrease at the same time. The fluid temperature at wellhead will

barely change if neither of these two important components in heat transfer is considered.

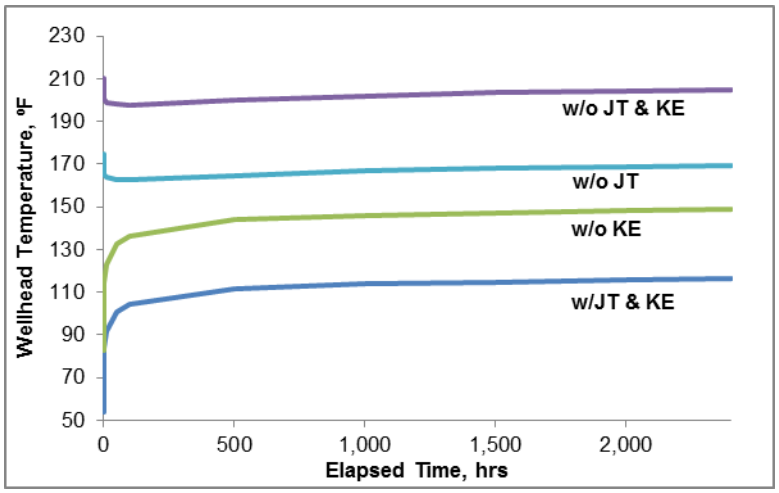

Figure 24. Wellhead temperature evolution considering different component in heat transfer

Figure 21 shows the results of the blowout evolution. Many of the reservoir variables; however, cannot be known accurately and may have great uncertainties in an actual setting. That aspect is especially true for wells in the exploration phase. We adopted a probabilistic simulation approach in this section to gain insights into how the various reservoir parameters influence a blowout event. Table 4 shows the range of four independent variables in this three-level design. Figure 25 shows the low, medium, and high-level cases, reflecting the range of each independent variable. To calculate production loss, we assumed that the blowout lasted for 300 days.

Table 4. Reservoir parameters with uncertainties for blowout model

	Low	Medium	High
Formation thickness, ft	50	100	150
Initial reservoir pressure, psia	5,387	5,985	6,584
Reservoir radius, ft	2,952	3,280	3,608
Permeability, md	1	2.3	5

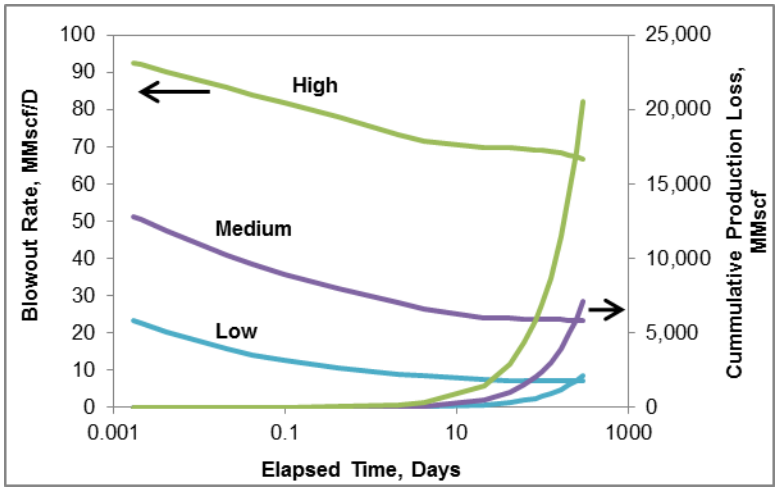

Figure 25. Probabilistic blowout behavior for Kikani *et al.* (1996) case

The folded-Plackett-Burman (Wolff, 2010) design of experiments helped quantify the significance of each independent variable. This design captures both nonlinearities and interactions between the variables. Cumulative production loss during a 100-day blowout constituted the dependent variable. Figure 26 presents the Pareto chart of this analysis, signifying that both permeability and formation thickness constitute important variables. The vertical line defines the results within the 95% confidence interval.

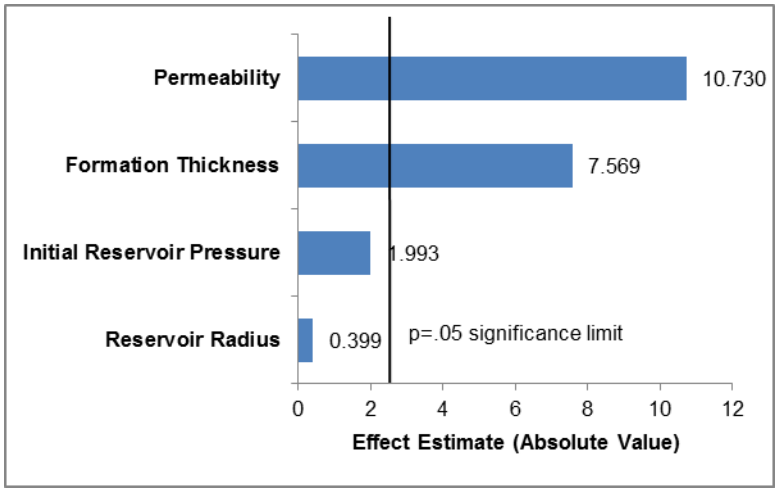

Figure 26. Pareto chart of total discharge amount during gas well blowout for folded-Packett-Burman design

Note that for certain combination of variables, the sonic velocity cannot be sustained. This item can be explored further by studying the tubing performance curve (TPC) and inflow performance relationship (IPR) curves. Figure 27 shows the TPC and IPR curve at low permeability of 1 md. The solid lines represent the IPR curves at different levels of reservoir pressure and the dashed line represents the TPC at constant wellhead pressure, which is close to atmosphere pressure. Note that nonlinearity of TPC is minimal because of the low-wellhead pressure. The operating points are between 6 and 9 MMscf/D. However, the choked flow rate of gas in this field example at standard conditions is about 19.8 MMscf/D. Thus for a low-permeability reservoir as in this example, sonic velocity will not be reached even when the wellhead pressure approaches atmospheric conditions. In contrast, Figure 28 presents the TPC and IPR curves for a

high-permeability reservoir (5 md). The operating points are between 50 and 70 MMscf/D, which are beyond the choked flow rate for this gas in the field example, indicating that the well will flow at sonic velocity.

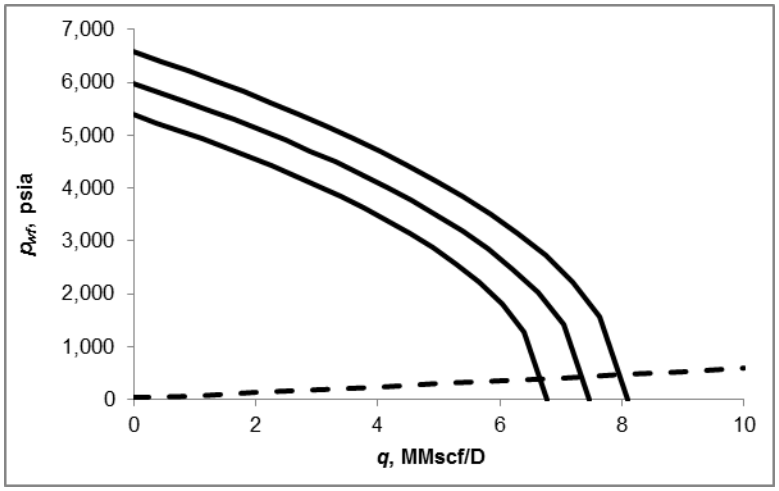

Figure 27. TPC and IPR curves at low level of permeability

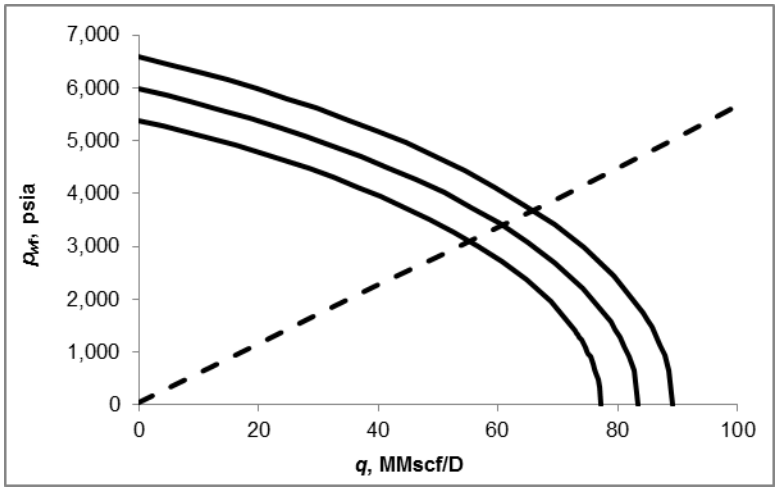

Figure 28. TPC and IPR curves at high level of permeability

The blowout model presented here is not only applicable for onshore gas wells, it also shows the potential application for offshore wells. For offshore wells, because of the hydrostatic pressure at a given water depth, the flow is unlikely to be choked. Therefore, the blowout behavior will be governed by the constant-wellhead pressure, but the other computational steps can follow the same procedure as discussed here. However, modeling the evolution of the oil plume and its dispersion in water will require a separate tool.

In addition, the blowout model can provide valuable information for the well control operations. For a certain blowout incident, given the reservoir and fluid properties, the blowout rate and bottomhole pressure can be obtained by coupling the wellbore with reservoir. Such results can be used to determine the type and properties of killing fluids and pump capacity. If the pump rate is not enough to kill the well, the depth of injection string can be increased. In addition, larger pumps can be added based on the pressure profile provided by the blowout model. If the calculated pump capacity cannot be achieved, other techniques can be considered, such as drilling of relief wells.

One difficulty with the proposed approach is that we assumed the blowout rate reaches the maximum value immediately after the occurrence of blowout. In reality, the blowout rate will increase from the normal production rate to the maximum value and then decline. Such increase of the rate in the beginning of the blowout event would take several minutes based on the study of Kikani *et al.* (1996). This short time period can be neglected when the blowout lasts for days. However, for blowouts lasting just a few

hours, the early period where the blowout rate increase occurs will become significant for the prediction of total discharge during the blowout event.

In this study, we provided a useful approach to modeling blowout events under the assumption of single tubing diameter, in absence of other wellhead restrictions. However, the model is capable of capturing geometry reflecting realistic situations. For example, following a blowout the wellhead may become dysfunctional but may still be in place, providing restrictions to fluid flow. This and other restrictions can be handled in the wellbore model, provided reasonable description of the geometry can be described.

2.6 Conclusions

The mechanism and corresponding physical phenomenon of blowout events are investigated in the section. Understanding the importance of heat transfer is essential to accurately estimate the consequence of gas well blowout. The reservoir, wellbore, and their interactions are coupled together to demonstrate a full picture of the potential gas well blowout. A well-established computational algorithm is developed to effectively estimate the blowout rate and total discharge amount during the blowout incidents. The statistical analysis identifies the independent variables responsible for the maximum discharge; both reservoir permeability and the connected reservoir volume are the key variables. The model could serve as the basis of the risk assessment of blowout events which are discussed in later chapters.

CHAPTER III

CONSEQUENCE MODELING OF OFFSHORE OIL WELL BLOWOUT

A number of similarities between the modeling of gas and oil well blowout are identified in this section. However, one of the important differences is the various flow patterns of multiphase flows that take place during an oil well blowout. Estimation of transition among different plow patterns could accurately determine the blowout rate and the total discharge amount in the offshore environment. In addition, given the hydrostatic pressure by the sea water at the wellhead, the choked flow is much less likely to occur when considering the consequence modeling.

3.1 Reservoir Model

Due to the high pressure of the reservoir, it is reasonable to assume that there is no occurrence of phase separation in the reservoir (*i.e.*, the reservoir pressure is always higher than the bubble point pressure). The material balance equation in this section to estimate the reservoir pressure is derived first based on the single phase oil and then expands to the two-phase flow.

Single phase oil contains no gas, so the gas solubility (R_s) is zero. The material balance for a single phase oil reservoir can be derived from thermodynamic knowledge. The basic thermodynamic equation is:

$$dV = (\frac{\partial V}{\partial p})_T dp + (\frac{\partial V}{\partial T})_P dT \tag{72}$$

Changing volume into density yields:

$$-\frac{d\rho}{\rho} = -\frac{1}{\rho}\left(\frac{\partial\rho}{\partial p}\right)_T dp - \frac{1}{\rho}\left(\frac{\partial\rho}{\partial T}\right)_p dT \tag{73}$$

The isothermal compressibility (c_w) and thermal expansion coefficient (β) are defined as follows:

$$c_w = \frac{1}{\rho}\left(\frac{\partial\rho}{\partial p}\right)_T \tag{74}$$

$$\beta = -\frac{1}{\rho}\left(\frac{\partial\rho}{\partial T}\right)_p \tag{75}$$

Then, an analytic expression for the density as a function of pressure and temperature can be obtained by combining Equations (73), (74) and (75):

$$\frac{d\rho}{\rho} = c_w dp - \beta dT \tag{76}$$

Equation (76) can be solved analytically:

$$\ln\frac{\rho}{\rho_{sc}} = c_w(p - p_{sc}) - \beta(T - T_{sc}) \tag{77}$$

where p_{sc} and T_{sc} represent the standard conditions (14.7 psi and 60 ℉). Therefore, the density of single phase oil can be calculated. At any time t, the amount of oil in the reservoir is calculated by the original oil in place and cumulative production/loss:

$$\textit{Original oil in place} - \textit{Oil in place at time } t = \textit{Cumulative loss from time } 0 \textit{ to } t \tag{78}$$

The differential form of Equation (78) is:

$$V_e d\rho = -w dt \tag{79}$$

where V_e is the drainage volume and w is the mass flow rate. Based on the definition of isothermal compressibility (c_w) given by Equation (74), Equation (79) is rewritten as:

$$-\frac{1}{\rho}\frac{w dt}{V_e d\bar{p}} = c_w \tag{80}$$

$$\frac{d\bar{p}}{dt} = -\frac{w}{\rho V_e c_w} \tag{81}$$

Since the oil density is an analytic function of pressure and temperature given by Equation (77), the average reservoir pressure can be obtained in field unit during the blowout by coupling Equations (77) and (81):

$$\bar{p} = p_i - \frac{0.234 qBt}{\phi c_t h(\pi r_e^2)} \tag{82}$$

where q is the volumetric flow rate at standard condition, B is oil formation volume factor, t is time, ϕ is porosity, c_t total compressibility, h is the thickness of pay zone, and r_e is the reservoir radius.

Havlena (1963 and 1964) applied the general material balance to a two-phase reservoir. They used the initial oil in place and the ratio of the initial hydrocarbon volume in the gas cap to the initial hydrocarbon volume in the drainage area. Later, Dake (1983) presented the generalized expression of the material balance for a two-phase

reservoir. Under the assumption of no water saturation in the reservoir, the expression is given as:

$$N_p[B_o + (R_p - R_s)B_g] = NB_{oi}[\frac{(B_o - B_{oi}) + B_g(R_{si} - R_s)}{B_{oi}} + m(\frac{B_g}{B_{gi}} - 1)] \qquad (83)$$

where N_p is the cumulative production/loss, B_o is the oil formation volume factor which is similar to the definition of B_g, R_p is the producing gas-oil ratio, R_s is the gas solubility that describes the volume of gas contained in oil phase, N is initial oil in place, and m is the ratio of the initial hydrocarbon volume in the gas cap to the initial hydrocarbon volume in the reservoir. The correlations of these variables are shown in Appendix A.

In this work, it is assumed that the pressure of the fluid in the reservoir will always be higher than the bubble point pressure to simplify the problem (*e.g.*, single phase). Therefore, Equation (81) still can be applied to the two-phase reservoir. But the analytic expression for the density of the fluid in the reservoir is not applicable as the oil contains a significant amount of gas now. The density of the fluid is calculated by using correlations based on field experience shown in Appendix A. Then the average reservoir pressure can be obtained.

3.2.1 Multiphase Flow Model

The basis of the multiphase flow model is similar to the single phase gas flow. Therefore, Equations (6) to (8) and (14) are still valid. Combining these equations, the pressure gradient in the wellbore could be calculated as:

$$(\frac{dp}{dz})_T = -(\rho g \sin\theta + \frac{fv^2\rho}{2d} + \rho v \frac{dv}{dz}) \tag{84}$$

Two- or three-phase fluid flows simultaneously through the same tubing always complicates the analysis of fluid flow in the wellbore. Even when the fluid coming from the reservoir at the bottomhole is single phase oil, the pressure and energy loss often results in separation of gas phase and oil phase. In this section, the main study objective is with two-phase flow—oil and gas in vertical and near-vertical systems.

When two-phase flow exists, the different phases show a number of distinct configurations, named flow patterns. Recognizing flow patterns facilitates the modeling of two-phase flow. Each of the flow regimes should be modeled separately, as the oil/gas ratio is different in every flow regime. Generally, there are four major flow patterns, named bubbly, slug, churn, and annular as shown in Figure 29.

At low gas velocity, the gas phase flow is distributed as small, nearly spherical bubbles through a continuous liquid medium; this is called bubbly flow. In vertical wells, bubbles flow uniformly throughout in the liquid phase. As the velocity of gas flow increases, the small bubbles in bubbly flow aggregate together, forming slug flow. In slug flow, the large gas bubbles have approximately the same diameter as the tubing and

are known as Taylor bubbles. The successive gas bubbles are separated from the wall of tubing by a thin film of liquid. As the velocity of gas flow further increases, the large gas bubbles are broken down and the flow becomes churn flow. In churn flow, the shapes of the bubbles are irregular throughout the liquid phase. This kind of flow has an oscillatory or time varying characteristic. Such flow regime is also known as slug-annular transition. At very high gas flow rates, the gas flow takes place in the core of the tubing, forming annular flow. The gas flow is continuous along the wellbore, so that it forms a gas core and liquid thin film. Some liquid droplets usually are distributed in the gas core. In some extreme situations (*e.g.,* blowout events), the liquid film will disappear, leaving only the gas core with a liquid mist.

The changes of pressure and temperature lead to different flow patterns at various depths along the wellbore. For example, if the bottomhole pressure is higher than the bubble point pressure, a single phase oil flow that contains a large amount of gas can be expected at the bottomhole. When the fluid flows upward, the pressure will gradually drop. As the pressure drops below the bubble point pressure, the gas contained in the oil phase will start to come out from the mixture, resulting in bubbly flow. If the pressure drops further with upward movement of the fluid, more and more gas will separate from the mixture, leading to the whole range of flow regimes, shown in Figure 30.

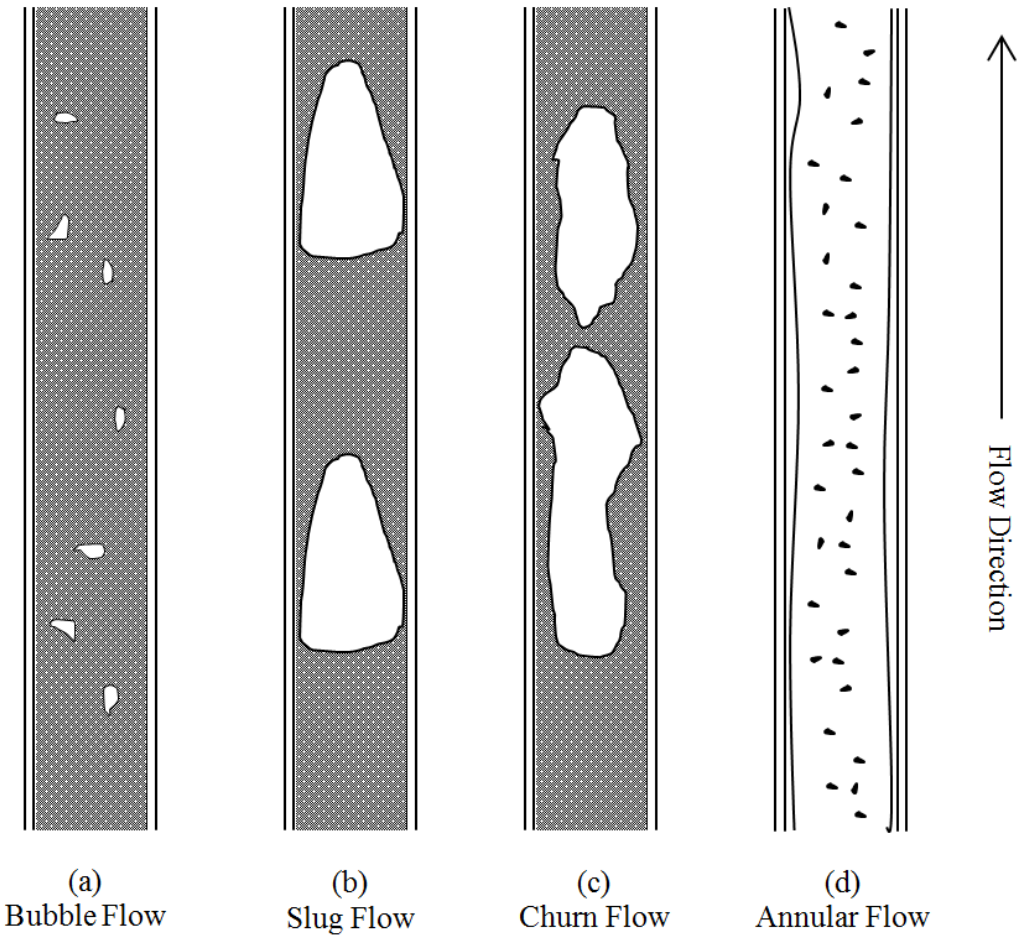

Figure 29. Two-phase flow in vertical wells

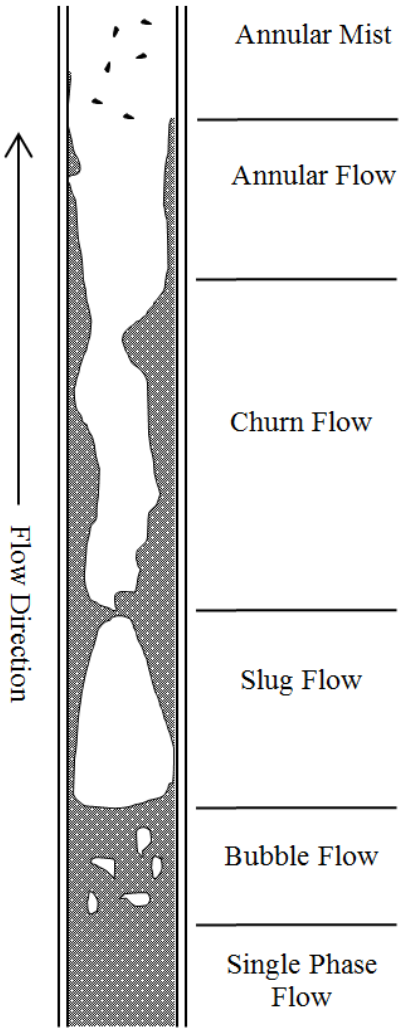

Figure 30. Development of flow patterns in a wellbore

A lot of effort has been made to recognize the flow patterns. Experimentally, some flow patterns can be observed at low flow rate in transparent pipes. A number of observation techniques have also been developed to aid the study of flow regimes, such as electrical, hot-wire, pressure, and optical probes. Signals provided by those probes can offer some indirect information for the analysis of flow patterns.

From a computational simulation point of view, there are two approaches to model the flow-pattern development—flow regime maps and individual transition criteria. A number of flow-pattern maps are proposed by different researchers. Some of them can match the experimental data quite well and have been used widely in industry. The main idea of these flow-pattern maps is to generalize a map by choosing different parameters that will indirectly influence the transition among flow regimes.

Figure 31 shows an example of flow-pattern map, which uses the superficial momentum flux of liquid and gas phases ($\rho_L v_{sL}^2$ and $\rho_g v_{sg}^2$) as the two axes. The typical flow-pattern map is based on an air and water mixture at low pressure, and steam and water data at high pressure from tubes with small diameters (1-3 cm). However, because the mixture in this map is water/air and steam/water mixtures, it might not capture some important properties of oil/gas mixtures. In addition, these empirical flow-pattern maps cannot aid modern computational models as they are difficult to be implemented into a computer program. Therefore, an alternative technique is needed to determine the flow regime transition and establish valid criteria for each transition.

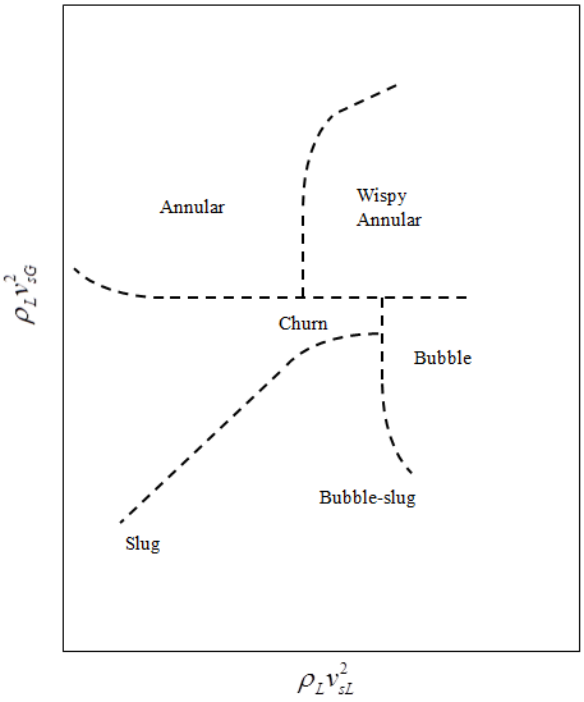

Figure 31. Example of flow-pattern map

Developing individual transition criteria is more flexible than the empirical flow-pattern maps. This alternative approach is used in this work to model two-phase flow in a wellbore.

Bubbly-Slug Flow Transition

The small, near spherical bubbles agglomerate together, forming Taylor bubbles that are large enough to fill the tubing cross section. This results in the transition from bubbly flow to slug flow. If the velocity of bubbles increases, the collision frequency will go up. Based on experimental data, a gas volume fraction, f_g, that is higher than 0.25 leads to the transition to slug flow (Hasan, 1988a and Hasan, 1988b). Therefore,

$f_g = 0.25$ might be considered as the criterion for the transition between bubbly flow and slug flow. The *in-situ* gas velocity, v_g, is affected by the mixture velocity, v_m, and buoyancy due to the density difference between the liquid and gas phases. The buoyancy can be expressed by the terminal rise velocity, v_∞.

$$v_g = C_0 v_m + v_\infty \tag{85}$$

where C_0 = 1.2 suggested by references (Hasan, 1988 and Ansari, 1994), and the terminal rise velocity, v_∞, follows the Harmathy equation (Harmathy, 1960).

$$v_\infty = 1.53[g(\rho_L - \rho_g)\sigma / \rho_L^2]^{0.25} \tag{86}$$

The *in-situ* velocity is hard to be measured in reality. Thus, *in-situ* velocity is related to superficial velocity, v_{sg}, by $v_g = v_{sg} / f_g$. Then, the following expression is used for gas volume fraction in bubbly flow:

$$f_g = \frac{v_{sg}}{C_0 v_m + v_\infty} \tag{87}$$

In Equation (87), the gas fraction needs to be larger than 0.25 to reach slug flow. Therefore, the resulting expression for the transition between bubbly and slug flow is:

$$v_{sg} > (0.429 v_{sL} + 0.357 v_\infty)\sin\theta \tag{88}$$

Slug-Churn Flow Transition

In slug flow (shown in Figure 29), a number of small bubbles are distributed axially and separate the Taylor bubbles. When the gas flow rate increases, the interaction between the small bubbles and Taylor bubbles becomes significant. The transition between slug and churn flow occurs when such interaction is high enough to break up the long Taylor bubbles. Many researches have been conducted on the transition from slug flow to churn flow with empirical, semi-theoretical, and theoretical analyses (Barnea, 1987; Hasan, 1988 and Weisman, 1981). However, these studies cannot satisfy the application in the oil field. Other researcher (Brauner, 1986) proposed that the gas volume fraction cannot exceed 0.52 to maintain stable slug flow. Thus, $C_0 = 0.52$ can be used in Equation (85) and lead to the following condition for the presence of churn flow:

$$v_{sg} > 1.66 v_{sL} + 2.66 v_{\infty} \tag{89}$$

Churn-Annular Flow Transition

At a high gas flow rate, the transition from churn flow to annular flow will happen. In this research, we follow the work by Taitel and others (Taitel, 1980), which suggested that the gas flow rate must be sufficiently high to support the liquid droplets in gas flow. Otherwise, the droplets will accumulate, resulting in churn or slug flow. The minimum required velocity to keep a droplet in suspension can be determined by performing a force balance on the droplet. Therefore, this analysis leads to the following expression for the minimum gas velocity to withstand annular flow in a wellbore:

$$v_{sg} > 3.1[g\sigma(\rho_L - \rho_g)/\rho_g^2]^{0.25} \tag{90}$$

Conclusion

The general pressure loss equation (Equation (84)) is still applicable to our analysis. However, all the properties need to be changed into the properties of oil and gas mixtures as follows:

$$(\frac{dp}{dz})_T = -(\rho_m g \sin\theta + \frac{f v_m{}^2 \rho_m}{2d} + \rho_m v_m \frac{dv_m}{dz}) \tag{91}$$

The properties of mixtures depend on the gas volume fraction, and therefore are related to the flow regime. The correlations of these properties for oil and gas mixtures can be found in Appendix A. It should be noted that for a pipe with a constant cross sectional area, the liquid phase acceleration is negligible. Therefore the pressure loss due to velocity change only depends on gas phase acceleration. As a result, Equations (18) and (20) are still applicable to the analysis of multi-phase flow in wellbore.

3.3 Reservoir and Wellbore Interaction

The unified model is adopted here to describe the reservoir and wellbore interaction during the blowout events. The concept is similar to the Section 2.3.3 except that the pseudo pressure is only required for gas given its PVT relationships. Therefore, Equation (68) becomes:

$$p_{wf} = p_i - \frac{q\mu}{2\pi kh}\left\{\frac{2t_{Dw}}{r_{eD}^2} + \ln r_{eD} - \frac{3}{4} + s + 2\sum_{n=1}^{\infty}\frac{\exp(-a_n^2 t_{Dw}) J_1^2(a_n r_{eD})}{a_n^2[J_1^2(a_n r_{eD}) - J_1^2(a_n)]}\right\} \tag{92}$$

All the remaining equations are same as in Section 2.3.3.

3.4 Computational Algorithm

The offshore oil well blowout duration is divided into small segments first, then at each time step:

1. Guess a flow rate in STB/D.
2. The average reservoir pressure could be obtained based on the guessed flow rate, initial reservoir pressure, and flow rate history by Equation (82).
3. The bottomhole pressure is then calculated by Equation (92).
4. Once the bottomhole pressure is known, a bottom-to-top calculation in wellbore could be performed so that the wellhead pressure can be calculated according to Equations (91).
    a) If the wellhead pressure is not equal to the hydrostatic pressure provided by sea water, go to Step 4 b); otherwise, go to Step 4 c)
    b) If the calculated wellhead pressure is larger than the hydrostatic pressure at wellhead, the flow rate needs to be increased; otherwise, it needs to be decreased. Apply the re-guessed flow rate and repeat Step 1 to 4 a) until convergence is reached. Then go to Step 5.
    c) Go to Step 5.
5. Go to next time step.

3.5 Results and Discussion

Figure 32 shows an example of the changes of the multiphase flow patterns in the wellbore during a subsurface offshore oil blowout event. The mudline is set as 0 ft and the well depth is 12,300 ft. As can be seen, from the bottom of the well to the well depth of 7,995 ft, the gas is dissolved in the oil phase, forming a single phase flow. The reduction in pressure with the upward movement of the fluid results in bubbly flow for depths between 1,230 ft and 7,995 ft, and churn flow for the depth above 1,230 ft. Along with changes in flow patterns and decreasing pressure, gas velocity increases exponentially. The primary mechanism of such increase of gas velocity is the rapid expansion of liberated gas. The increased free gas lowers the mixture density, resulting in the increase of the mixture velocity. High fluid velocity, which favors more significant friction and kinetic energy loss, leads to the increase of the fluid pressure gradient. When the local fluid pressure is low, the decrease of mixture density is expected, which further increases the velocity and pressure gradient. Therefore, as the fluid approaches the wellhead, the gas velocity increases exponentially.

Similar to Chapter II, the reservoir and wellbore interaction model is validated with commercial software. As can be seen in Figure 33, the results from a commercial package and our blowout model shows a very good agreement, showing a smooth transition between early-time transient period and late-time pseudo steady-state at around 250 hr.

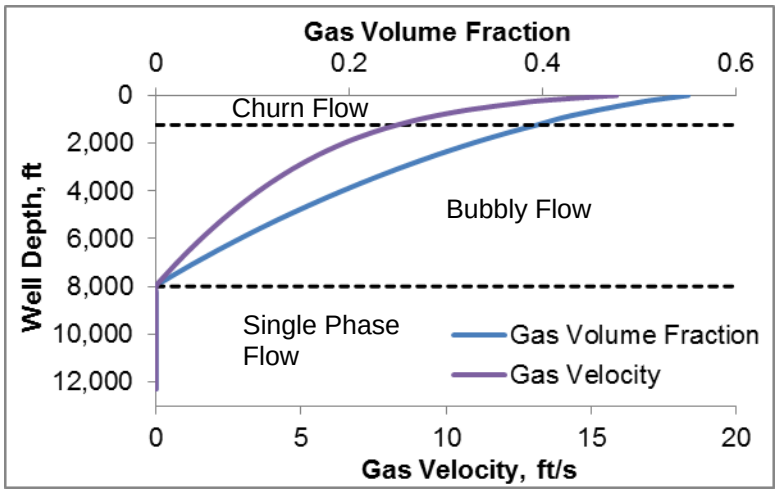

Figure 32. Multiphase fluid flow model in wellbore during blowout event

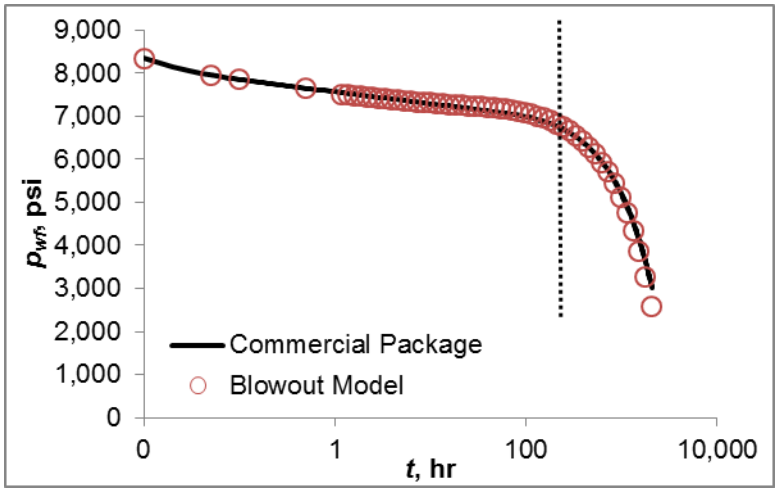

Figure 33. Constant rate drawdown test of oil reservoir

To validate the oil well blowout model presented in this dissertation, Deepwater Horizon incident is selected. The Macondo well was located in the Mississippi Canyon Block 252 of the Gulf of Mexico, 130 miles away from New Orleans. In April 20, 2010, the explosion of Deepwater Horizon drilling platform led to a blowout of the Macondo

well for 87 days, killing 11 operators. The blowout was finally capped on July 15, 2010. It is considered as one of the largest incidental marine oil spill in the history of oil and gas industry. The incident severely damaged the underwater equipment including the riser. In the beginning of the incident, there were two main leak points (Plume Calculation team, 2010). The main leak came from the broken end of the riser until the severing operations, which was far away from Blowout Preventer (BOP). After May 1, 2010, a second leak source appeared in the kinked riser above the BOP. During the incident, a number of strategies to stop the flow of oil were proposed. Since it is difficult to access the well, and the prevention operations needed to be performed at the seafloor where the temperature is low and the pressure is high, none of these strategies was successful to cap the uncontrolled release. Public started to pay attention to the accurate estimation of the magnitude of the oil and gas discharged into the environment. This information is important for evaluating the environmental consequences of oil and gas release, developing proper control strategies and evaluating the liability of the operating companies for the environmental damage.

The oil spill caused by Macondo incident was only collected up to 25,000 barrels per day by surface ships during the latter portion of the incident. The actual release observed from the bottom of the sea by camera was higher than the collection rate. Therefore, estimation of volume of oil discharged cannot rely on the collection data. Different government agencies, researchers, and companies calculated the blowout rate of Macondo well by various techniques. Some of the examples are shown in Table 5.

Table 5. Example of blowout rate estimations for Macondo incident (Plume Calculation Team, 2010 and DOI 2011)

Estimation techniques	Estimation of blowout rate (STB/D)
Using probability distributions to model the uncertainty implied in experts' assessment	46,000
Analysis of videos of discharging flow	45,000
Analysis of videos of discharging flow	30,000 to 40,000
Analysis of videos of discharging flow	68000
Measuring oil jet velocities using manual Feature Tracking Velocimetry	$61{,}000 \pm 15{,}000$
Analyzing the velocity profile and trajectory profile of oil leak jets using established theory of turbulent jets	89,000 with a range of 62,000 to 116,000
Simulating the trajectory of a buoyant oil leak jet using computational fluid dynamics	55,000 to 70,200
Acoustics analysis	60,000
Reservoir modeling from 3-D seismic data	27,000 to 102,000
Well modeling	30,000 to 118,000

Oldenburg *et al.* (2012) used the software of T2Well and iTOUGH2 to couple the reservoir/wellbore flow to estimate the initial blowout rate for the Macondo well. They concluded that the most likely initial oil flow rate was 105,000 bbl/day assuming

100 ft of penetration depth. 500 Monte Carlo simulations were carried out to analyze the uncertainties of the reservoir and fluid properties. They found that the initial flow rate was strongly sensitive to the reservoir permeability. Table 6 shows the parameters in Oldenburg's model. These parameters are used as the inputs for the oil blowout model presented in this dissertation to examine its validity.

Table 6. Parameters used in Oldenburg study (2012)

Parameters	Value
Temperature at the sea floor	41 ℉
Depth to the sea floor	5,067 ft
Pressure at the sea floor	2,241 psia
Length of 9 7⁄8 in casing	7,700 ft
ID of 9 7⁄8 in casing	8.6 in
Length of 7 ½ in casing	5,500 ft
ID of 7 ½ in casing	6.1 in
Depth below sea floor	13,300 ft
Thickness	100 ft
Porosity	22%
Permeability	500 md

Table 6. Continued

Parameters	Value
Pressure	12,000 psia
Temperature	260 ℉
Oil gravity	35 API
Gas-oil ratio	3000 scf/bbl
Gas gravity	0.8

Figure 34 shows the results of the oil well blowout model based on Oldenburg's data. The initial blowout rate, as can be seen, is 109,511 bbl/day, shwoing a very good agreement with Oldenburg's estimation with only 4% difference. This obtained initial blowout rate also agrees with the BP internal documents that estimates the initial blowout rate for hypothetical worst-case could reach about 100,000 bbl/day (DOJ, 2012). The advantage of the oil well blowout analysis presented here is that it is an integrated tool that couples reservoir and wellbore together, so that no separate tools are needed. This convenience also enables us to calculate the dynamic blowout rate. Due to the reservoir pressure depletion, the simulation shows that the blowout rate at the end of the Macondo incident drops down to 52,039 bbl/day, and the total amount of discharge reaches over 6.25 million barrels of oil.

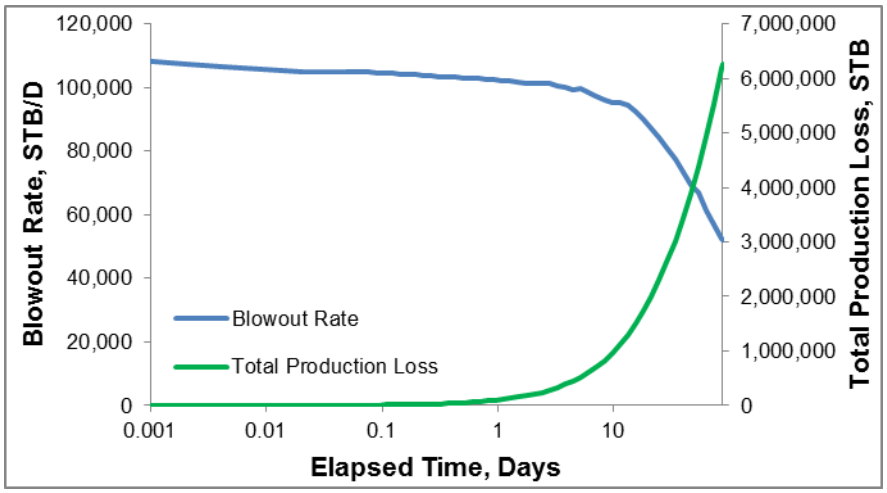

Figure 34. Blowout rate and total production loss for Macondo well

However, all the above estimations are based on the worst-case scenarios, and several conservative assumptions, such as no BOP restriction at wellhead, maximizes the blowout rate. BP, during the Macondo incident, measured the flowing pressure above and below the BOP, and concluded that 850 psig pressure was applied to the flow at wellhead due to the BOP restriction and additional 400 psig was created by other flow restrictions. Therefore, a more realistic wellhead flowing pressure would be 3,491 psig. Figure 35 shows the blowout rate and total discharge amount profile when such restrictions are taken into account. As can be seen, the initial blowout rate decreases to 96,807 bbls/d and the total discharge amount drops to 5.41 million barrels.

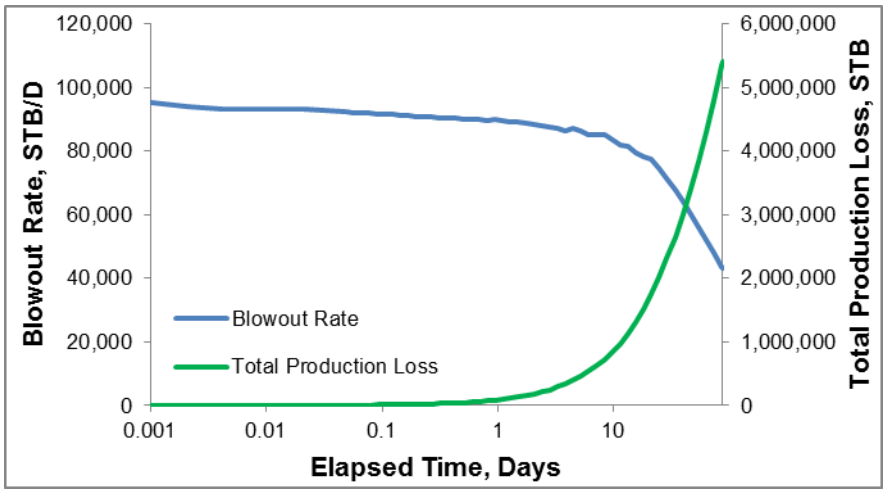

Figure 35. Blowout rate and total production loss considering BOP restriction

Similar to Section 2.5, a folded-Plackett-Burman design of experiments is performed to determine the significance of each independent variable. The variables selected here include the permeability, formation thickness, initial reservoir pressure, and reservoir radius. Three levels (*i.e.*, low, medium, and high) are assigned for each of the variables, as shown in Table 7. Total amount of discharge during an 87 days blowout constituted the dependent variable. Figure 36 presents the Pareto chart of this analysis, signifying that permeability is the most important variable. The vertical line defines the results within the 95% confidence interval. This finding also matches the conclusion of the Oldenburg study.

Table 7. Independent variables variation for design of experiments

	Low	Medium	High
Formation thickness, ft	80	100	120
Initial reservoir pressure, psia	9,600	12,000	14,400
Reservoir radius, ft	2,886	3,608	4,330
Permeability, md	400	500	600

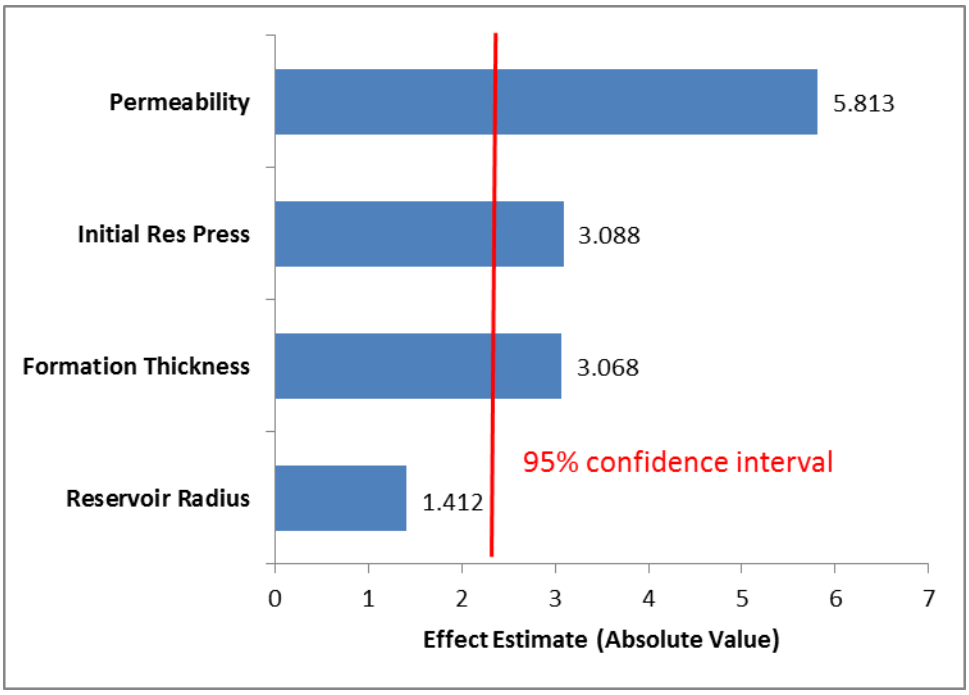

Figure 36. Pareto chart of total discharge amount of oil well blowout for folded-Packett-Burman design

3.6 Conclusions

The oil well blowout mechanism and physics are evaluated in this chapter. The behavior of multi-phase flow is implemented into the consequence model to accurately estimate the blowout rate and total discharge amount based on a well-established

computational algorithm. The model shows that under different pressure and temperature, the oil and gas phases could form bubbly flow, slug flow, churn flow or even annular flow. The results of the model are compared with other studies for the Macondo incident and show a good agreement. The statistical analysis identifies the independent variables responsible for the maximum discharge; reservoir permeability, initial reservoir pressure and the formation thickness are the key variables. Among these three variables, the blowout rate and total discharge amount is strongly sensitive to the change of permeability. The model could serve as the basis of the risk assessment of blowout events which are discussed in later chapters.

CHAPTER IV

PREVENTION AND MITIGATION OF BLOWOUT EVENTS[2]

The definition of prevention is (CCPS, 2016):

"*The process of eliminating or preventing the hazards or risks associated with a particular activity. Prevention is sometimes used to describe actions taken in advance to reduce the likelihood of an undesired event.*"

The definition of mitigation is (CCPS, 2016):

"*Lessening the risk of an incident event sequence by acting on the source in a preventive way by reducing the likelihood of occurrence of the event, or in a protective way by reducing the magnitude of the event and/or the exposure of local persons or property.*"

As can be seen, the prevention and mitigation are always associated with the likelihood and consequence of an incident event. Although a number of techniques, such as Bow-Tie and Layer of Protection Analysis (LOPA), could qualitatively or semi-quantitatively evaluate prevention and mitigation actions, the quantitative determination of the prevention and mitigation measurements effectiveness requires a comprehensive understanding to the risk associated with blowout events. In this section, both consequence- and risk-based assessment of blowout events are presented. The

[2] Part of this chapter is reprinted with permission from "Flow rate and total discharge estimation in gas-well blowouts" by Liu, R., Hasan, A. R. and Mannan, M. S. (2015). *Journal of Natural Gas Science and Engineering*, 26, 438-445. Copyright 2015 Elsevier.

effectiveness of the prevention and mitigation measurements and the risk reduction plan are discussed as well.

4.1 Consequence-based Assessment of Blowout Events

When a blowout happens, significant amount of fluid will be spewed out of the wellbore. Hydrocarbons coming out of the wellbore are flammable and hazardous. Thus, during an onshore blowout one of the following scenarios may play out given different conditions:

- In the absence of an ignition source, the gas will disperse to the surroundings; the dispersion will be influenced by the wind speed. The toxicity, plume dispersion, and the consequent hazard need to be investigated.
- In the presence of an ignition source, the gas/air mixture may ignite and result in jet fires and explosions. To evaluate fire and explosion hazards, we used heat flux intensity associated with jet fire and overpressure caused by explosion.

Such hazardous scenarios are the major concerns for the personnel on the offshore platforms, or the surrounding population near the onshore wells. In the following section, an onshore sour gas well blowout is used an example to illustrate the consequence-based assessment to the blowout event.

4.1.1 Plume Boundary

To fully appreciate and quantify the risks associated with these hazards, we need to understand the details of a blowout. The methodology presented in this dissertation

provides an opportunity for all concerned to capture the evolution of blowout events under different operational conditions. The quantitative assessment of the risk related to blowout can also help the operational personnel to make the right decisions at right time.

In the absence of ignition, a plume will form because of the dispersion of toxic/flammable gas. The shape of the plume depends on the wind speed and buoyancy effect. To gain a better understanding of the plume evolution, we considered low (9.8 ft/sec), moderate (16.4 ft/sec), and strong (26.2 ft/sec) wind speeds to study the shape of the plume. The blowout is similar to the leak of a high-pressure tank to some extent. The blowout rate is the source-term on ground. If we assume that the blowout rate remains constant in short time period, the concentration of gas released in the plume is given by the following expression given by Crowl (Crowl, 2011):

$$< C > (x, y, z) = \frac{Q_m}{2\pi x\sqrt{K_x K_y}} \exp\left[-\frac{v}{4x}\left(\frac{y^2}{K_y} + \frac{z^2}{K_z}\right)\right] \tag{93}$$

Given that the preparedness and emergency response may be insufficient at the event's inception, the first hour of a blowout event is considered. As the base case, we use the field data in Kikani's work (Kikani, 1996) and assume the blowout rate to be constant in each time segment. Table 8 shows the blowout rate change within each time interval.

Table 8. Blowout rate change within time based on field example

Time (Hours)	Blowout Rate (MMscf/D)
0-0.1	48.0
0.1-0.5	41.3
0.5-1	38.8

Figure 37, Figure 38, and Figure 39 show the evolution of the plume under different wind speeds generated with a commercial software package PHAST (OGP, 2010). This software package is a hazard-analysis tool that is often used by the chemical process industries, but is not very well known in the upstream side of the petroleum industry. The software can be used to model different scenarios, those involving discharge and dispersion, flammable situations, and explosions. Conservations of mass and momentum constitute the centerline of the dispersion plume. Gaussian distribution is then applied at centerline to determine the concentration and width of the plume. Overall, this tool adopts a unified modeling approach capturing jet, and heavy and passive phases.

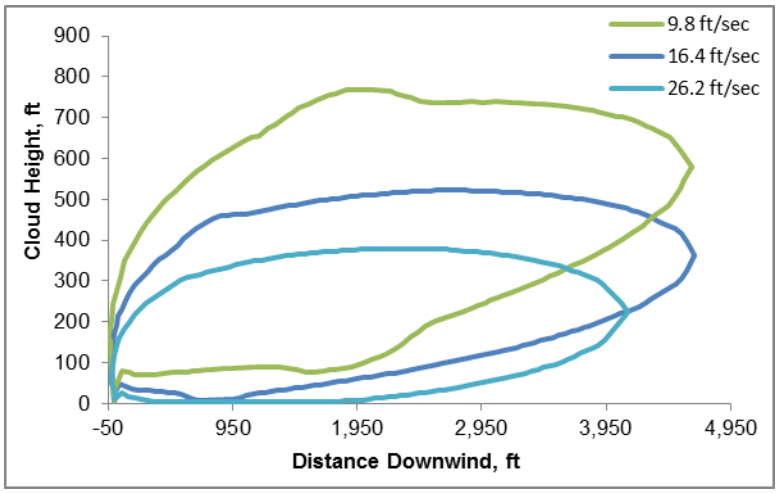

Figure 37. Side view of plume caused by gas well blowout after 360 seconds

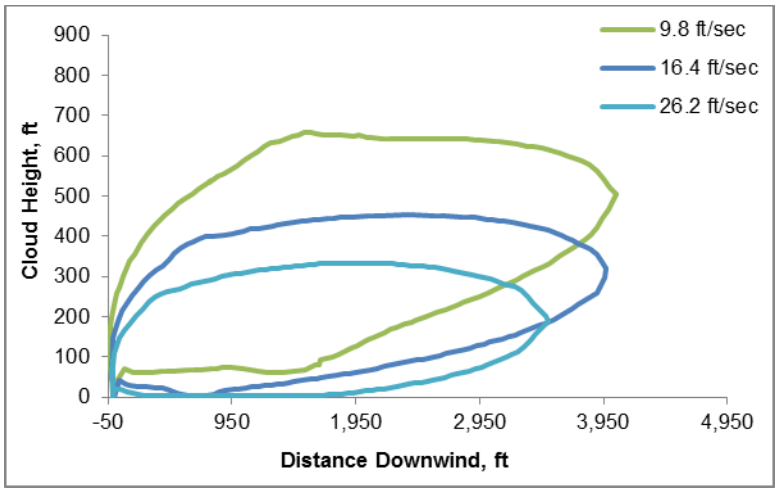

Figure 38. Side view of plume caused by gas well blowout after 1,800 seconds

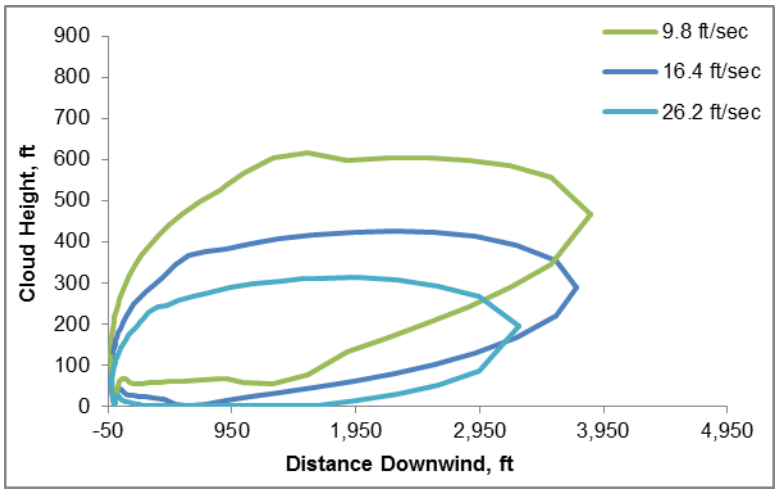

Figure 39. Side view of plume caused by gas well blowout after 3,600 seconds

Figure 37 through Figure 39 illustrate the plume boundary wherein the concentration of gas is 100 ppm. Note that the top of the plume is higher for the low wind speed situation than others because of the buoyancy effect. At higher speeds, the buoyancy effect is reduced and the plume begins to descend onto the ground, causing health and safety concerns for personnel in the area. Thus, the mixing effect of released gas and air is enhanced with the increase of wind speed. Therefore, the plume affects larger area in low wind speed compared to the strong wind situations. In contrast, the decreasing blowout rate causes the shrinkage of the plume as can be observed in Figure 38 and Figure 39. The plume could reach up to 4,700 feet away from the blowout location, prompting the need for evacuation of the residents and personnel in that area.

4.1.2 Explosions

When there is an ignition source near the wellbore, the gas/air mixture may be ignited, leading to explosion and fire. The explosion of gas leads to a reaction front moving away from the ignition source, accompanied by a shock wave. Even when the reaction material is exhausted, the movement of the shock wave does not stop. The pressure resulting from the shock wave over normal atmospheric pressure is called overpressure. Overpressure is an important characterization of the consequence of an explosion. Table 9 shows the damage to common structures based on overpressure, following the work of Clancey (1972).

Table 9. Damage estimates for common structures based on overpressure

Overpressure (psi)	Damage
10	Total destruction of buildings
5-7	Nearly complete destruction of houses
2	Partial collapse of walls and roofs of houses
0.3	"Safe distance" 95% probability of no serious damage
0.03	Occasional breaking of large glass windows already under strain

Here, we used TNT equivalency method to evaluate the overpressure situation. The equivalent mass of TNT is first calculated:

$$m_{TNT} = \frac{\eta m \Delta H_c}{E_{TNT}} \tag{94}$$

In Equation (94), E_{TNT} denotes the energy of explosion of TNT, which typically equals to 2,016 Btu/lbm. The overpressure can be empirically estimated by the equivalent mas of TNT and the distance from the explosion point based on the experiments of explosives (Glasstone, 1962 and Baker, 1973):

$$\frac{p_o}{p_a} = \frac{1616\left[1+\left(\frac{z_e}{4.5}\right)^2\right]}{\sqrt{1+\left(\frac{z_e}{0.048}\right)^2}\sqrt{1+\left(\frac{z_e}{0.32}\right)^2}\sqrt{1+\left(\frac{z_e}{1.35}\right)^2}} \tag{95}$$

where

$$z_e = \frac{r}{m_{TNT}^{1/3}} \tag{96}$$

When the effect of explosion is evaluated conservatively, the realistic worst-case scenario is always considered, meaning that the ignition source is present right after the initiation of blowout. During this period the plume of the released gas has the largest volume, leading to the largest area affected by of explosion. Figure 40 presents the worst-case scenario of the explosion when the ignition source is 5 ft away from the well. The circle indicates an overpressure of 0.3 psi, which is considered a safety limitation to buildings and personnel. Any buildings and personnel inside the circle will be in danger if explosion occurred soon after the blowout event. As Figure 40 shows, distance of 150 ft away from the blowout source is covered by the overpressure higher than 0.3 psi when the wind speed is 9.8 ft/sec. With the increase of wind speed, the unsafe area becomes smaller.

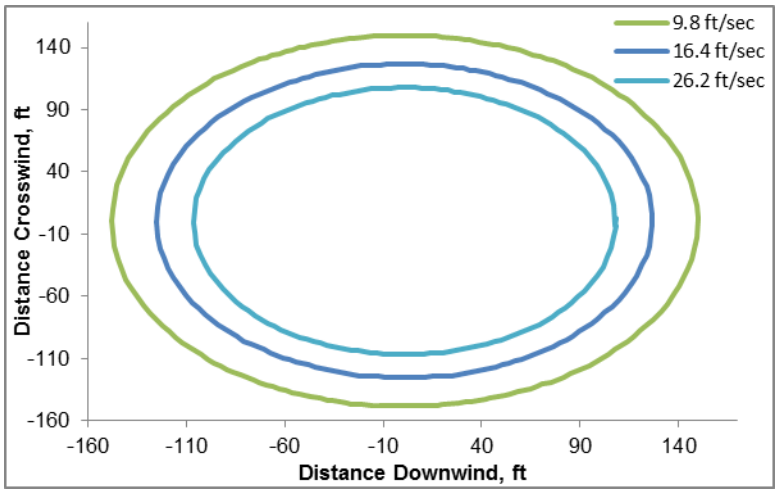

Figure 40. Late explosion or worst-case scenario caused by blowout incident

4.1.3 Jet Fire

In addition to explosions, a gas well blowout could lead to jet fire. A jet fire is a flame with turbulent diffusion owing to the combustion of continuous released hydrocarbon gas in a particular direction. Many of the jet fires are followed by explosion. The jet fires may occur right after the blowout incident in presence of an ignition source. In that case, the radiation generated by jet fire must be taken into account. HSE (2004) suggested that personnel are able to survive and escape from the exposure to heat flux less than 1,584 Btu/hr-ft^2. Figure 41 shows the safe distance for personnel in presence of a jet fire resulting from the blowout incident. The circles indicate the heat flux of 1,584 Btu/hr-ft^2 under different wind speeds. When wind speed increases, the circle starts to shift in the direction of wind and the affected area depends on the shape of the plume.

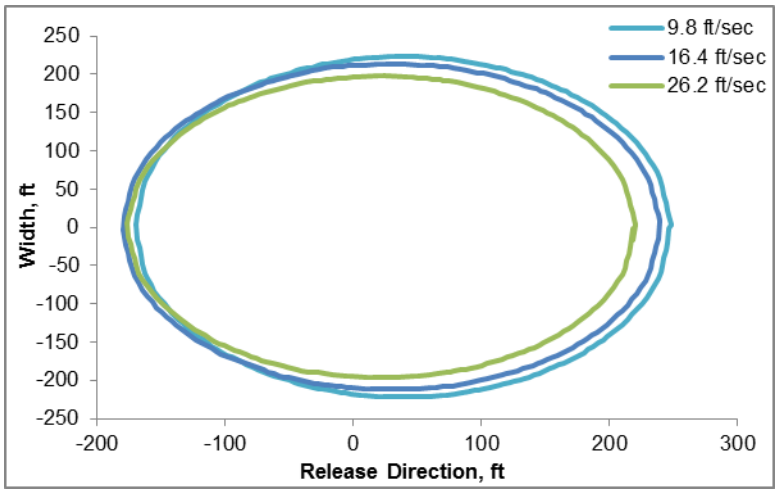

Figure 41. Heat flux intensity radius for jet fire caused by blowout incident

4.1.4 Discussion

Compared to the WCD scenarios, this methodology, as a consequence-based approach, provides more realistic worst-case scenario assessment. The areas which could be potentially affected by the blowout events need to be taken into consideration during the selection of drilling locations. Minimum population should be allowed in such area with proper toxic/flammable gas sensors and appropriate emergency response plan, to avoid tragedies like Kaixian gas well blowout from happening again.

In addition, using PHAST to evaluate the impacted area is only one of the options. PHAST is specialized to model dispersion behavior in open field. One of the important assumptions is that it does not consider the obstruction effect of the trees, hills, and buildings. Such assumption leads to a conservative assessment of the consequence of the blowout events. If more accurate results are desired, the detailed surrounding neighborhood information and CFD tools should be used.

Moreover, the wind is assumed to be from one direction only since no probability distribution is considered in the consequence-based approach. In the real application, the wind direction should always be towards the direction that could result in the most severe consequences.

In this section, TNT equivalent approach is adopted to evaluate the consequence of the potential explosions due to the gas well blowout. When lacking other information, TNT equivalent model is usually used to estimate the energy of the explosion. However, literature reveals that TNT equivalent model always estimates higher peak overpressure in the near field, and lower in the far field compared to other models (Mannan, 2012). In other words, TNT equivalent model is conservative in the near field and not conservative in the far field. Additional methods are also available in PHAST if more information of the surroundings of the site could be provided such as TNO multi-energy model or Baker-Strehlow-Tang (BST) model.

4.2 Risk-Based Assessment of Blowout Events

The risk-based assessment of blowout events can quantitatively determine the blowout risk for the wells not only in the planning phase but also in the operational phase. A well-established blowout consequence model couples the nature of transient-fluid flow in the reservoir and the fluid and heat flows in the wellbore. Combining the consequence model and the uncertainties from both historical database and well-specific parameters provide great opportunities to understand and manage the blowout risk. In addition, a case study is presented to demonstrate how this method could be practically

applied in typical industrial settings. The risk reduction plan is also discussed in the later sections by statistical and sensitivity analysis.

4.2.1 Methodology

Blowout events, categorized into three groups – surface blowout, subsurface blowout and underground blowouts – could occur during various offshore operations. This research focuses on the subsurface blowout as it imposes greatest impact to the marine environment. The NORSOK Standard D-010 (NORSOK, 2004) requires two independent barriers to be present during all well operations. The primary barrier is typically the drilling mud that could balance the pore pressure, while casing, cement, BOP and other associated equipment are generally considered as the secondary barriers. Here the investigation of interest is how the secondary barriers could affect the offshore drilling well blowout risk, as we assume that the blowout incident has happened, indicating the failure of primary barrier.

It is a common practice to acquire historical data and statistics from the database for the purpose of risk assessment study. SINTEF (2013) database documents blowout occurrence information, including locations, type of operation when blowout happens, well configurations, types of blowout, consequences and so on. The database is updated and an annual report is issued every year. Scandpower summarizes the SINTEF database and issues Blowout and Well Release Frequencies Report Based on SINTEF Offshore Blowout Database. Such databases are considered the main information source when

conducting Environmental Risk Analysis and Quantitative Risk Assessments of blowout events.

However, the basic idea of historical generic data is to normalize all the information of well blowout events to provide representative cases for the study purpose. These databases, therefore, lose the uniqueness that each well has. The consequences of a blowout event depends on specific reservoir conditions, operations, and well configurations. The risk level associated with each well is unique due to such factors, which cannot be reflected in the generic data. More importantly, the representative case provides only the frequency of blowout based on the historical data, but gives very limited consideration to the blowout risk reduction and mitigation measures. Thus, we propose a "hybrid" risk model in this paper, which takes not only the historical incident statistics but also the unique information of the well (*i.e.*, geographical uncertainties, well configuration and the types of operations) into account.

Generic Data

Many parameters influence the consequences of well blowouts; these variables can be obtained from historical database. Here we select some important ones including: blowout duration, blowout path, and BOP restriction.

Various efforts, such as bridging, crew intervention, capping, and drilling the relief wells, could terminate a blowout incident. These actions require differing amount of time to be implemented and activated. For example, natural bridging may only take several days to self-kill the blowout, while drilling a relief well might need about 75

days (ACONA, 2012). Figure 42 shows the cumulative probability of blowout duration taking all the control methods into account based on the SINTEF database.

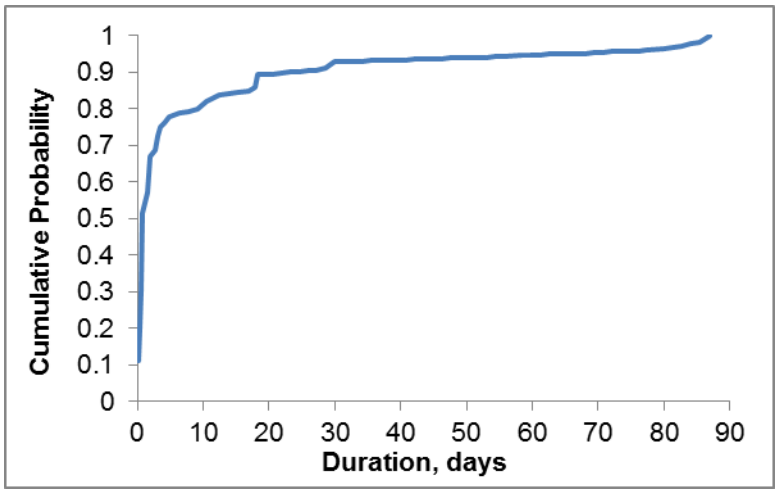

Figure 42. Cumulative probability of blowout duration from SINTEF database

The probability of blowout duration is calculated by a conservative approach. The upper bound of each range is selected as the representative duration, except for the duration larger than 14 days. The probability distribution of blowout duration is shown in the table below.

Table 10. Probability distribution of blowout durations

Duration Range (days)	<2	2-14	>14
Representative duration (days)	2	14	50
Probability	0.67	0.17	0.16

As mentioned earlier, once blowout occurs, the fluid could flow through the drill string, the annulus, or the open hole, depending on the BOP status and the position of drill string. Among these three paths, the flow through annulus is considered as the most likely scenario. When the pore pressure is predicted inaccurately, and the primary barrier is compromised, the influx of hydrocarbons from high pressure payzone would occur through the annulus. In addition, the swabbing effect – pulling the drill string out of the borehole – could decrease wellbore pressure, possibly allowing a blowout with the hydrocarbons flow through the annulus. The flow through drill strings requires not only the influx from the reservoir, but also the failure of drill string safety valve which is one of the barriers to prevent back flow in drill string. In addition, it is unlikely that the hydrocarbons would flow through the drilling string due to the downward influx of the drilling fluid. Moreover, when a possible hydrocarbon influx happens without the presence of drill strings in the wellbore (*e.g.*, when completely pulled out of the wellbore), an open hole blowout event could occur. But taking the well-maintained drilling fluid weight into consideration, this scenario is in general unlikely. The table below provides the flow path probability distribution during drilling operation according to the SINTEF database.

Table 11. Probability distribution of blowout flow paths

Flow Path	Probability
Drilling String	0.06
Annulus	0.88
Open Hole	0.06

BOP, as one of the secondary barriers, is considered as highly reliable equipment with several independent rams inside. The risk of a total failure of a BOP, therefore, would be low. However, once a blowout occurs, it is obvious that the BOP has either completely or partially failed. The probability of BOP partially functioning is assumed to be 0.7, while the probability of complete failure of BOP is 0.3 based on the OLF guidelines (OLF, 2004). When the BOP only closes partly, the opening fraction of BOP is assumed to be 5%.

Well Specific Parameter

Each well is specific in terms of geographical information and well configurations. The geographical information investigated here includes reservoir pressure, porosity, permeability and so forth. Different tubing and casing diameters and the penetration depths could be readily handled in our blowout simulation tool. The reservoir pressure that can be obtained dynamically with the progress of drilling activities is not considered as an uncertainty in this model, but as an important input to determine the blowout behaviors. The porosity and permeability information relies on the seismic data and generally becomes available with significant uncertainties. The distributions of such highly location dependent parameters are discussed in the case study in later section.

Scenario Probability

Combining the multiple uncertainties distribution discussed above, the spectrum of blowout scenarios with different ranges of potential blowout rate and total discharge amount could be estimated. Each blowout scenario accompanies a unique probability depending on the assumptions of the probability distribution and availability of geographical data. The sum of the probability associated with each scenario equals one. Figure 43 presents some of the potential blowout scenarios and how the potential blowout scenarios are determined. It should be noted that the probability distributions of porosity and permeability is only for illustrative purpose, and these distributions should be obtained specifically depending on the locations of the wells. Our method provides opportunities to combine generic historical data with well specific uncertainties. One potential blowout scenario probability is calculated by multiplying the conditional probabilities. For example, when hydrocarbons flow through high porosity and low permeability formation, leading to a blowout through drill string for 2 days with the completed failure of BOP, the probability of this scenario would be: $P = 0.06 \times 0.67 \times 0.3 \times 0.21 \times 0.29 = 0.000734$.

The dynamic blowout rate and total amount of oil spill could be calculated for each potential blowout scenario. The product summation of the total amount of oil spill and corresponding probability yields the well specific blowout risk. This serves as the base case for the further barrier effectiveness and risk reduction studies.

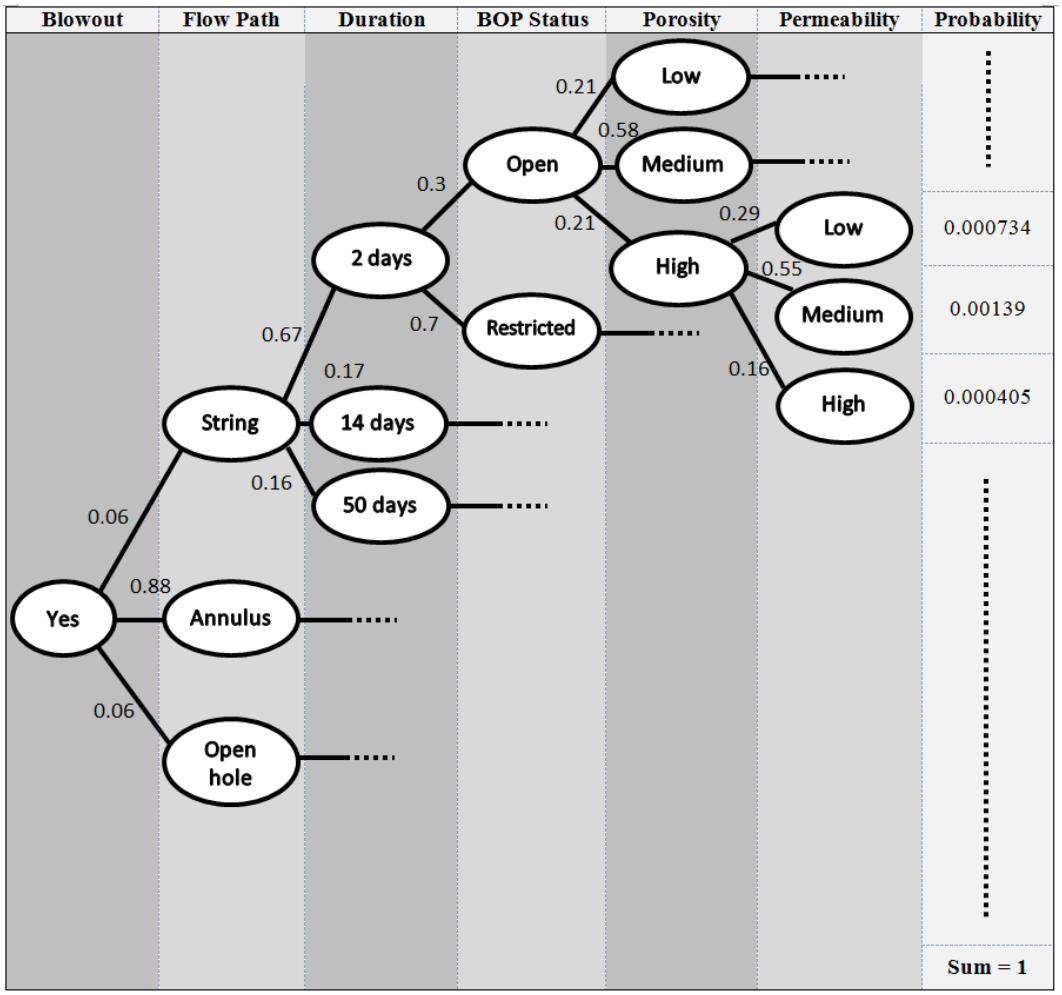

Figure 43. Illustration of scenario probability calculation for blowout risk

4.2.2 Case Study

In this section we present a case study using the flow modeling simulator we have developed combined with the generic and specific probabilities to illustrate how this approach could be practically used in the industry application. As discussed above, the geographical uncertainties such as permeability and porosity are dependent on the location of wells. Figure 44 and Figure 45 show the porosity and permeability

distribution at two offshore wells in the Bredasdrop Basin located near the south coast of South Africa (Hanson Mbi, 2006). Three levels of porosity are selected (*i.e.*, low, medium and high) with respect to the probability distribution as shown in Table 12. Clear dependency between the porosity and permeability could be observed from Figure 44 and Figure 45. Therefore, the probability distribution of permeability is determined at each level of porosity separately. As shown in Table 13, at low and medium level of porosity, due to lack of enough data points, only two levels are selected for permeability (*i.e.*, low and high), and three levels (*i.e.* low, medium and high) are identified at high level of porosity. Both parameters are weighted averaged at each level and such averages serve as the representative values for the potential blowout scenarios.

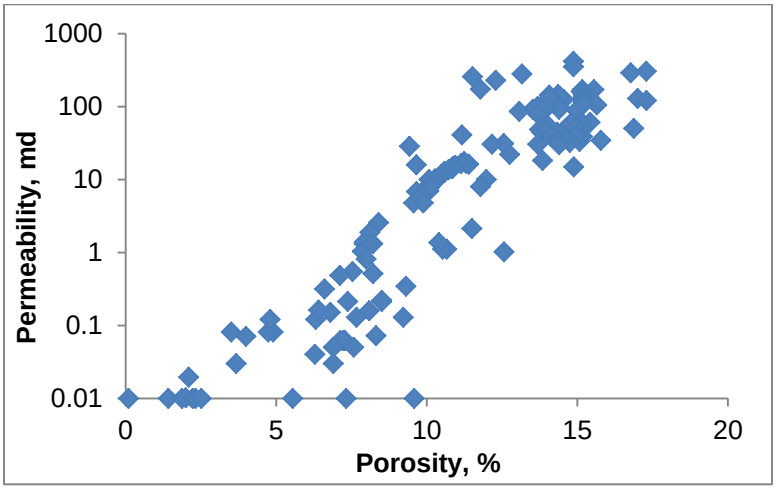

Figure 44. Porosity-permeability scatter plot for well E-AD1

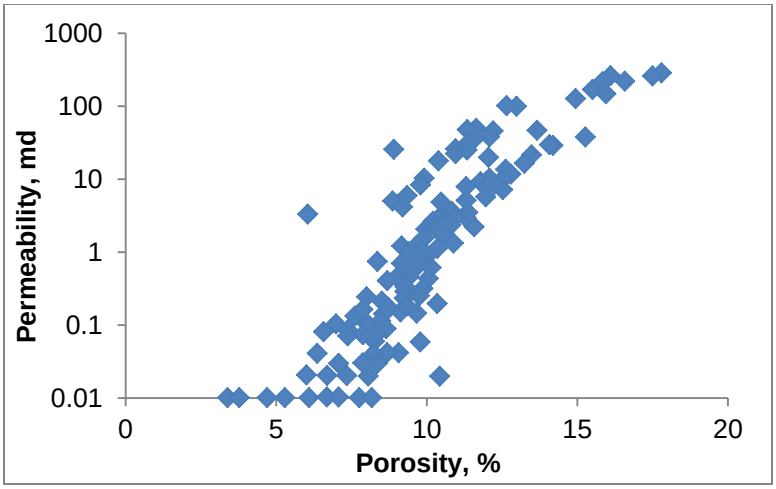

Figure 45. Porosity-permeability scatter plot for Well E-CA1

Table 12. Representative values and probability of porosity for wells at Bredasdrop Basin

Porosity Level	Min. Value (%)	Max. Value (%)	Weighted Average (%)	Probability
Low	0	8	5.8	0.21
Medium	8	14	10.6	0.58
High	14	18	15.3	0.21

Table 13. Representative values and probability of permeability for wells at Bredasdrop Basin

Porosity Level	Permeability Level	Min. Value (md)	Max. Value (md)	Weighted Average (md)	Probability
Low	Low	0	0.1	0.05	0.70
	High	0.1	4	0.8	0.30
Medium	Low	0	10	5.0	0.63
	High	10	275	49.3	0.37
High	Low	10	50	35.6	0.29
	Medium	50	200	112.5	0.55
	High	200	450	297.2	0.16

The wellbore and reservoir in the case study are hypothetical but based on the typical parameter values used in practice. The well and reservoir parameters are presented in Table 14. A total of 126 potential blowout scenarios are established with unique probabilities to include all the variations of the uncertainties discussed above. Although the reservoir pressure and penetration depth are considered as inputs in this case, real-time measurements of these parameters could be dynamically updated to reflect accurate risk results in real field application.

Table 14. Parameter used in case study

Parameters	Value
Water Depth, ft	4,911
Well Depth, ft	12,300
Casing Inner Diameter, in	9
Drill String Inner Diameter, in	3.5
Penetration Depth, ft	100
Reservoir Radius, ft	3,608
Reservoir Pressure, psia	11,856
Reservoir Temperature, °F	276.8
Oil gravity, API	35
Gas-oil ratio, scf/bbl	1,600
Gas gravity	0.83

After simulating all the potential blowout scenarios, the results are rounded up and the probabilities of similar results are combined together to reflect the major contributors to the blowout probability. As can be seen in Figure 46, the minimal amount of potential oil spill is about 200 bbls, while the maximum oil spill could potentially reach 1.3 million bbls. The total risk of potential oil spill for this hypothetical well is around 40,000 bbls. Figure 46 also indicates that the tragedy like Macondo incident, in which the total amount of production discharge is in the millions of barrels, belongs to the category of high-consequence and low-probability event.

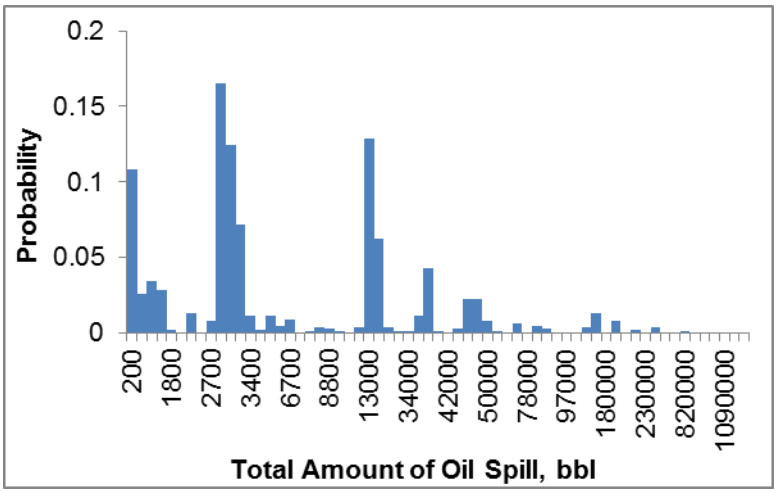

Figure 46. Probability and total amount of oil spill for all potential blowout scenarios

4.2.3 Prevention and Mitigation

Understanding Significance of Uncertainties

Figure 46 presents a comprehensive picture of potential blowout risk. The effects of uncertainties in the blowout risk, however, are not fully demonstrated. It is important to quantify the significance of the uncertainties so that the appropriate barriers could be added or enhanced to better manage the blowout risk. The folded-Plackett-Burman design of experiments (Wolff, 2010) is adopted here to understand how the uncertainties would affect the risk results. This method captures both nonlinearities and interactions between the uncertainties. Only the uncertainties, including blowout duration, flow path and BOP status that could be reduced by prevention or mitigation barriers are selected to guide the barrier management strategies. Three levels – low, medium, and high – are assigned to each uncertainty. The weighted average of the oil spill amount, taking uncertainties both from generic data and well-specific parameters into account, serves as

the dependent variable. Figure 47 shows the Pareto chart of this analysis, indicating that all the uncertainties are important to the total blowout risk. The vertical line defines the results within the 95% confidence interval. Compared to the single WCD value, this method enables operators to identify and manage the important barriers to better control the risk associated with the uncontrolled wellbore flow events. For example, as indicated in Figure 47, blowout duration is important to determine the blowout risk. Operators can only accurately estimate the potential amount of the oil discharge by coupling the blowout duration with the dynamic blowout rate, and therefore could demonstrate the blowout risk of their planning wells and manage the risk to the acceptable level.

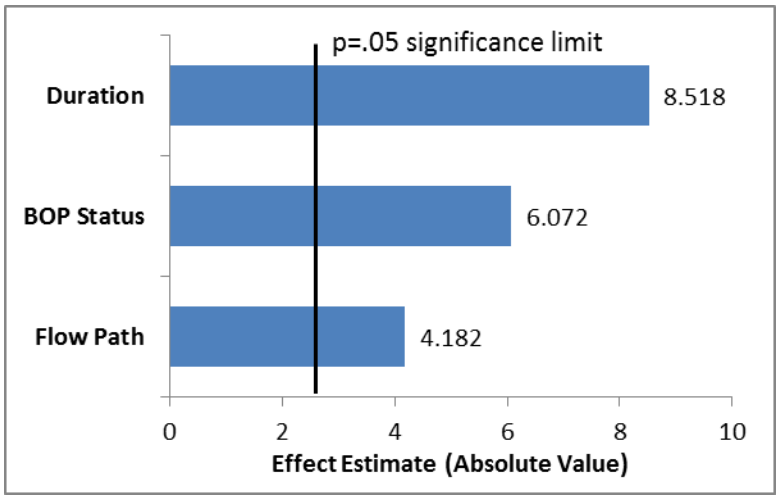

Figure 47. Pareto chart for folded-Packett-Burman design

Values of Barriers

For the purpose of barrier management, evaluating the values of the barriers could help to reasonably allocate limited resources to enhance the safety performance. The blowout risk assessment in this paper provides operators a great opportunity to identify the important barriers. When a barrier is added or removed, the total risk of blowout will change accordingly. For example, as shown in Figure 48, assuming additional blind rams could completely prevent the open hole blowout from happening, the total risk is reduced by 3.1%. On the other hand, missing drill string safety valve could fail to stop the hydrocarbon flow through tubing, leading to an open hole blowout with higher probability. Figure 48 indicates that missing drill string safety valve could result in an increase of total blowout risk by 4.9%. Another example illustrated by Figure 49 is that the risk could be reduced by up to 67.5% when the BOP complete failure probability decreases from 30% for the base case to 0% for an ideal case. An effective maintenance and inspection program for BOP system is required to reduce the BOP complete failure probability.

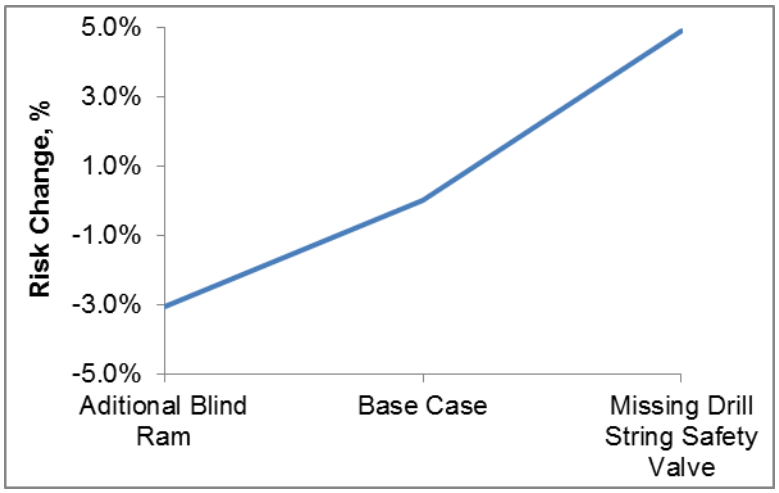

Figure 48. Example of risk change when adding or removing barriers

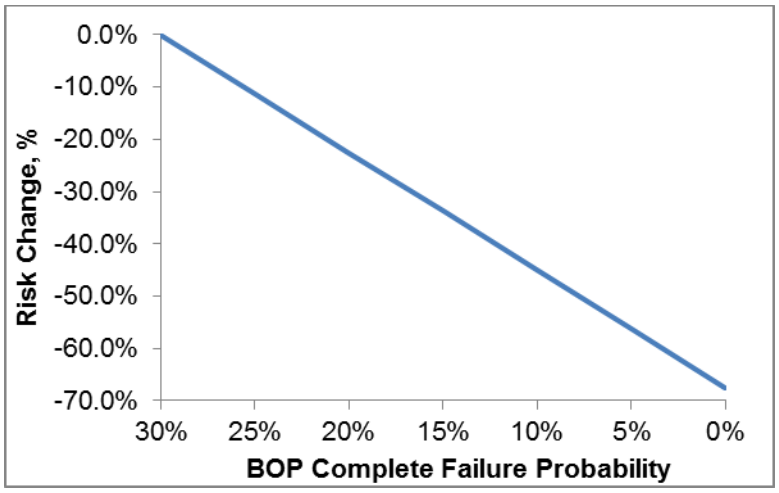

Figure 49. Example of effect of BOP maintenance and inspection to blowout risk

Risk Reduction Plan

Figure 46 also provides valuable information to identify the major risk contributors. The smaller spills do not contribute significantly to the blowout risk although their probabilities are high. Table 15 shows the all the risk contributors to the

total blowout risk for this case. As can be seen, most of the major risk contributors are associated with long blowout duration and complete failure of BOP with significant amount of oil spill over 100,000 bbls. The only exception can be found at the risk contributor (No. 4) with less severe consequence but much higher probability. It indicates that identification of major risk contributors cannot solely rely on the determination of consequence or probability, and hence a comprehensive risk assessment is needed. Table 15 also suggests that the risk reduction plan, as a part of the risk assessment study, should focus on reducing the likelihood or the consequences of such hazardous scenarios.

Table 15. Risk contributors to total blowout risk in case study

Risk Ranking	Scenarios					Total Spill (bbl)	Probability	Risk Contribution
	Flow Path	Duration (days)	BOP Opening Fraction	Porosity (%)	Perm. (md)			
1	Annulus	50	100%	10.6	49.3	816428	0.009065	18.8445%
2	Annulus	50	100%	15.3	112.5	994439	0.004879	12.3537%
3	Annulus	50	100%	10.6	5	236995	0.015434	9.3142%
4	Annulus	50	5%	10.6	5	66811	0.036014	6.1267%
5	Annulus	50	100%	15.3	35.6	776430	0.002572	5.0858%
6	Annulus	50	5%	10.6	49.3	78181	0.021151	4.2106%
7	Annulus	9	100%	10.6	49.3	166413	0.009631	4.0811%
8	Annulus	50	100%	15.3	297.2	1082677	0.001419	3.9127%
9	Annulus	2	100%	10.6	49.3	38478	0.037958	3.7191%
10	Annulus	9	100%	15.3	112.5	198756	0.005184	2.6234%
11	Annulus	2	100%	15.3	112.5	45341	0.02043	2.3586%
12	Annulus	50	5%	15.3	112.5	79064	0.011384	2.2918%
13	Annulus	9	100%	10.6	5	48561	0.016399	2.0278%
14	Annulus	2	100%	10.6	5	12087	0.064632	1.9892%
15	Open hole	50	100%	10.6	49.3	926884	0.000618	1.4587%

Table 15. Continued

Risk Ranking	Scenarios					Total Spill (bbl)	Probability	Risk Contribution
	Flow Path	Duration (days)	BOP Opening Fraction	Porosity (%)	Perm. (md)			
16	Annulus	9	5%	10.6	5	12467	0.038265	1.2147%
17	Annulus	50	5%	15.3	35.6	78022	0.006002	1.1925%
18	Annulus	2	5%	10.6	5	2844	0.150808	1.0922%
19	Annulus	9	100%	15.3	35.6	152878	0.002733	1.0640%
20	Open hole	50	100%	15.3	112.5	1161211	0.000333	0.9836%
21	Annulus	2	100%	15.3	35.6	35439	0.010772	0.9721%
22	Annulus	9	100%	15.3	297.2	218432	0.001508	0.8387%
23	Annulus	9	5%	10.6	49.3	14238	0.022473	0.8147%
24	Annulus	2	100%	15.3	297.2	49671	0.005943	0.7517%
25	Annulus	2	5%	10.6	49.3	3190	0.08857	0.7193%
26	Annulus	50	5%	15.3	297.2	79418	0.003312	0.6697%
27	Open hole	50	100%	10.6	5	239392	0.001052	0.6415%
28	Annulus	50	5%	5.8	0.8	33721	0.006209	0.5332%
29	Open hole	50	5%	10.6	5	77856	0.002455	0.4868%
30	Annulus	9	5%	15.3	112.5	14442	0.012095	0.4448%
31	Annulus	2	5%	15.3	112.5	3229	0.047669	0.3919%
32	Open hole	50	100%	15.3	35.6	875136	0.000175	0.3908%
33	Tubing	50	100%	10.6	5	135717	0.001052	0.3637%
34	Open hole	50	5%	10.6	49.3	94765	0.001442	0.3480%
35	Tubing	50	100%	10.6	49.3	208411	0.000618	0.3280%
36	Open hole	9	100%	10.6	49.3	191980	0.000657	0.3210%
37	Open hole	50	100%	15.3	297.2	1283607	9.68E-05	0.3163%
38	Open hole	2	100%	10.6	49.3	44684	0.002588	0.2945%
39	Annulus	50	100%	5.8	0.8	41806	0.002661	0.2833%
40	Annulus	9	5%	15.3	35.6	14257	0.006377	0.2315%
41	Open hole	9	100%	15.3	112.5	236252	0.000353	0.2126%
42	Annulus	2	5%	15.3	35.6	3190	0.025135	0.2041%
43	Open hole	2	100%	15.3	112.5	54153	0.001393	0.1921%
44	Open hole	50	5%	15.3	112.5	96392	0.000776	0.1905%
45	Tubing	50	100%	15.3	112.5	218640	0.000333	0.1852%
46	Open	9	100%	10.6	5	49244	0.001118	0.1402%

Table 15. Continued

Risk Ranking	Scenarios					Total Spill (bbl)	Probability	Risk Contribution
	Flow Path	Duration (days)	BOP Opening Fraction	Porosity (%)	Perm. (md)			
	hole							
47	Open hole	2	100%	10.6	5	12310	0.004407	0.1381%
48	Annulus	9	5%	15.3	297.2	14400	0.003519	0.1290%
49	Annulus	50	5%	5.8	0.05	3234	0.014488	0.1193%
50	Annulus	2	5%	15.3	297.2	3220	0.013867	0.1137%
51	Annulus	9	5%	5.8	0.8	6674	0.006597	0.1121%
52	Annulus	2	5%	5.8	0.8	1613	0.026001	0.1068%
53	Open hole	50	5%	15.3	35.6	94208	0.000409	0.0982%
54	Tubing	50	100%	15.3	35.6	205856	0.000175	0.0919%
55	Tubing	50	5%	10.6	5	14520	0.002455	0.0908%
56	Open hole	2	5%	10.6	5	3339	0.010282	0.0874%
57	Open hole	9	100%	15.3	35.6	174296	0.000186	0.0827%
58	Open hole	2	100%	15.3	35.6	40631	0.000734	0.0760%
59	Tubing	9	100%	10.6	5	25850	0.001118	0.0736%
60	Open hole	9	100%	15.3	297.2	264467	0.000103	0.0692%
61	Open hole	9	5%	10.6	49.3	17472	0.001532	0.0682%
62	Tubing	2	100%	10.6	5	6018	0.004407	0.0675%
63	Tubing	9	100%	10.6	49.3	38793	0.000657	0.0649%
64	Annulus	2	100%	5.8	0.8	2216	0.011143	0.0629%
65	Open hole	9	5%	10.6	5	9440	0.002609	0.0627%
66	Annulus	9	100%	5.8	0.8	8687	0.002827	0.0625%
67	Open hole	2	100%	15.3	297.2	60405	0.000405	0.0623%
68	Open hole	2	5%	10.6	49.3	3900	0.006039	0.0600%
69	Tubing	2	100%	10.6	49.3	8710	0.002588	0.0574%
70	Open hole	50	5%	15.3	297.2	96835	0.000226	0.0557%
71	Tubing	50	100%	15.3	297.2	222620	9.68E-05	0.0549%
72	Tubing	50	5%	10.6	49.3	14831	0.001442	0.0545%
73	Annulus	50	100%	5.8	0.05	3238	0.006209	0.0512%
74	Open hole	50	5%	5.8	0.8	35919	0.000423	0.0387%
75	Open hole	9	5%	15.3	112.5	17651	0.000825	0.0371%

Table 15. Continued

Risk Ranking	Scenarios					Total Spill (bbl)	Probability	Risk Contribution
	Flow Path	Duration (days)	BOP Opening Fraction	Porosity (%)	Perm. (md)			
76	Tubing	9	100%	15.3	112.5	40304	0.000353	0.0363%
77	Open hole	2	5%	15.3	112.5	3948	0.00325	0.0327%
78	Tubing	2	100%	15.3	112.5	9012	0.001393	0.0320%
79	Tubing	50	5%	15.3	112.5	14850	0.000776	0.0293%
80	Annulus	2	5%	5.8	0.05	182	0.06067	0.0281%
81	Annulus	9	5%	5.8	0.05	690	0.015394	0.0271%
82	Open hole	50	100%	5.8	0.8	41653	0.000181	0.0192%
83	Tubing	50	100%	5.8	0.8	41559	0.000181	0.0192%
84	Open hole	9	5%	15.3	35.6	17275	0.000435	0.0191%
85	Tubing	9	100%	15.3	35.6	38006	0.000186	0.0180%
86	Tubing	9	5%	10.6	5	2639	0.002609	0.0175%
87	Open hole	2	5%	15.3	35.6	3889	0.001714	0.0170%
88	Tubing	2	100%	15.3	35.6	8541	0.000734	0.0160%
89	Tubing	50	5%	15.3	35.6	14835	0.000409	0.0155%
90	Tubing	2	5%	10.6	5	590	0.010282	0.0155%
91	Tubing	50	5%	5.8	0.8	12933	0.000423	0.0139%
92	Annulus	2	100%	5.8	0.05	183	0.026001	0.0121%
93	Annulus	9	100%	5.8	0.05	692	0.006597	0.0116%
94	Open hole	9	5%	15.3	297.2	17625	0.00024	0.0108%
95	Tubing	9	100%	15.3	297.2	41056	0.000103	0.0107%
96	Tubing	9	5%	10.6	49.3	2680	0.001532	0.0105%
97	Open hole	2	5%	15.3	297.2	3941	0.000946	0.0095%
98	Tubing	2	100%	15.3	297.2	9170	0.000405	0.0095%
99	Tubing	2	5%	10.6	49.3	597	0.006039	0.0092%
100	Tubing	50	5%	15.3	297.2	14869	0.000226	0.0085%
101	Tubing	50	5%	5.8	0.05	3269	0.000988	0.0082%
102	Open hole	9	5%	5.8	0.8	7108	0.00045	0.0081%
103	Open hole	50	5%	5.8	0.05	3234	0.000988	0.0081%
104	Open hole	2	5%	5.8	0.8	1736	0.001773	0.0078%
105	Tubing	9	5%	15.3	112.5	2687	0.000825	0.0056%
106	Tubing	2	5%	15.3	112.5	599	0.00325	0.0050%
107	Open	2	100%	5.8	0.8	2208	0.00076	0.0043%

Table 15. Continued

Risk Ranking	Scenarios					Total Spill (bbl)	Probability	Risk Contribution
	Flow Path	Duration (days)	BOP Opening Fraction	Porosity (%)	Perm. (md)			
	hole							
108	Open hole	9	100%	5.8	0.8	8656	0.000193	0.0042%
109	Tubing	9	100%	5.8	0.8	8528	0.000193	0.0042%
110	Tubing	2	100%	5.8	0. 8	2142	0.00076	0.0041%
111	Tubing	50	100%	5.8	0.05	3243	0.000423	0.0035%
112	Open hole	50	100%	5.8	0.05	3237	0.000423	0.0035%
113	Tubing	9	5%	15.3	35.6	2676	0.000435	0.0030%
114	Tubing	9	5%	5.8	0.8	2384	0.00045	0.0027%
115	Tubing	2	5%	15.3	35.6	597	0.001714	0.0026%
116	Tubing	2	5%	5.8	0.8	540	0.001773	0.0024%
117	Open hole	2	5%	5.8	0.05	182	0.004137	0.0019%
118	Tubing	9	5%	5.8	0.05	699	0.00105	0.0019%
119	Open hole	9	5%	5.8	0.05	690	0.00105	0.0018%
120	Tubing	2	5%	5.8	0.05	172	0.004137	0.0018%
121	Tubing	9	5%	15.3	297.2	2690	0.00024	0.0016%
122	Tubing	2	5%	15.3	297.2	599	0.000946	0.0014%
123	Tubing	2	100%	5.8	0.05	185	0.001773	0.0008%
124	Open hole	2	100%	5.8	0.05	182	0.001773	0.0008%
125	Tubing	9	100%	5.8	0.05	693	0.00045	0.0008%
126	Open hole	9	100%	5.8	0.05	691	0.00045	0.0008%

Various measures could effectively reduce the likelihood of potential blowout scenarios with significant consequences. For example, a well-prepared emergency response plan could be sufficient to reduce the likelihood of long blowout duration (*i.e.*, 50 days). Literature shows that capping is widely used as an intervention measure for subsea blowout events, and could reduce the overall duration of blowout (OGP/IPIECA, 2013). Typically, it takes around 10 days for the capping devices to be assembled

(ACONA, 2012). Thus, a good capping plan could greatly reduce the probability of long blowout duration. In addition, the BOP control system failure has been found as the major cause for the blowout event (Mide, 2010). A study concluded that 86% of the blowout incidents could be attributed to the failure of BOP control system (DNV, 1999). The BOP complete failure probability could be reduced by effective risk-based inspection, maintenance and additional redundancy of control system (He, 2014). Moreover, multiple layers of protection could prevent the open hole blowout from happening, such as drilling string safety valves. They may fail to close and suffer lock-up when experiencing high pressure flow. The selection of low-torque drilling string safety valve under certain operating conditions could help reduce the failure rate and, therefore, decrease the likelihood of open hole blowouts (Stephens, 1998).

A sensitivity study is conducted to determine how to allocate limited resources to prioritize the barriers that can effectively reduce the likelihood, and thus, the blowout risk. Figure 50 shows how the total blowout risk is reduced when the probabilities of long blowout duration, BOP complete failure, or open hole blowouts are decreased from base case to zero. As can be seen, the reduction of BOP complete failure probability could decrease the risk up to 68%, while efforts to avoid open hole blowout only contribute 3% of risk reduction. Consequently, operators should pay more attention to the barriers that could prevent BOP complete failure and reduce the blowout duration to manage the blowout risk in this case.

Mitigating the serious consequences of top risk contributors could also lower the total blowout risk. As can be seen in Table 15, most of the top risk scenarios are

associated with 100% BOP opening fraction. A proper risk-based inspection and maintenance program of the BOP system could not only reduce the likelihood of the complete failure scenario but also mitigate the scale of the failure consequence (*i.e.*, less than 100% BOP opening fraction under the worst failure scenario). Figure 51 shows the relationship between the total blowout risk and the BOP opening fraction of the worst failure case. Unlike the probability reduction case, a non-linear relationship is demonstrated. Given the typical non-linear curve for the cost versus the risk, this non-linear relationship at the benefit side emphasizes the necessity of a cost-benefit analysis. As can be seen, when the BOP opening fraction is reduced by 95% (5% opening fraction), the total risk decreases by 73%.

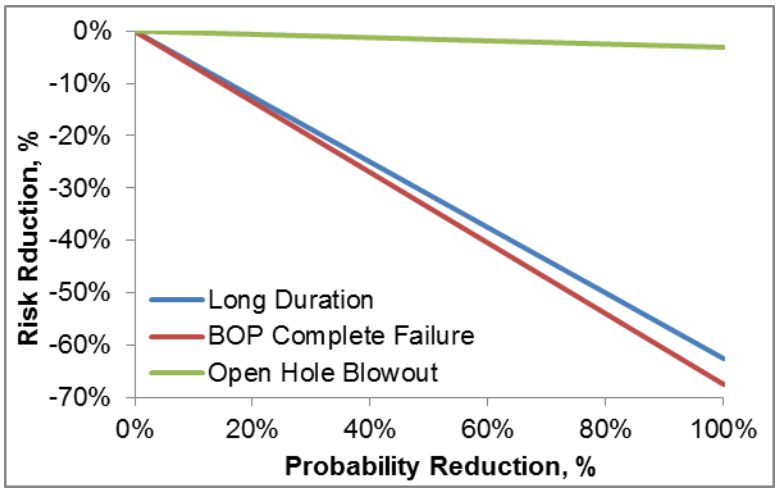

Figure 50. Example of risk reduction due to likelihood mitigation

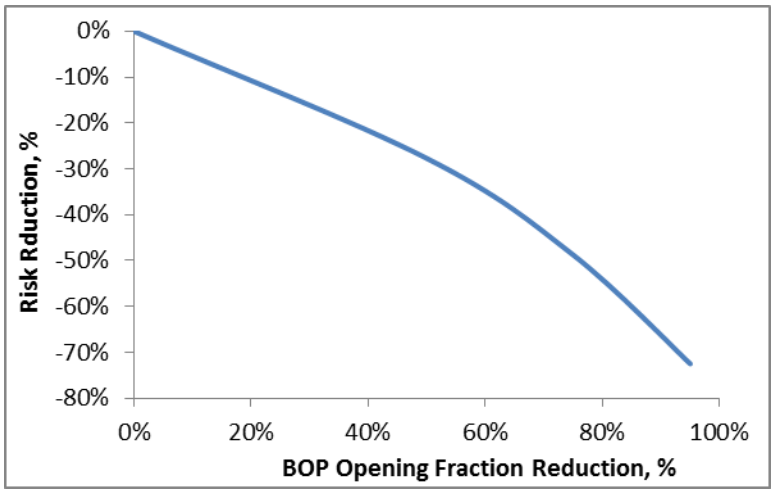

Figure 51. Example of risk reduction due to consequence mitigation

4.2.4 Discussion

The primary goal of the proposed methodology is to integrate the well blowout simulation modeling with other functionalities to achieve the risk-based operational excellence. It is envisioned that this concept, if fully developed, would be applicable throughout the entire lifecycle of well operations (drilling, completions, intervention and abandonment). This risk-based blowout risk assessment method can be practiced as a part of well planning. The well engineer will create the well schematic which will identify the flow paths and proposed barriers to be installed. The well schematic and well information determined by the engineers could then be imported into the modeling as input parameters to evaluate the blowout risk. Engineers could easily switch between multiple well designs until an optimum well design has been established. This optimum shall be based on considerations of operational efficiency, acceptable risk levels based on blowout probability profile, and cost. A log of all the well design simulations could

be stored in the database and easy comparative reports could be generated for discussions or management approvals. Such reports could also be the furnished to regulatory well permit approving body to showcase decision rationale for selecting a particular well design.

In addition, this method to determine the blowout risk could be implemented in to the barrier management. This would require the operations team to generate a bowtie specific to the operation being planned to identify threats, hazards, and prevention and mitigation barriers, as shown in Figure 52. For each barrier identified, barrier requirements would be established as defined in regulations, such as NORSOK D-010 or API RP 96. Also barrier assurance parameters could be defined which would be monitored during the well operations to establish barrier assurance levels. This exercise would be similar to performance standards workshop and could be easily done in a workshop setting. All the results of the workshop including performance standards and bowties would reside in the database. Most organizations have already identified and created enterprise level Major Incident Hazards (MAHs) bowties; these could be easily imported into this tool and serve as the starting point for this exercise.

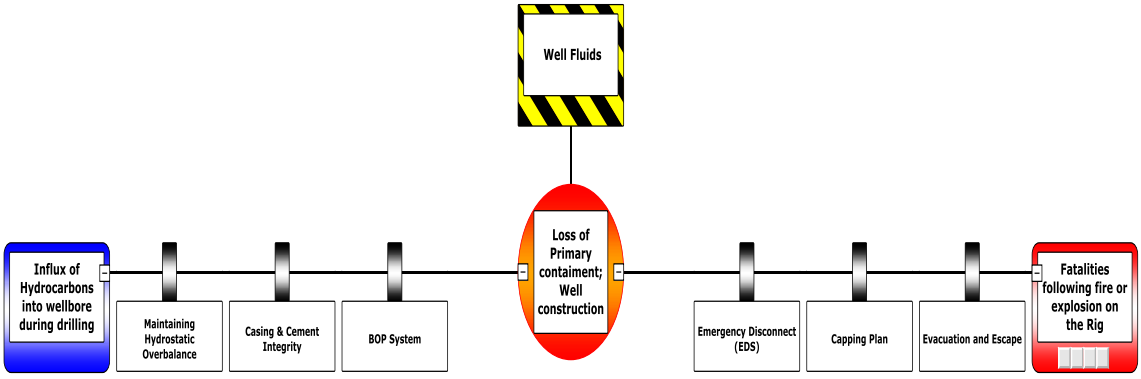

Figure 52. MAH Bowtie (simplified for purpose of this dissertation)

Moreover, the proposed practice could also be dynamically updated, such as potential flow paths and the current status of barriers, as the drilling operation continues in the field. Most updated reservoir information would be automatically obtained via the downhole logging tools and fed into the blowout simulation model to depict an updated and more accurate blowout risk picture. Similarly barrier information would be frequently fed into the database via the well reports, inspections, testing, and the rig systems. Based on results of the information, a risk profile could be generated for the specific operations. Any deviation from the accepted risk profile would require the intervention from the appropriate personnel or parties. This would make the operations take a more proactive and a focused approach to risk management rather than a reactive one as personnel in remote office have information on most probable blowout flow path (probability percentage), current barrier status and also the ability to detect effect on other systems (barrier link to other MAH bowties).

Another benefit of the proposed method is that it can facilitate the analysis of the relationships amongst well economics, cost information, and safety performance. Operators can input the specific cost information of the barriers and evaluate the multiple barriers requirement for a certain flow path; or a comparison of similar type of barriers available from different vendors. The barrier reliability data provided by the vendor to the operator based on history of use or testing could be utilized to aid this decision making. Figure 53 showcases a simplified case of how the cost-benefit analysis for safety barrier (*i.e.*, isolation packers or centralizer) selection is performed. Three similar barriers (Barrier 1A, 1B and 1C), which could reduce the likelihood of the open hole blowout events, are available for procurement from three different vendors (A, B and C). The risk reduction percentage is established based on each of the barriers' reliability information (*e.g.*, probability of failure on demand) and the technology adopted along with the overall cost during the installation and maintenance. A risk-based decision for the selection between Barrier 1A, 1B and 1C therefore can be made. The figure shows that Barrier 1B is a cost-effective option over Barrier 1C since the overall risk reduction is similar to Barrier 1C but the cost savings is on the scale of USD 250,000. The rationale behind such a higher cost for Barrier 1C could be based on the assumption that it is a newer technology or a newly developed product from vendor C, and hence, is being sold at a premium price. The selection of Barrier 1B rather than1A is based on the relatively small cost difference between two products but a much better overall risk reduction level. It is important to note that this example only serves as a

simplified one; real field applications require consideration of other factors, such as the compatibility with other barriers.

Barrier Type	Overal Cost (USD)	Overall Risk Reduction (%)	Vendor
Barrier 1A	150000	30	A
Barrier 1B	250000	60	B
Barrier 1C	500000	62	C

Figure 53. Example of risk base barrier selection

4.3 Conclusion

In this section, both consequence-based and risk-based approaches are discussed. The application of such approaches is demonstrated by the case study. The consequence-based approach is easier to be implemented and provide guidance to the operators based on the realistic worst-case scenario. It would be useful in the drilling site location selection and preparation of emergency response plan. On the other hand, the risk-based approach enables the operators to have a comprehensive understanding of the particular well that they are working on, so that the risk associated with the blowout events can be effectively managed and controlled. It should be noted that the application of the risk-based approach requires the input from onsite personnel to depict a more accurate risk picture.

CHAPTER V

CONCLUSIONS AND RECOMMENDATIONS

5.1 Conclusions

A fully integrated analytical model that couples the reservoir and wellbore has been proposed to investigate the fluid behaviors during the blowout events. This model could be used to simulate any potential blowout events for gas, oil, or oil/gas wells at onshore or offshore facilities.

The material balance is considered in the oil reservoir model to obtain the dynamic average reservoir pressure. Additional PVT relationship of the gas needs to be considered for the gas reservoir. The fluid dynamics and heat transfer are taken into account to calculate the pressure drop when the fluid flows along the wellbore. The particular concern for gas wells is the potential existence of sonic velocity at the wellhead. The determination of sonic velocity requires a proper energy balance to be established as the sonic velocity is temperature dependent. For oil wells, the multi-phase flow may exhibit various flow patterns in the wellbore depending on the local pressure, temperature, and the fluid properties. The reservoir and wellbore interaction is an important factor to determine the blowout rate. Analytical equations are used to capture the relationship between reservoir pressure and wellbore bottomhole pressure during the transient period and pseudo steady-state period. All the physical models are combined together to obtain the dynamic blowout rate and total amount of discharge during the blowout events.

Field examples are presented in this dissertation to validate the onshore and offshore gas well blowout model and offshore oil well blowout. The results show that the proposed model shows a good agreement with the field examples, existing studies, and commercial software. The advantage of this model is to avoid using separate tools to simulate the reservoir and wellbore fluid, which may fail to capture the important interaction between reservoir and wellbore. Design of experiments is adopted to demonstrate the important uncertainties that could affect the blowout behaviors. It could be concluded that the blowout rate is strongly sensitive to the change of permeability and the reservoir pore-volume connected to the well.

The results of the simulation can serve as the basis for a series of study. In this dissertation, the model is imbedded into consequence-based and risk-based assessment tools so that the effectiveness of prevention and mitigation measurements could be quantitatively evaluated. The consequence-based assessment couples the blowout model and dispersion model to demonstrate the area which could under effect of the potential blowout events due to toxic gas dispersion, explosion, and fires. This assessment provides a more realistic blowout scenario compared to the WCD required in the US Gulf of Mexico region. A proper emergency response plan, toxic/flammable gas sensor placement, and drilling site selection could benefit from the consequence-based assessment.

The risk-based assessment, on the other hand, presents a more comprehensive risk picture associate with the potential blowout events. The uncertainties from generic historical database, such as the blowout duration and flow paths, are considered here. In

addition, some well-specific parameters distribution, including permeability and porosity, are combined with uncertainties obtained from historical databases to create a spectrum of potential blowout scenarios. Each scenario is associated with a unique probability and consequence. Coupling the probability and consequence together, the well-specific blowout risk could be fully assessed.

The results of the risk-based assessment have a variety of applications. The effectiveness and values of both prevention and mitigation barriers could be evaluated in terms of the risk reduction fraction. It can also help to allocate the limited resources to important barriers to improve the safety performance. In addition, cost-benefit analysis can acquire valuable information from this risk-based approach to aid the decision making process.

In general, the work presented here shows a promising approach for conducting a detailed study to the consequence and risk associated with the blowout events during different operational phases. By considering the physics in the reservoir, wellbore, and their interactions, the consequence model can readily couple with the uncertainties obtained from historical database and well-specific testing data to illustrate the full picture of blowout risk. Sensitivity analysis can provide guidance for the determination of the effectiveness of prevention and mitigation barriers. Moreover, the analysis from this work can serve as an engineering benchmark in the assessment of blowout risk and the development of the risk reduction plan.

5.2 Recommendations for Further Research

This research proposed a consequence modeling to simulate the blowout events, based on which the consequence-based and risk-based assessments to blowout risk were developed. The occurrence of blowout events indicates the failure of the primary barrier – drilling mud. Therefore, no probability of failure of the primary barrier is considered in this research. The failure of the primary barrier should be taken into account when evaluating the risk associated with the kick events which are considered as the leading indicator of blowout events. Physical model is required to determine the consequence of kick events and historical database could provide their likelihood. Combining the consequence and likelihood of kick events leads to a risk model that could be implemented into the blowout risk assessment approach in this research to evaluate the risks of both kick and blowout events.

In addition, this research assumes when BOP fails to function, it is either partially closed (5% opening) or fully opened (100% opening). The probability distribution is based on the suggestion from the industry guidelines. A BOP reliability model and BOP failure mode and effects analysis (FMEA) need to be investigated to further determine such probability distribution so that more realistic blowout risk results can be obtained. Moreover, human failure, which has been responsible for over 70% of the causes in offshore incidents, could be taken into account (Reason, 1997). At present, a number of studies have addressed the effect of human factors in the onshore and offshore operations. Such investigation could be integrated into the current model to reflect the effect of human behaviors to the blowout risk.

In this research, we assumed the blowout rate reaches the maximum value immediately after the occurrence of blowout. In reality, the blowout rate will increase to the maximum value and then decline. Such increase of the rate in the beginning of the blowout event would take several minutes. This short time period can be neglected when the blowout lasts for days. Moreover, as shown in Chapter IV, the blowout scenarios with short blowout duration belongs to the high likelihood and low consequence category and is not as significant as the scenarios with long blowout duration. However, when simulating blowouts with short duration or kick events, the early period where the blowout rate increase occurs will become significant for the prediction of total discharge amount during the blowout event. A fully transient wellbore fluid model will be required to address the blowout rate increase in early period.

In this research, the consequence modeling of blowout events is applied to the risk assessment with regard to the environmental impact. Other studies could also utilize the results of such models. For example, the blowout rate could serve as an important input for the oil plume and drift modeling. The oil composition, weather condition, and marine environment are also coupled together for a better oil spill preparedness and response plan. The impact due to the blowout to the personnel and equipment on the offshore facilities can be evaluated based on the consequence models presented here. Blowout is one of the important considerations for the design of fire and blast walls and facility siting at the platform against incidental loads. Currently, one design of incidental loads is based on the effect of the fire and explosion due to blowout events in which the blowout rate, several times higher than the normal production rate, is assumed to be

constant. The approach proposed here can provide either a consequence-based or a risk-based basis for a better design and construction for the offshore facilities.

The primary goal of this research is to develop a blowout risk assessment tool which can be used by not only the engineers but also the onsite operators. This tool could dynamically update the risk associated with any operations, including drilling, completion, intervention and production. The safety performance of each prevention and mitigation barriers is considered in this tool. The human factor and kick events can also integrated into the assessment to enable operators to ensure a safe and sound operational environment.

REFERENCES

ACONA. (2011). *Report: blowout risk evaluation at Labrador Sea south-west of Greenland*.

Ahmed, T. (2010). *Reservoir engineering handbook*. Fourth ed. Burlington, MA: Elsevier.

Al-Hussainy, R., Ramey. Jr. H. J., & Crawford, P. B. (1966). The flow of real gases through porous media. *Journal of Petroleum Technology, 18,* 624-636.

Ansari, A. M., Sylvester, N. D., Sarica, C., Shoham, O., & Brill, J. P. (1994). A comprehensive mechanistic model for upward two-phase flow in wellbores. *SPE Production & Operations, 9*, 143-151.

API. (2013). *API RP 96: Deepwater well design and construction*, First Edition.

Aziz, K., Govier, G. W., & Fogarasi, M. (1972). Pressure drop in wells producing oil and gas. *Journal of Canadian Petroleum Technology, 11,* 38-40.

Baker, W.E. (1973). *Explosions in air*. University of Texas Press, Austin, Texas.

Barnea, D. (1987). A unified model for predicting flow-pattern transitions for the whole range of pipe inclinations. *International Journal of Multiphase Flow, 13,* 1-12.

Beggs, H. D. & Robinson J. R. (1975). Estimating the viscosity of crude oil systems. *Journal of Petroleum Technology, 27,* 1140-1141.

BOEMRE. (2010). *Information requirements for EPs, DPPs, and DOCDs on the OCS – frequent asked questions*.

BOEMRE. (2014). *National notice to lessees and operators of federal oil and gas leases, Outer Continental Shelf (OCS), NTL No. 2010-N06*.

Bourgoyne, A. T., Millheim, K.K., Chenevert, M. E. & Young, Jr. F. S. (1991). *Applied drilling engineering*. Richardson, Texas: Society of Petroleum Engineering.

BP. (2009). *Initial exploration plan Mississippi Canyon Block 252 OCS-G 32306*.

BP. (2015). *Second quarter and half year 2015(a) report*.

Brauner, N. & Barnea D. (1986). Slug/Churn transition in upward gas-liquid flow. *Chemical Engineering Science, 41*, 159-163.

CCPS. (2016). *Guidelines for integrating management systems and metrics to improve process safety performance*, John Wiley & Sons.

CSB, (2010). *Investigation report: explosion and fire at the Macondo well, Volume 2*.

Chen, N. H. (1979). An explicit equation for friction factor in pipe. *Industrial & Engineering Chemistry Fundamentals, 18,* 296-297.

Clancey, V. J. (1972). Diagnostic features of explosion damage. Paper presented at *6th International Meeting on Forensic Sciences, Edinburgh, Scotland.*

Clark, A. R. & Perkins, T. K. (1981). Wellbore and near-surface hydraulics of a blown-out oil well. *Journal of Petroleum Technology, 33,* 2181-2188.

Crawl, D. A. & Louvar, J. F. (2011). *Chemical process safety: fundamentals with applications*, 3rd Edition. Prentice-Hall.

Dake, L. P. (1983). *Fundamentals of reservoir engineering*. Elesvier.

Darcy, H. (1856). *Les fontaines publiques de la ville de dijon. in victor dalmont*. Paris.

Department of Justice (DOJ). (2012). *Information for Seaman's Manslaughter, Clean Water Act, Migratory Bird Treaty Act and obstruction of congress.*

Department of Interior (DOI) (2011). *Assessment of flow rate estimates for the deepwater horizon / Macondo well oil spill,* National Incident Command, Interagency Solution Group and Flow Rate Technical Group.

DNV. (1999). *Reliability of subsea BOP systems for deepwater application, phase II DW.*

DNV. (2010). *Report: environmental risk assessment of exploration drilling in Nordland VI.*

Dranchuk, P. M. & Abou-Kassem H. (1975). Calculation of Z factors for natural gases using equations of state, *Petroleum Society of Canada, 14,* 34-36.

Dropkin, D. & Somerscales E. (1965). Heat transfer by natural convection in liquids confined by two parallel plates which are inclined at various angles with respect to the horizontal. *Journal of Heat Transfer, 87,* 77-82.

Earlougher, R. C. (1977). *Advances in well test analysis*. Dallas: Society of Petroleum Engineers.

Economides, M. J., Daniel, A. H., Ehlig-Economides, C. & Zhu D. (2013). *Petroleum production systems*. Second Edition. Prentice Hall.

Everdingen, A. F. V. & Hurst, W. (1949). The application of the Laplace transformation to flow problems in reservoirs, *Journal of Petroleum Technology, 1*, 305-324.

Glasstone, S. & Dolan, P. J. (1977). *The effects of nuclear weapons*, 3rd edition. United States Department of Defense and Energy Research and Development Administration.

Goldenberg, S. (2010). Marine scientist study ocean-floor film of Deepwater oil leak, in *the Guardian*, May 13, 2010.

Grace, R. D., Cudd, B. Carden, R. S. & Shursen, J. L. (2003). *Blowout and well control handbook*. Elsevier.

Harmathy, T. Z. (1960). Velocity of large drops and bubbles in media of infinite or restricted extent. *AIChE Journal, 6,* 281-288.

Hasan, A. R. & Kabir, C. S. (1988). A study of multiphase flow behavior in vertical wells. *SPE Production Engineering, 3,* 263-272.

Hasan, A. R. & Kabir C. S. (2012). Wellbore heat-transfer modeling and applications. *Journal of Petroleum Science and Engineering, 86–87, 127*-136.

Hasan, A. R. & Kabir C. S. (1994). Aspects of wellbore heat transfer during two-phase flow (includes associated papers 30226 and 30970). *SPE Production & Operations, 9,* 211-216.

Hasan, A. R., Kabir, C. S. & Rahman R. (1988). Predicting liquid gradient in a pumping-well annulus. *SPE Production Engineering, 3,* 113-120.

Hasan, A. R., Kabir, C. S., & Lin, D. (2000). Modeling wellbore dynamics during oil well blowout. *International Oil and Gas Conference and Exhibition in China*. Beijing, China, 2000.

Hasan, A.R. (1988). Void fraction in bubbly, slug and churn flow in vertical two-phase up-flow. *Chemical Engineering Communications, 66,* 101-111.

Havlena, D. & Odeh, A. S. (1963). The material balance as an equation of a straight line. *Journal of Petroleum Technology, 15,* 896-900.

Havlena, D. & Odeh, A. S. (1964). The material balance as an equation of a straight line—part II, field cases. *Journal of Petroleum Technology, 16,* 815-822.

He, X., Sorman, J., Alme, I. A. & Roper, S. (2014). BOP risk model development and applications, *Probabilistic Safety Assessment and Management PASM 12*, Honolulu, Hawaii, US.

Health & Safety Executive (HSE). (2004). *Fire and explosion strategy-issues 1*.

Hewitt, G. F. & Roberts, D.N. (1969). *Studies of two-phase flow patterns by simultaneous x-ray and flash photography*.

Holand, P. (1997). *Offshore blowouts: causes and control*. Elsevier.

HSE. *Well Construction Standards, SPC/TECH/GEN/42*, (http://www.hse.gov.uk/foi/internalops/hid_circs/technical_general/spc_tech_gen_42.htm), Last Retrieved, 01/27/2016.

Kabir, C.S. (2006). What is the real measure of gas-well deliverability potential? *SPE Reservoir Evaluation & Engineering, 9*, 126-134.

Khordagui, H. & Al-Ajmi, D. (1993). Environmental impact of the Gulf War: An integrated preliminary assessment. *Environmental Management, 17*, 557-562.

Kieffer, S. W. (1977). Sound speed in liquid-gas mixtures: water-air and water-steam. *Journal of Geophysical Research. 82*, 2895-2904.

Kikani, J., Heinrich, S. & Graute, J. (1996). A method for blowout rate prediction for sour gas Wells–Oldenburg fields, Germany. SPE Reservoir Engineering, 11, 158-162.

Lake, L. W. (2007). *Petroleum engineering handbook*. Vol. III. Society of Petroleum Engineers.

Landrey, W. G. (1991). Oil slick in Gulf likely to spread, in *St. Petersburg Times*, 30 January, 1991.

Li, J., Zhang, B., Wang, Y. & Liu, M. (2009). The unfolding of '12.23' Kaixian blowout incident in China, *Safety Science, 47*, 1107-1117.

Liu, R., Hasan, A. R. & Mannan, M. S. (2015). Flow rate and total discharge estimations in gas-well blowouts, *Journal of Natural Gas Science and Engineering, 26*, 438-445.

Mannan. M. S. (2012). *Lees' loss prevention in the process industries: hazard identification, assessment and control*, 4th Edition, Elsevier.

Matthews, C. S. & Russell, D. G. (1967). *Pressure buildup and flow tests in wells*. Society of Petroleum Engineers.

Matthews, C. S., Brons, F. & Hazebroek, P. (1954). A method for determination of average pressure in a bounded reservoir. *Petroleum Transactions, AIME, 201*, 182-191.

McCabe, W., Smith, J. & Harriott P. (2004). Unit operations of chemical engineering. seventh edition. McGraw-Hill Book Co. Inc.

Mide Technology Corporation. (2010). *Deep water drilling risk reduction assessment*.

Moody, L. F. (1944). Friction factors for pipe flow. *Transactions of the ASME, 66,* 671-684.

NORSOK. (2004). *NORSOK standard D-010: well integrity in drilling and well operations*, Rev.3.

NORSOK. (2001). *NORSOK standard Z-013: risk and emergency preparedness analysis*, Rev.2.

OGP. (2010). *Risk assessment data directory, blowout frequencies*, Report No. 434-2.

OGP. (2010). *Risk assessment data directory: consequence modelling*. Report No. 434-7.

OGP/IPIECA. (2013). *Report: oil spill risk assessment and response planning for offshore installations*.

Oldenburg, C. M., Freifeld, B. M., Pruess, K. Pan, L., Finsterle, S. & Moridis, G. J., Numerical simulations of the Macondo well blowout reveal strong control of oil flow by reservoir permeability and exsolution of gas, *Proceedings of the National Academy of Sciences, 109,* 20254-20259.

OLF. (2005). *Barriers against spills – fact sheet*.

OLF. (2004). *Retningslinjer for beregning av utblåsningsrater og varigheter til bruk ved analyse av miljørisiko (Guidelines on estimation of blowout rates and duration for the use in risk analysis).*

Oudeman, P. (1998). Analysis of surface and wellbore hydraulics provides key to efficient blowout control. *SPE Drilling & Completion, 13*, 163-173.

Oudeman, P. (2006). Oil fallout in the vicinity of an onshore blowout: observations on a field case. *SPE Projects, Facilities & Construction, 1*, 1-7.

Oudeman, P. (2010). Validation of blowout-rate calculations for subsea wells. *SPE Drilling & Completion, 25,* 282-289.

Plume Calculation Team. (2010). *Deepwater Horizon release estimate of rate by PIV*.

Reason, J. T. (1997). *Managing the risk of organizational incidents.* Hampshire: Ashgate.

Scandpower. (2011). *Report: blowout and well release frequencies,* Report No. 19.101.001-3009/2001/R3.

Schneider, D. *How to drill a relief well, (http://spectrum.ieee.org/energy/fossil-fuels/how-to-drill-a-relief-well),* Last Retrieved, 01/27/2016

SINTEF. (2013). *Report: blowout and well release characteristics and frequencies*.

Skalle, P., Jinjun H. & Podio, A. L. (1999). Killing methods and consequences of 1120 gulf coast blowouts during 1960–1996, in *Latin American and Caribbean Petroleum Engineering Conference1999, Caracas, Venezuela*.

Smith, J. M., Van Ness H. C. & Abbott, M. M. (2005). Introduction to chemical engineering thermodynamics, Seventh Edition. McGraw-Hill Book Co. Inc.

SPE. (2015). *Technical report: calculation of Worst-Case Discharge (WCD).*

Stephens, L. E., Coleman, E. D., Casemore, M. A. & Core, Jr. T. T. (1998). Drill string safety valve reliability: experimental measurements of actuating torque, *Transaction of the ASME, 120*, 84-89.

Taitel, Y., Bornea D. & Dukler, A. E. (1980). Modelling flow pattern transitions for steady upward gas-liquid flow in vertical tubes. *AIChE Journal, 26,* 345-354.

US Committee on Merchant Marine and Fisheries. (1992). *Congress report: the environmental role of the national oceanic and atmospheric administration and the U.S. coast guard in the Persian Gulf conflict*.

Van den Berg, A. C. (1985). The multi-energy method, a framework for vapor cloud explosion blast prediction, *Journal of Hazardous Materials, 12,* 1-10.

Vazquez, M. & Beggs H. D. (1980). Correlations for fluid physical property prediction. *Journal of Petroleum Technology, 32,* 968-970.

Weisman, J. & Kang S. Y. (1981). Flow pattern transitions in vertical and upwardly inclined lines. *International Journal of Multiphase Flow, 7,* 271-291.

Wolff, M. (2010). Probabilistic subsurface forecasting—what do we really know? *Journal of Petroleum Technology, 62,* 86–92.

Xu, L., Wu, J. & Hong, Q. (2005). Analysis on environment impact of Chongqing Kaixian blowout, *China Safety Science Journal, 15*, 84-87.

APPENDIX A

CORRELATIONS OF OIL/GAS PROPERTIES

Experimentally, all the properties of crude oil and gas can be obtained in a laboratory. Based on the experimental results, different curves are generated for use in the field. However, different gas volume fractions in gas/oil mixtures complicate the application of such curves. In addition, they cannot aid the computational simulation due to implementation issues. In the absence of experimental data of properties of the reservoir fluid, it is necessary to determine the properties from empirical correlations. Therefore, a number of researchers developed a wide variety of correlations for the properties of oil/gas mixtures. In this chapter, the correlations that are used in this work are shown.

A.1 Compressibility Factor

The compressibility factor is one of the most important parameters for the PVT relationship of gas. It is a non-linear function of reduced pressure and reduced temperature, which results in the difficulties during implementation into computational program. In this research, a reduced density is introduced (Dranchuk, 1975):

$$\rho_r = \frac{Z_0 P_r}{Z T_r} \tag{97}$$

where

$$Z = 1 + (A_1 + \frac{A_2}{T_r} + \frac{A_3}{T_r^3} + \frac{A_4}{T_r^4} + \frac{A_5}{T_r^5})\rho_r + (A_6 + \frac{A_7}{T_r} + \frac{A_8}{T_r^2})\rho_r^2 - A_9(\frac{A_7}{T_r} + \frac{A_8}{T_r^2})\rho_r^5 + A_{10}(1 + A_{11}\rho_r^2)\frac{\rho_r^2}{T_r^3}\exp(-A_{11}\rho_r^2) \quad (98)$$

and Z_0 is assumed to be 0.270. Then Equation (97) becomes:

$$f(\rho) = \rho_r Z T_r - Z_0 P_r = 0 \quad (99)$$

The constants in Equation (98) are listed in the table below. Then the iterative Newton Raphson Method is adopted with an initial guess of $Z = 1$ to get convergence of ρ_r as shown in Equation (100). The converged value of ρ_r is plugged into Equation (98) to get the value of the compressibility factor.

$$\rho_{new} = \rho_{old} - \frac{f(\rho_{old})}{f'(\rho_{old})} \quad (100)$$

Table 16. Constants value in Equation (98)

Constant	Value
A_1	0.3265
A_2	-1.0700
A_3	0.5339
A_4	0.01569
A_5	-0.05165
A_6	0.5475
A_7	-0.7361
A_8	0.1844
A_9	0.1056
A_{10}	0.6134
A_{11}	0.7210

A.2 Bubble Point Pressure

Bubble point describes the conditions of temperature and pressure at which the first bubble of gas comes out of the liquid oil/gas mixture. In the reservoir, the temperature is considered as a constant. Bubble point pressure is the criteria of phase separation phenomenon in the reservoir. The Vasquez-Beggs Correlation (Vasquez, 1980) is used in this work:

$$p_b = [\frac{R_{sb}}{C_1 \gamma_{gs} \exp(C_3 API / (T + 460))}]^{1/C_2} \quad (101)$$

where R_{sb} is the gas solubility at the bubble point pressure and reservoir temperature, γ_{gs} is the specific gravity of gas measured at the separator, and T is reservoir temperature in $^\circ$F. γ_{gs} can be obtained from a separator pressure of 100 psig because it represents the average field separator conditions. The following equation could adjust γ_g at any separator condition to the referenced separator conditions:

$$\gamma_{gs} = \gamma_g [1 + 5.912(10^{-5})(API) T_{sep} \log(\frac{p_{sep}}{114.7})] \quad (102)$$

If the separator conditions are unknown, the unadjusted gas gravity may also be used. The coefficients C_1, C_2, and C_3 are shown in the following table:

Table 17. Values of the coefficients used in Equation (101)

Coefficient	**API $\leq$ 30**	**API > 30**
C_1	0.0362	0.0178
C_2	1.0937	1.1870
C_3	25.7240	23.9310

A.3 Gas Solubility

The gas solubility R_s is defined as the amount of gas in standard cubic feet that can dissolve in one stock-tank barrel of crude oil at a specified pressure and temperature. It is a strong function of the pressure, temperature, oil gravity, and gas gravity. The gas solubility increases with an increase of pressure at constant temperature until the gas solubility reaches its maximum value. Figure 54 shows a typical gas solubility curve as a function of pressure for undersaturated oil. The gas solubility remains constant if the reservoir pressure is higher than bubble point pressure, and decreases if the reservoir pressure drops below bubble point pressure.

Vasques and Beggs (Vasquez, 1980) proposed an empirical correlation of R_s based on 5,008 experimental data points. The measured data was divided into two groups depending on the oil gravity. The expression of the proposed correlation is:

$$Rs = C_1 \gamma_{gs} p^{C_2} \exp[API/(T+460)] \tag{103}$$

where the coefficients C_1, C_2, and C_3 are the same as the equation used to calculate the bubble point pressure.

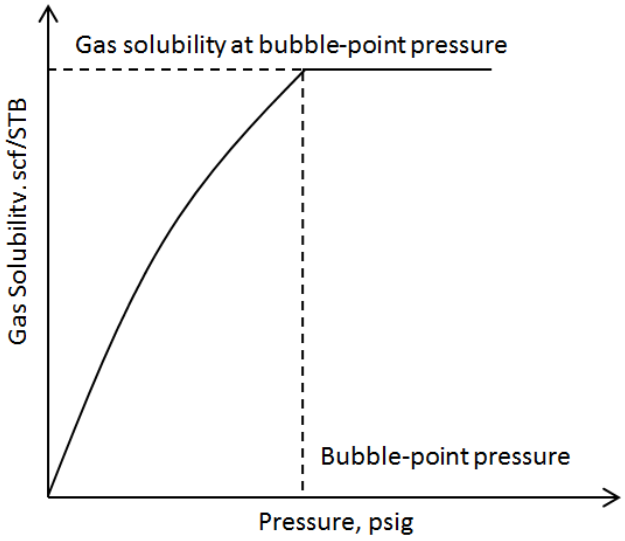

Figure 54. Gas solubility pressure diagram

A.4 Oil Formation Volume Factor

The oil formation volume factor B_o is defined as the ratio of the volume of oil at reservoir conditions to the volume of oil at standard conditions. The mathematical expression of B_o is given by:

$$B_o = \frac{(V_o)_{p,T}}{(V_o)_{sc}} \tag{104}$$

A typical oil formation factor curve is a function of pressure at constant temperature as shown in Figure 55. If the pressure is above the bubble point pressure, the decrease in pressure results in an increase in oil formation volume factor because of the oil expansion. When the pressure is less than bubble point pressure, the oil formation volume factor will decrease with the pressure going down owing to the gas liberation.

Vasquez and Beggs (Vasquez, 1980) used 6,000 measurements of B_o at different pressures to propose a correlation:

$$B_o = 1.0 + C_1 R_s + (T - 60)(\frac{API}{\gamma_{gs}})[C_2 + C_3 R_s] \tag{105}$$

for $p \le p_b$, and

$$B_o = B_{ob} \exp[-c_0 (p - p_b)] \tag{106}$$

for $p \ge p_b$, c_0 is given by:

$$c_0 = \frac{-1433 + 5R_s + 17.2T - 1180\gamma_{gs} + 12.61API}{10^5 p} \tag{107}$$

where R_s is the value at the bubble point pressure and reservoir temperature, γ_{gs} is the specific gravity of gas measured at the separator, and T is reservoir temperature in $^\circ$F. c_0 is also the regression of isothermal compressibility. The coefficients C_1, C_2, and C_3 are shown in the following table:

Table 18. Values of the coefficients used in Equation (105)

Coefficient	API ≤ 30	API > 30
C_1	4.677×10^{-4}	4.670×10^{-4}
C_2	1.751×10^{-5}	1.100×10^{-5}
C_3	-1.811×10^{-8}	1.337×10^{-9}

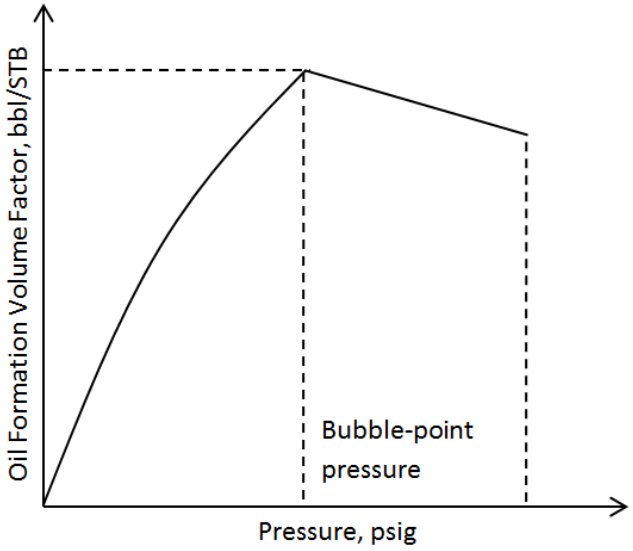

Figure 55. Oil formation volume factor pressure diagram

A.5 Viscosity

The viscosity of crude oil is an important physical property since it governs the flow through porous media and pipes. It is usually considered an internal resistance of fluid flow. When lacking laboratory measurements, some correlations of oil viscosity

may be used. Beggs and Robinson (1975) proposed an empirical equation based on 2,073 observations of saturated oil viscosity. The expression is given by:

$$\mu = a(\mu_{od})^b \tag{108}$$

where

$$a = 10.715(R_s + 100)^{-0.515} \tag{109}$$

$$b = 5.44(R_s + 150)^{-0.338} \tag{110}$$

μ_{od} in Equation (108) is the viscosity of dead oil that is defined as the viscosity of crude oil with no gas in the solution at atmospheric pressure. Beggs and Robinson (Beggs, 1975) also proposed the correlation of μ_{od} after analyzing 460 dead oil viscosity data points as follows:

$$\mu_{od} = 10^X - 1 \tag{111}$$

where

$$X = Y(T - 460)^{-1.163} \tag{112}$$

$$Y = 10^Z \tag{113}$$

$$Z = 3.0324 - 0.02023API \tag{114}$$

For undersaturated oil, the Vasquez-Beggs correlation is used in this work. The viscosity at pressures above the bubble point pressure is a function of viscosity at bubble point pressure, μ_{ob}, pressure, p, and bubble point pressure, p_b:

$$\mu_o = \mu_{ob}(\frac{p}{p_b})^m \tag{115}$$

where

$$m = 2.6p^{1.187}\exp(-11.514 - 8.98\times10^{-5}p) \tag{116}$$

When $p = p_b$, Equation (115) is equivalent to Equation (108).

APPENDIX B

NOMENCLATURE

a_n	series roots of Equation (71)
B	oil formation volume factor, bbl/STB
B_g	current gas formation volume factor, rcf/scf
B_{gi}	initial gas formation volume factor, rcf/scf
c	sonic velocity of gas, ft/sec
C_J	Joule-Thomson coefficient, ℉/psi
<C>	average concentration in plume, ppm
c_p	heat capacity, Btu/(lbm- ℉)
c_t	total compressibility, psi-1
D	non-Darcy flow coefficient, D/Mscf
d	pipe diameter, ft
E_{TNT}	energy of explosion of TNT, 2016 Btu/lbm
f	Moody friction factor, dimensionless
f_g	gas volume fraction, fraction
g	acceleration owing to gravity, ft/sec2
G	current gas-in-place, Mscf
g_c	conversion factor, 32.17 (lbm-ft)/(lbf-sec2)
g_G	geothermal gradient, ℉/ft
G_i	initial gas-in-place, Mscf

G_p	cumulative production, Mscf
Gr	Grashof number, dimensionless
h	net pay, ft
h_c	annular fluid convective heat transfer coefficient, Btu/(hr•ft2• ºF)
h_{to}	tubing fluid convective heat transfer coefficient, Btu/(hr•ft2• ºF)
J	mechanical equivalent heat, 778 (ft-lbf)/Btu
J_1	Bessel functions of the first kind
k	permeability, md
K	eddy diffusivity, ft2/sec
k_e	reservoir heat conductivity, Btu/(hr•ft• ºF)
L	well depth, ft
L_R	relaxation distance parameter, 1/ft
m	mass of hydrocarbon, lbm
M	molecular weight, lbm/lb-mol
m(p)	pseudopressure, psia2/cp
m_{TNT}	equivalent mass of TNT, lbm
n	number of moles, mol
Nu	Nusselt number, dimensionless
$\bar{p}$	average reservoir pressure, psia
p_a	ambient pressure, psig
p_i	initial reservoir pressure, psia
p_o	peak side-on overpressure, psig

Pr	Prandtl number, dimensionless
p_{wf}	flowing bottomhole pressure, psia
q	fluid flow rate at standard conditions, Mscf/D
Q	heat flow rate, Btu/(lbm• ºF)
Q_m	gas mass flow rate, lbm/D
r	distance from the ground-zero point of explosion, ft
R	universal gas constant
r_{ci}	casing inner radius, ft
r_{co}	casing outer radius, ft
r_e	reservoir drainage radius, ft
Re	Reynolds number, dimensionless
r_{eD}	dimensionless reservoir drainage radius with respect to wellbore radius, dimensionless
r_{inv}	radius of investigation, ft
r_{ti}	tubing inner radius, ft
r_{to}	tubing outer radius, ft
r_w	wellbore radius, ft
s	mechanical skin, dimensionless
s_g	gas saturation, fraction
t	blowout duration, hr
T	temperature, ℉
t_{Dw}	dimensionless time

T_e	reservoir temperature, ℉
T_{ei}	formation temperature at initial condition, ℉
T_{eibh}	initial bottomhole temperature, ℉
T_f	fluid temperature, ℉
v	fluid velocity, ft/sec
v_∞	terminal rise velocity, ft/s
V_e	volume of reservoir, ft3
v_g	in-site gas velocity, ft/s
v_m	mixture velocity, ft/s
v_{sg}	velocity of gas, ft/s
v_{sL}	superficial liquid velocity, ft/s
Y1	Bessel functions of the second kind
Z	gas compressibility factor, dimensionless
z_e	scaled distance, ft/lbm1/3
Z_i	initial gas compressibility factor, dimensionless
z_w	variable well depth from surface, ft
α	wellbore inclination with horizontal, degrees
γ	heat capacity ration, dimensionless
Δ Hc	energy of explosion of the flammable gas, Btu/lbm
ϵ	pipe roughness, 1/ft
η	empirical explosion efficiency, dimensionless
μ	viscosity, cp

ρ_g	gas density, lbm/ft3
ρ_L	liquid density, lbm/ft3
σ	surface tension, lbm/s2
ϕ	porosity, fraction

B.1 Abbreviation

API	American Petroleum Institute
BOEMRE	Bureau of Ocean Energy Management, Regulation, and Enforcement
BOP	Blowout preventer
BSEE	Bureau of Safety and Environmental Enforcement
DOCD	Development and Coordination Document
DOI	Department of Interior
DOJ	Department of Justice
DPP	Development of Production Plan
EP	Exploration Plan
ERCB	Energy Resource Conservation Board
GOM	Gulf of Mexico
HSE	Health and Safety Executive
IPR	Inflow Performance cure
JT	Joule-Thomson Effect
KE	Kinetic energy
MAH	Major Incident Hazard
MMS	Minerals Management Service
MOC	Management of Change
NAF	Neal Adams Firefighters

OCS	Outer Continental Shelf
OGP	International Association of Oil & Gas Producers
RP	Recommended Practice
TPC	Tubing performance curve
WCD	Worst-Case Discharge
WOAD	World Offshore Incident Databank